Electrodeposition of Metal Powders[1]

GUSTAF WRANGLEN

Division of Applied Electrochemistry, Royal Institute of Technology, Stockholm, Sweden

ABSTRACT

Metal powders may be produced electrolytically by two different methods: (*a*) direct deposition on the cathode, and (*b*) grinding of a brittle deposit. The principles underlying method (*a*) are dealt with in this paper. Three factors are shown to be responsible for the formation of powdery or spongy deposits: (1) low metal overvoltage, (2) depletion of the metal content of the cathode film, and (3) hydroxide formation in the cathode film. These factors may operate together or they may be operative under different conditions of electrolysis. Powder formation on the cathode in the electrolysis of copper, iron, nickel, zinc, and cadmium is described and analyzed.

INTRODUCTION

Metal powders may be prepared electrolytically by two different methods: (*a*) the metal may be deposited on the cathode as a powdery or even spongy material which will give a powder either directly or after light rubbing and (*b*) the metal may be obtained also as a coherent but brittle electrodeposit which may be ground to a powder. The two forms in which the metals are deposited may be related to metal overvoltage.

Method (*a*) is most important for low overvoltage metals; method (*b*) for the iron group metals, which form coherent deposits because of high metal overvoltage, and are easily obtained in a brittle condition, owing to the codeposition of a finely divided basic material (hydroxide). However, even metals such as copper (low overvoltage) can be obtained in brittle form by addition agents.

In this paper, the principles of method (*a*) are reviewed, but method (*b*) will not be dealt with further. The literature on the subject consists mainly of patents. They were abstracted by Rossman (1, 2) and by Skaupy (3). The whole field was reviewed previously by Passer (4), but the treatment of the principles involved was not adequate. A more complete discussion is given in this paper. Experimental results are included here to illustrate the principles outlined. A more detailed account of the work was given elsewhere (20).

Factors Causing Formation of Powdery and Spongy Deposits on the Cathode

The following factors are of importance for the formation of powdery and spongy metal deposits on the cathode.

1. Low metal overvoltage.
2. Depletion of the metal content of the cathode film.
3. Formation of basic material in the cathode film.

1. Low Metal Overvoltage

The metals which deposit with low metal overvoltage, e.g., silver, lead, zinc, and cadmium, tend to form needles and dendritic outgrowths, when deposited from their simple salts. It is easy, therefore, to obtain them in loosely coherent deposits, giving a crystalline powder. In fused salt electrolysis (5, 6) all metals (even those of the iron group) deposit with virtually no overvoltage and, therefore, powdery deposits are almost invariably obtained in this case. (High viscosity of the melt and depletion may also be important here.) Complex formation and addition agents increase the overvoltage of the metal deposition, thereby retarding the formation of powdery deposits.

2. Depletion of Metal Content of the Cathode Film

Under conditions favoring a high depletion of metal ions in the cathode film, the deposited metal cannot form a coherent coating, but tends to grow away from the cathode and out into the bulk solution where the metal ion concentration is higher.

Conditions favoring depletion of the metal content of the cathode film are: initial low concentration of the metal, low temperature, high current density, stationary electrolyte, and the presence of neutral salts in high concentrations. Under such circumstances, and especially in the deposition of metals with low overvoltage, loosely coherent deposits of needle-like, dendritic, or arboreal crystal formations are easily obtained. If the crystal formations are very small, the loose deposit is referred to as spongy. An extreme case of the depletion effect is the formation of so-called metal blacks (7, 8) on the cathode at very small metal ion concentrations and/or very high current densities; it is particularly favored by

[1] Manuscript received June 13, 1949. This paper prepared for delivery before the Buffalo Meeting, October 11 to 13, 1950.

the presence of neutral salts. The best known example is platinum black.

The addition of a neutral salt to the electrolyte affects a powdery deposit in two opposing ways. First, by increasing the conductivity of the bath it increases the throwing power and hence counteracts the formation of long outgrowths. Second, it increases the depletion of the depositable cation in the cathode film. This effect occurs because the neutral cations carry part of the current and, therefore, fewer metal ions are brought in by electrical transference. Thus a larger proportion of the depositable cations has to reach the cathode surface by diffusion which results in a higher difference of concentration between the metal in the solution and at the cathode surface. The outcome is that a sufficiently large addition of a neutral salt results in a finer powder. An examination of the literature showed that the importance of the addition of neutral salts had not been fully appreciated previously. Therefore, this subject will be given special attention in the experiments to follow.

3. Formation of Basic Material in the Cathode Film

Precipitated flocks of hydroxide, present in the cathode film, may settle down on the cathode surface, insulate the metal beneath, and prevent it from growing, whereas free parts of the cathode continue to grow. In this way a noncoherent deposit will be formed.

Precipitation of hydroxide in the cathode film is promoted, aside from the use of a neutral or only slightly acid solution, by conditions fostering hydrogen evolution, that is, a low cathode current efficiency. This causes depletion of the hydrogen ions in the vicinity of the cathode. The pH may be several units higher in the cathode film than in the bulk solution, as can be seen from the formation of hydroxides in the cathode film even at low pH in the bulk. The pH in the cathode film is usually higher at low temperatures, owing to slower diffusion of hydrogen ions, and in the presence of conducting salts unless the latter are also buffering.

A low cathode current efficiency, and hence a high pH of the cathode film, is favored for a given metal by shifting the conditions of deposition in a direction such that the ratio, hydrogen overvoltage/metal overvoltage, decreases. For the same reason, powder formation is promoted by contaminants consisting of metals with low hydrogen overvoltage. The presence of oxidizing agents in the electrolyte also favors powder formation due to hydroxide formation.

It is important to notice that only precipitated hydroxide (i.e., in gel-form) causes the formation of a powdery or spongy deposit. Basic material in colloidal solution (sol-form) in the cathode film often has a quite contrary effect, fostering the deposition of fine-grained, smooth, and hard deposits in the same way as do added organic colloids. If the hydroxide is flocculated, however, it is adsorbed locally on the cathode surface and causes the formation of a noncoherent, so-called burnt deposit. Furthermore, the basic material provides support for hydrogen bubbles, which make the deposit still looser.

Cooperation of Powder-forming Factors

Two or more of the powder-forming factors may be operative at the same time. Depletion and a low current efficiency are often favored by the same conditions of electrolysis, involving a cooperation of the factors 2 and 3 (e.g., deposition of iron powder at a high current density and a low temperature). Sometimes, however, the factors are influenced in opposite directions by the plating variables. An increase in temperature, for instance, counteracts depletion but lowers the metal overvoltage. An example where the hydroxide effect, but not depletion, is operative is the electrodeposition of zinc sponge from a neutral solution at a high temperature and a low current density. These conditions favor a low current efficiency (because hydrogen overvoltage is low under these conditions) but result in no appreciable depletion of metal ions.

Hydrogen evolution is often a supplementary factor in powder deposition, aiding in loosening the deposit. However, hydrogen evolution is by no means necessary for the formation of a powdery deposit. Thus, spongy dark red deposits of copper and, in the case of the noble metals, even black deposits may be formed without a simultaneous evolution of hydrogen. Actually, hydrogen evolution may sometimes make the powder coarser because of the agitation which counteracts depletion.

The general principles of powder formation on the cathode outlined above will now be illustrated by some qualitative experiments.

Formation of Powdery and Spongy Deposits on the Cathode

Copper

In the deposition of copper powder, depletion of metal ions at the cathode is the main cause of formation of powder. Typical commercial conditions are: 10 g/l of Cu, 175 g/l of H_2SO_4, 30°C, 10 amp/dm^2. Although hydrogen evolution occurs under these conditions, the high acidity of the solution prevents the formation of basic material at the cathode.

Experimental

The influence of copper concentration, current density, and temperature on the particle size of the

electrodeposited powder is well known. The influence of acidity and of additions of neutral salts has not been clearly demonstrated and, therefore, some experiments were carried out to obtain information on this point. The solution used contained 12 g/l of copper as $CuSO_4$. Vertical square electrodes (10 cm^2 x 10 cm^2) were used. No stirring was provided. The experiments were carried out at 50°C and 4 amp/dm^2. The time of electrolysis was ½ hour in every run, and the deposit remained on the cathode during this time. The results obtained are summarized in Table I.

TABLE I. *Effect of additions of H_2SO_4 and Na_2SO_4 on appearance and relative particle size of copper powder deposited at 50°C and 4 amp/dm^2 from a solution containing 12 g/l of copper.*

Expt. No.	Addition to solution		Nature of deposit	Relative particle size*
	H_2SO_4	Na_2SO_4		
	g/l	g/l		
1	—	—	Coherent deposit and large dendrites	1
2	10	—	Red sponge and fine dendrites	3
3	100	—	Fine dendrites	2
4	—	50	Uniform red sponge	4
5	—	200	Brown sponge	5
6	—	400	Brownish-black, dense sponge. Impalpable	7
7	10	50	Dark red, dense sponge. Impalpable	6
8	10	200	Voluminous red sponge. Impalpable	6
9	10	400	Voluminous red sponge. Impalpable	6

* The larger the number, the smaller the relative particle size of the powder.

It is evident from Table I that additions of sulfuric acid or sodium sulfate give finer powders (cf., 1 with following experiments). It was established in repeated experiments that 10 g/l H_2SO_4 has a greater effect than 100 g/l, which is probably due to the agitation of the hydrogen evolution occurring at the higher acid concentration, whereas there was none at the lower acid concentration.

In neutral solutions, containing high concentrations of sodium sulfate (cf., 4 to 6), brownish-black powders were formed which, on treatment with sulfuric acid, partly dissolved and became considerably lighter in color. Such powders probably contained finely divided copper hydroxide inclusions in the metal, increasing its reactivity. Such powders are not of commercial value.

From experiments 7 to 9 the conclusion may be drawn that a fine impalpable copper powder may be produced at a lower current density and a higher temperature than is used commercially (see above), if agitation of any kind, including that caused by hydrogen evolution, is avoided. This is accomplished by the presence of neutral salts and by keeping the acidity low, at about 10 g/l of H_2SO_4. This concentration is quite enough to prevent any contamination of oxides. The salt additions also make the powder more uniform than does acid alone, in the sense that the sponge may be allowed to grow for a longer time on the cathode without the formation of larger crystal aggregates on the surface.

Iron

Although electrolytic iron powder is produced commercially by grinding a coherent, brittle deposit, there are many patents dealing with the direct deposition of iron powder. The method recommended by Friedrich (11) was investigated in some detail. He recommended a neutral solution containing 15 g/l of iron as $FeCl_2$ and 100 g/l of NH_4Cl; room temperature; and a current density of 10 amp/dm^2.

Experimental

The experiments were carried out on a beaker scale with ordinary square vertical electrodes (a steel cathode between iron anodes). Propeller stirring of well-defined and constant intensity was provided. The pH of the solution was kept constant within 0.2 units by means of an antimony electrode in the bath and continuous addition of hydrochloric acid. About 40 grams of Fe/dm^2 were deposited in each run. The surface appearance and cross-sections of the deposits were studied microscopically. For the latter purpose the powdery deposits were soaked with bakelite solution, dried, and then molded in bakelite powder. The results of the experiments are summarized in Table II.

In order to investigate the influence of pH, a series of experiments was made at a current density of 10 amp/dm^2 and at several different pH's: 3, 4, 5, 6, and 6.5, both at 20°C (Expt. 1–5) and at 50°C (Expt. 6–10). At the higher temperature, a coherent deposit was obtained at pH 3, 4, 5, and 6, as shown in Fig. 1. However, as soon as ferrous hydroxide was precipitated in the solution, at pH 6.5 (Expt. 10), the deposit changed immediately to a powdery structure as shown in Fig. 2. At 20°C (Expt. 1–5), on the other hand, there was a gradual rather than sudden change in the form of the deposit as the pH was raised. This difference is explained by the greater difference in pH between the cathode film and the bulk solution at a low temperature. In neutral solution, pH 6.5−7, the deposit becomes as easily powdery at 50°C as at 20°C. It is advantageous, therefore, for reasons of economy to work at a somewhat elevated temperature in this case. However, there is a limit to the temperature that can be used,

because at 90°C (Expt. 11) a coherent deposit is formed, the other conditions being the same, even without stirring.

At higher current density, a finer powder is formed but the great influence of pH and hydroxide formation is still evident, as shown in Fig. 3 and 4 (Expt. 12–13). Even in the case of iron, a powdery deposit may be formed due to the depletion effect alone. In experiment 14 a powder was obtained although the solution was free from ferrous hydroxide. The conditions mentioned are similar to those used by Gardam (12) for the direct deposition of iron powder. As the pH was increased to 3.5 with the subsequent precipitation of ferric hydroxide, no appreciable change in the deposit was obtained. However, a much finer and looser deposit may be obtained from a neutral solution containing ferrous hydroxide.

TABLE II. *Influence of temperature, current density, and pH on the character of iron deposited from a solution containing 15 g/l of Fe as $FeCl_2$ and 100 g/l of NH_4Cl*

Expt. No.	Temp	Current density	pH	Nature of deposit	Remarks
	°C	amp/dm²			
1–5	20	10	3.0, 4.0, 5.0, 6.0, 6.5	Gradual change from coherent to powdery deposit	
6–9	50	10	3.0, 4.0, 5.0, 6.0	Coherent (Fig. 1)	Solution clear
10	50	10	6.5	Powdery (Fig. 2)	Solution contained ferrous hydroxide
11	90	10	6.5	Coherent	Solution contained ferrous hydroxide
12	50	20	4.0	Coherent (Fig. 3)	Solution clear
13	50	20	6.5	Powdery (Fig. 4)	Solution contained ferrous hydroxide
14	25	20	2.5	Coarse powder	No stirring. Solution clear. Depletion effect
15	25	20	3.5	Coarse powder as in previous case	No stirring. Solution contained ferric hydrate. Depletion effect

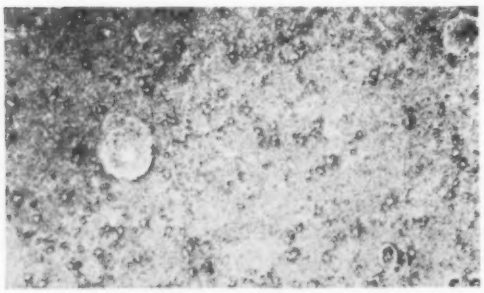

FIG. 1. Fe, $pH_{20°}$ = 3, 4, 5, 6
50°C, 10 amp/dm², 30×

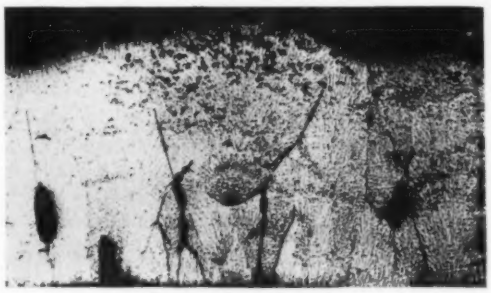

FIG. 3. Fe, $pH_{20°}$ = 4
50°C, 20 amp/dm², 100×

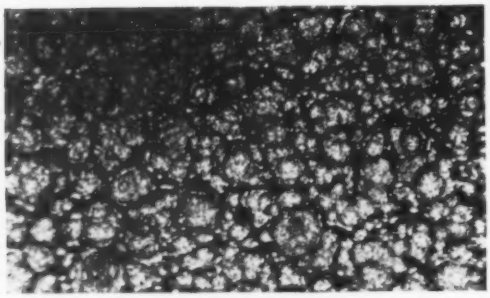

FIG. 2. Fe, $pH_{20°}$ = 6.5
50°C, 10 amp/dm², 30×

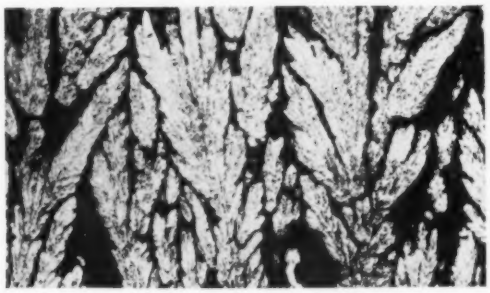

FIG. 4. Fe, $pH_{20°}$ = 6.5
50°C, 20 amp/dm², 100×

The influence of stirring is shown in Fig. 5 and 6. Stirring interferes with the production of powder because it counteracts depletion of both metal and hydrogen ions and removes hydroxide flocks and hydrogen bubbles from the cathode before they can interfere with the growth of the metal.

Nickel

It is more difficult to obtain a powdery deposit of nickel than of iron. This result is partially explained

by the higher metal overvoltage of nickel. If a nickel salt solution is electrolyzed under conditions usually favorable to powder formation, often the only result is a deposit of basic material on the cathode. If ammonium salts are added, nickel, free from visible basic inclusions, is obtained with good current efficiency, even at low temperatures in neutral solutions containing suspended hydroxide.

However, an entirely powdery deposit, similar to those of iron, as reported above, was obtained readily in ammoniacal nickel solutions. Thus, under the

FIG. 5. Fe, no stirring, pH 7
50°C, 10 amp/dm², 100×

FIG. 6. Fe, vigorous stirring, pH 7
50°C, 10 amp/dm², 100×

conditions: 10 g/l of Ni as $NiCl_2$, 250 ml/l of concentrated NH_4OH (giving a pH of about 11), 15 amp/dm², 50°C, and a stationary electrolyte, a fine powder was obtained with a current efficiency of 90 per cent. It could be removed from the cathode by spraying with water. Although the solution mentioned was slightly turbid, it is likely that the depletion factor was more important than the presence of basic material in the formation of the powder.

Zinc

The following discussion will show that spongy deposits of zinc may be obtained under three substantially different conditions of electrolysis, viz.:

1. In acid zinc salt solutions at *high* current density and *low* temperature. The cause is the *depletion* of zinc ions in the cathode film.

2. In neutral zinc salt solutions at *low* current density and *high* temperature. The cause is the precipitation of *hydroxide* in the cathode film.

3. In alkaline zincate solutions at *high* current density and *low* temperature. The cause is the *depletion* of zincate ions in the cathode film.

The first condition is analogous to deposition of copper sponge from acid solutions. The second condition corresponds to the zinc sponge formation encountered as a difficulty in the early experiments on electrowinning of zinc (13). It was early suggested that zinc hydroxide was the cause of this sponge formation (14). This theory was later rejected when it was found that a similar sponge could readily be obtained from an alkaline zincate solution (case no. 3) where zinc hydroxide should not be precipitated (15). Secondary oxidation at the cathode has also been suggested as a cause of formation of zinc sponge (16). In recent work on zinc powder production from zincate solutions (17, 18) the cause was again assumed to be basic material in the cathode film.

Experimental

To decide whether depletion might not be the determining factor in alkaline solutions, the influence of current density and temperature was investigated. If the powder formation were caused by depletion, it should be favored by high current densities and low temperatures. Some experiments were made with a solution containing 200 g/l of NaOH and in which zinc had been dissolved electrolytically to a concentration of 20 g/l. When subjected to electrolysis between zinc electrodes, this solution showed a marked tendency toward sponge formation which, however, decreased as the temperature was raised and the current density lowered. Indeed, at 90°C and 0.5 amp/dm² a coherent deposit was formed and there was no trace of sponge formation even after many hours' electrolysis. Hence, it is obvious that the depletion effect is the governing factor in zincate solutions as it is in acid solutions.

Cadmium

Cadmium has more tendency than zinc to deposit in the form of needles and dendritic outgrowths obviously owing to a very low metal overvoltage. A loose crystalline powder is almost invariably formed if solutions of simple cadmium salts are electrolyzed. Variations of this method are utilized to prepare cadmium powder for analytical purposes (19) and cadmium sponge for alkaline storage batteries of the Swedish type.

In order to study the application of the general principles, which have previously been outlined, to the production of cadmium powders, the effects of

several variables were investigated. The following discussion will show that spongy cadmium deposits may be obtained under two different conditions of electrolysis.

1. In acid solution at *high* current density and *low* temperature, under which conditions depletion is the important factor.

2. In neutral solution at *low* current density and *high* temperature, under which conditions the formation of basic material is the important factor.

TABLE III. *Influence of temperature, current density, and acidity on appearance and relative particle size of cadmium powder. The solutions all contained 50 g/l of Cd as $CdCl_2$*

Expt. No.	NaCl	pH	Temp	Current density	Appearance of deposit	Relative particle size*
			Acid solutions			
	g/l		°C	amp/dm²		
1	—	1	20	5	Long needles (Fig. 7)	7
2	100	1	20	5	Compact aggregations of well-developed crystals (Fig. 8)	3
3	300	1	20	5	Coarse gray sponge (Fig. 9)	10
4	—	1	30	40	Black sponge	12
5	—	1	90	40	Fine crystal needles	9
6	100	1	20	0.5	Large crystal aggregations	1
7	100	1	20	5	Compact aggregations of well-developed crystals (Fig. 8)	3
8	100	1	80	0.5	Well-developed crystal plates (Fig. 10)	2
9	100	1	80	5	Crystal aggregations	5
			Neutral solutions			
10	100	6	20	0.5	Partly dense sponge, partly larger crystals (Fig. 12)	8
11	100	6	20	5	Thin scaley flakes	4
12	100	6	80	0.5	Gray sponge (Fig. 11)	11
13	100	6	80	5	Crystal aggregations	6

* The larger the number, the smaller the particle size of the powder.

Experimental

The plating solutions contained 50 grams of cadmium per liter, as chloride, and varying concentrations of sodium chloride. The acid solution was 0.1*N* in hydrochloric acid (approximately pH 1). The neutral solution was prepared by adding NaOH to the cadmium chloride solution until a permanent turbidity was produced. This solution had a pH of about 6. The electrolysis was done in a 500-ml beaker with a cadmium rod as anode and a cadmium-coated nickel cylinder as cathode with an area of about 2 dm². The anode was placed at the axis of the cylinder and the deposit was produced on the inside surface of the cylinder. The solution was not stirred. In each experiment deposition was carried out to the extent of 4 amp-hr. The results of the experiments are summarized in Table III.

Effect of sodium chloride.—The most important plating variable governing the formation of cadmium sponge by electrolysis was found to be the presence of sodium chloride in the electrolyte. Sponges were obtained in experiments 3, 10, and 12. If the NaCl were omitted from these experiments, no sponges were obtained. On the other hand, in a series of parallel experiments (not recorded here), similar to experiments 6 to 13 in which the content of sodium chloride was increased to 300 g/l, a gray or black sponge was obtained in every experiment. At this high concentration of sodium chloride the hydroxide effect and the depletion effect seem to merge.

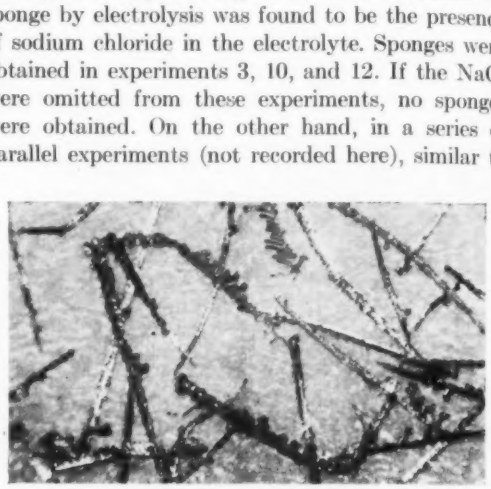

FIG. 7. Cd, no NaCl, pH 1
20°C, 5 amp/dm², 30×

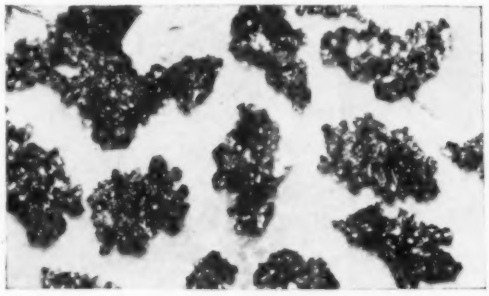

FIG. 8. Cd, 100 g/l NaCl, pH 1
20°C, 5 amp/dm², 30×

The effectiveness of sodium chloride in enabling sponges to be obtained from acid solutions at a current density of 5 amp/dm² is illustrated in Fig. 7 to 9 (Expt. 1–3). Without the sodium chloride, long needles are formed. In the presence of 100 grams of sodium chloride per liter, aggregates of well-developed crystals are obtained, and in the presence of 300 grams of sodium chloride per liter a finely crystalline spongy deposit is obtained. In the absence of sodium chloride, a current density of 40

amp/dm² must be used to obtain a sponge in the acid solution (Expt. 4).

Effect of plating conditions.—In the presence of 100 g/l of NaCl in the solution, the effects of pH, current density, and temperature were brought out most clearly, and these data are contained in experiments 6 to 13. The deposits obtained in these experiments varied considerably in fineness, comprising both sponge and large crystals. These experiments are discussed in detail in the following paragraphs.

Effect of acidity of solution.—The experiments (Table III) made in runs 6 to 9 are similar to those in experiments 10 to 13 in all respects except for the

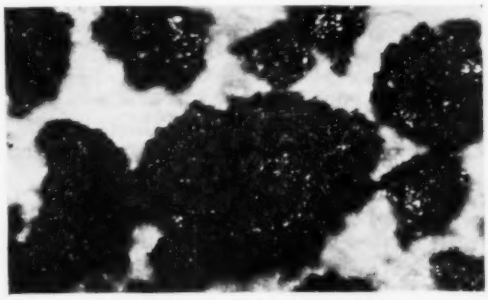

FIG. 9. Cd, 300 g/l NaCl, pH 1
20°C, 5 amp/dm², 30×

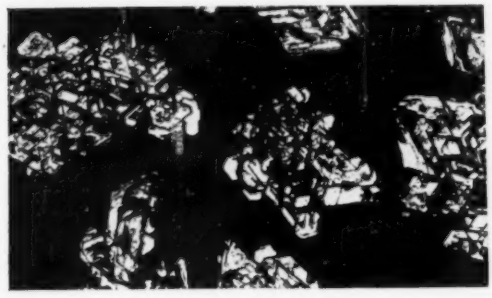

FIG. 10. Cd, pH 1
80°C, 0.5 amp/dm², 30×

acidity of the solution. The former set of runs were from acid solutions of pH 1, and the latter runs from a neutral solution of pH 6. The table shows that a powder obtained from a neutral solution is always finer than the corresponding powder obtained in an acid solution, the other conditions being the same. The effect of acidity is strikingly illustrated by Fig. 10 and 11. Fig. 10 shows large, well-developed hexagonal cadmium crystals formed in the acid solution. Fig. 11 shows the spongy deposit obtained from the neutral solution at the same current density and temperature.

Effect of current density.—Variation in the current density has opposite effects in neutral and in acid solutions. This is because hydroxide formation is the most important factor in neutral solutions, whereas in acid solutions low overvoltage and depletion are operative. In neutral solution an increase in current density retards the sponge formation (cf. Expt. 10 and 11, 12 and 13), owing to increased current efficiency. In acid solution an increase in current density gives a finer crystal powder (cf. Expt. 6 and 7, 8 and 9) and finally a sponge (Expt. 4).

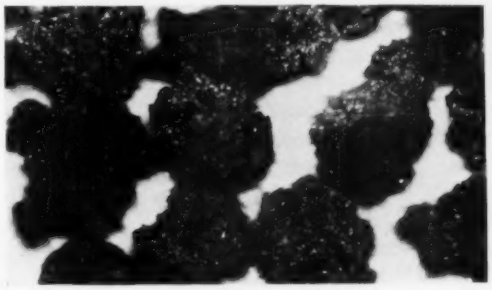

FIG. 11. Cd, pH 6
80°C, 0.5 amp/dm², 30×

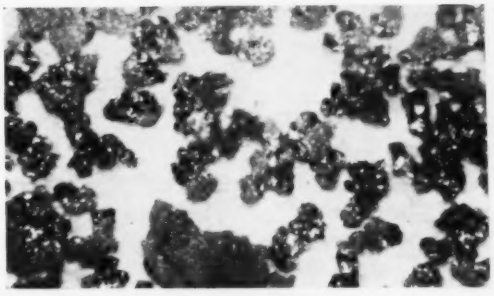

FIG. 12. Cd, pH 6
20°C, 0.5 amp/dm², 30×

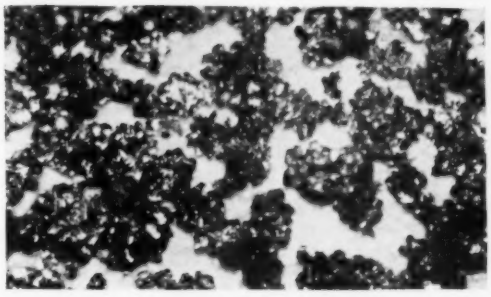

FIG. 13. Cd, pH 6
80°C, 5 amp/dm², 30×

The different effect of current density in neutral and acid solutions is also illustrated by the following observations. The sponge formation in neutral solutions starts at the upper part of the cathode, which is the low current density area, spreads from there and becomes more and more pronounced as the

cathode surface increases and the current density correspondingly decreases during deposition. The sponge formation in acid solution at high current density, on the other hand, is most pronounced at the edges of the electrode (cf. Expt. 4, which, as No. 5, was made with a flat electrode) and it is retarded more and more as the cathode surface is increased in the deposition process.

Effect of temperature.—The effect of temperature on the particle size of electrodeposited cadmium powders is more complicated. In acid solutions the coarse crystalline powders formed at relatively low current densities, where depletion is not yet important, become finer with a rise in temperature (cf. Expt. 6 and 8, 7 and 9), which may be attributed to a lowering in the metal overvoltage. The fine sponge formed at a high current density, however, where depletion is the important factor, is retarded by an increase in temperature (cf. Expt. 4 and 5) as expected. In neutral solutions, the sponge formation at a low current density is more pronounced at a high temperature (cf. Expt. 10 and 12), favoring a low current efficiency and hence hydroxide formation, which is more important than metal overvoltage in this case.

Acknowledgments

The author wishes to express his thanks to Professor G. Angel, Head, Department of Chemical Engineering, Royal Institute of Technology, Stockholm, who suggested and supervised this investigation. The work was promoted by a grant from the Swedish Technical Research Council.

Any discussion of this paper will appear in a Discussion Section, to be published in the June 1951 issue of the JOURNAL.

REFERENCES

1. J. ROSSMAN, *Metal Ind.* N. Y., **30**, 321, 396, 436, 468 (1932).
2. J. ROSSMAN, *Trans. Electrochem. Soc.*, **85**, 169 (1944).
3. F. SKAUPY, "Metallkeramik," p. 25–26, 21, Verlag Chemie, Berlin (1943).
4. M. PASSER, *Kolloid-Z.*, **97**, 272 (1941).
5. J. ANDRIEUX, *Rev. mét.*, **45**, 49 (1948).
6. W. J. KROLL, *Trans. Electrochem. Soc.*, **87**, 551 (1945).
7. F. MYLIUS AND O. FROMM, *Ber.*, **27**, 630 (1894).
8. V. KOHLSCHÜTTER AND TH. TOROPOFF, *Z. Elektrochem.*, **19**, 161 (1913).
9. A. HOTHERSALL AND G. GARDAM, *Metal Ind. London*, **66**, 234 (1945).
10. BIOS INVESTIGATORS, *Metal Ind. London*, **71**, 226 (1947).
11. Allgemeine Elektrizitäts-Gesellschaft, German Pat. 316, 748, Dec. 5, 1919.
12. G. GARDAM, Iron & Steel Inst. (London), Special Report No. 38, "Symposium on Powder Metallurgy," 2nd ed., p. 3, 1947.
13. W. PFANHAUSER, "Galvanotechnik," p. 51–53, Akademische Verlagsgesellschaft, Leipzig (1941).
14. F. FOERSTER AND O. GÜNTHER, *Z. Elektrochem.*, **5**, 16 (1898–99).
15. F. FOERSTER AND O. GÜNTHER, *Z. Elektrochem.*, **6**, 301 (1900).
16. O. K. KUDRA AND K. N. IVANOV, *J. Phys. Chem.*, **40**, 769 (1936).
17. M. PASSER AND G. HÄNSEL, *Wiss. Veröffentl. Siemens-Werken*, **18**, 124 (1940).
18. W. ECKHARDT, *U. S. Bur. Mines Circ.* No. 7466 (1948).
19. W. D. TREADWELL, *Helv. Chim. Acta*, **4**, 551 (1921); **5**, 732, 806 (1922).
20. G. WRANGLEN, *Trans. Roy. Inst. Technol. Stockholm*, No. 37 (1950).

Plating Experiments with Aqueous Solutions at High Temperatures[1]

SEYMOUR SENDEROFF AND ABNER BRENNER

National Bureau of Standards, Washington, D. C.

ABSTRACT

Aqueous solutions of salts of chromium, copper, molybdenum, nickel, titanium, tungsten, vanadium, and zirconium were electrolyzed under pressure at temperatures up to 300°C. Under these conditions, intermediate reduction steps were favored over reduction to metal. Instability of the solutions was frequently encountered but anodic processes were improved in some instances.

INTRODUCTION

As part of a project on the electrodeposition of refractory metals sponsored by the Department of the Navy, a study of the electrolysis of aqueous solutions at high temperatures was undertaken.

No studies have been reported on the electrodeposition of metals from aqueous solutions at temperatures much above 100°C. It is known that between room temperature and 100°C the electrodeposition of metals from many solutions improves with increasing temperature. Higher plating rates, higher cathode current efficiencies, more ductile deposits, and, frequently, brighter deposits may be obtained at elevated temperatures (1) from plating solutions which do not yield these results at room temperature. As an example, deposits of tungsten alloys are sound and smooth when plated at 90°C, while at 30°C they are usually rough and brittle (2). It was thought advisable to investigate the temperature range between 100° and 300°C with particular reference to the possibility of depositing those metals which have hitherto not been deposited from aqueous solution at normal temperature.

Three factors are involved in an appreciable increase of temperature which might facilitate the deposition of these metals. First, if the inability to deposit them is due to some irreversibility in the complex series of processes at the cathode, i.e., a slow step with a high energy barrier, the higher temperature would overcome this. Those electrode processes where irreversibility has been observed, as shown by their overvoltage, are made more reversible as the temperature is increased (3). Second, if the inability to deposit these metals is associated with their presence in a nonreducible complex structure (ion or molecule), the high temperature may dissociate this complex so that the metal will be present in solution in a reducible form. Third, if the deposition of these metals is prevented by the formation of cathodic oxide films, the overvoltage or resistivity of which interferes with metal deposition, a higher temperature might decompose these oxides or make them more soluble in the electrolyte.

The temperature range, 100° to 300°C, was selected for investigation because the upper limit is still safely below the critical temperature of water, thereby eliminating the possibility of difficulties due to changes in state and reducing the problems of pressure control, and because it represents an approximate doubling of the absolute temperature compared to room temperature, so that any changes resulting from the temperature change should be large enough to observe. Since the vapor pressure of water at 300°C is approximately 90 kg/cm² (1275 lb/in.²), and since it rises very rapidly with temperature at this point, it was necessary to use high-pressure, high-temperature, corrosion resistant equipment for this study and to operate it by remote control as far as possible.

The equipment finally assembled consisted of a stainless steel reaction vessel[2], 1400 cm³ capacity, with modification of the head to accommodate electrical leads, anode and cathode holders, thermowell, and sampling condenser. Fig. 1 is a schematic diagram of this equipment. Of particular interest are the electrical leads and seals used for bringing current into the interior of the bomb. The usual method of passing a wire through a soapstone cone and crushing the cone in its seat to make an insulating pressure seal failed because of the porosity of the powdered soapstone which permitted absorption of plating solution. A chromic acid solution attacked the soapstone sufficiently to cause it to blow out at 140 kg/cm² (2000 lb/in.²). Replacement of the soapstone with Teflon gave an insulating seal that was sufficiently stable to chemicals, but not to heat. It extruded and failed at about 225°C. A satisfactory

[1] Manuscript received June 23, 1950. This paper prepared for delivery before the Buffalo Meeting, October 11 to 13, 1950.

[2] American Instrument Company Superpressure Vessel, Catalog No. 406-25J3.

electrical lead was made by sealing 60-mil tungsten rod in a Nonex (or Corning #772) glass tube (the seal extending the full length of the glass) with about one inch of tungsten exposed at each end. The glass was then coated with silver by chemical reduction and electroplated with 0.005 inch of nickel. About one inch of glass at each end was left exposed. The nickel was machined to true round and a silver cone fitted over the nickel (see Fig. 2). The silver cone and conical seat in the bomb-head were painted with a silicone resin (GE #9989-1) and the assembly was set in place. Pressure was applied by tightening the nut in the bomb-head to seat the cone accurately and to compress the cone around the nickel deposit. These leads were found to be satisfactory at 300°C and 210 kg/cm² (3000 lb/in.²) and to resist chemical attack by acids and oxidizing agents, but failed with strong alkalies after several experiments owing to attack of the glass by the alkali at high temperature. The resistance between the lead and bomb-head was greater than one megohm and no gas leaks were observed.

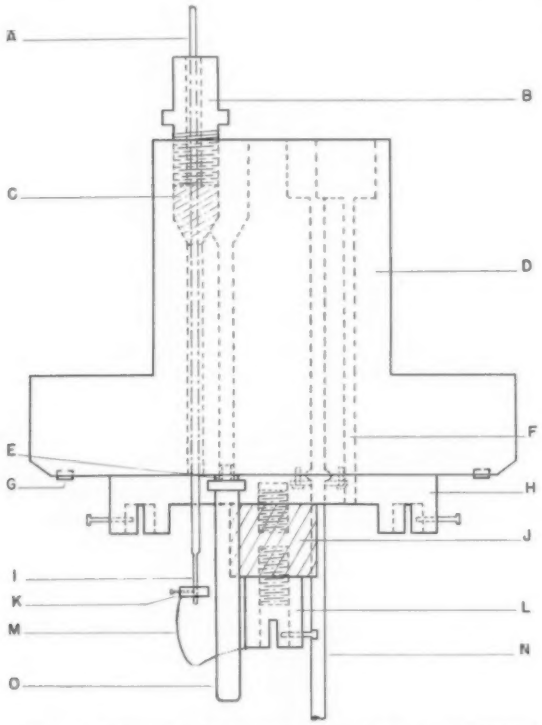

FIG. 1. Schematic diagram of bomb-head. A—Electrical lead-in, B—tightening nut, C—silver cone, D—stainless steel bomb-head, E—gold gasket, F—gas port, G—stainless steel gasket, H—stainless steel holder for anodes, I—tungsten rod, J—ceramic insulator, K—stainless steel collar, L—cathode holder (stainless steel), M—gold wire, N—solution outlet tube, O—stainless steel thermowell.

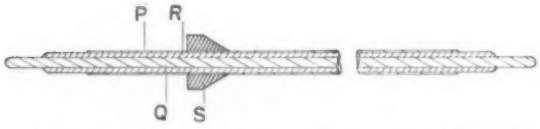

FIG. 2. Detail of lead-in. P—Electrodeposited nickel, 0.005-in. wall thickness, Q—tungsten rod, 0.060-in. diameter, R—"Nonex" glass tube, 0.030-in. wall thickness, S—silver cone.

EXPERIMENTAL WORK

Copper.—In an effort to determine the high temperature properties of ordinary plating solutions, acid copper and Watts nickel solutions were investigated. A solution containing 200 g/l of copper sulfate pentahydrate and 30 ml/l of sulfuric acid was electrolyzed with copper anodes at 300°C, and at the end of the run an accumulation of fine crystalline copper powder was found at the bottom of the beaker. A similar run with copper rods immersed in the solution, but without the use of current, produced a similar deposit. In this case, the copper powder was agglomerated in a spongy mass of very low coherence. At this high temperature the copper evidently dissolves in the plating solution as Cu^{+}, which then disproportionates to $Cu + Cu^{++}$ (4). Determination of the copper and sulfuric acid in the solution before and after this run showed that the Cu/H_2SO_4 ratio decreased by about 8 per cent. This result can be explained only if some cuprous hydroxide precipitated in addition to the copper which came out of the solution.

Nickel.—The work with nickel is summarized in Table I. The inability to obtain any nickel plate in runs 3 and 4 was due to almost complete removal of nickel ion from the solution at this temperature. Nickel sulfate had previously been found to be practically insoluble in water at 230°C (5). Even at 200°C enough precipitates so that good plates cannot be obtained at a current density greater than 5 amp/dm² (see runs 2, 5, 6, 9). This shows that the expected increase of the limiting current density with increasing temperature is more than offset by the decrease in solubility. Nickel chloride is more soluble at 300°C than nickel sulfate, but it too is less soluble at higher temperatures.

On analysis the precipitate obtained from solution 4 corresponded to the formula $NiSO_4 \cdot 2H_2O$. It was very difficultly soluble in water but dissolved in warm hydrochloric acid. The pH of the water solution was about 7. On standing for about one week in water, enough salt dissolved to make a 5 per cent solution. The complete precipitation of this lower hydrate of nickel sulfate from water solution (pH = 2) at high temperature represents one of the more extreme ex-

amples of the instability of aqueous solutions under these conditions.

Three borderline elements (i.e., elements that are plated only as alloys or at low efficiency from aqueous solution) were then investigated. These were chromium, molybdenum, and tungsten.

atmosphere above it gave identical results. This indicates that pressure variations have no significant effect on chromium plating in this range. When electrolyzed at 150°C, however, the cathode efficiency was reduced to 1 per cent, and at 300°C the plating solution decomposed, precipitating chromic

TABLE I. *Electrolysis of nickel solutions under pressure at elevated temperatures**

Expt. No.	Solution	Temp	Current density	Cathode current efficiency	Remarks
		°C	amp/dm²	%	
1	2*N* $NiSO_4$, pH = 2	90	5	98	—
2	2*N* $NiSO_4$, pH = 2	200	5	99.2	Small precipitate, satisfactory Ni deposit
3	2*N* $NiSO_4$, pH = 2	250	5	0	Large precipitate, no plate
4	2*N* $NiSO_4$, pH = 2	300	5	0	Large precipitate, no plate
5	2*N* $NiSO_4$, pH = 2	200	50	—	Burned deposit
6	2*N* $NiSO_4$, pH = 2	200	20	—	Treed deposit
7	2*N* $NiCl_2$, pH = 2	300	5	91	Treed deposit
8	2*N* $NiCl_2$, pH = 2	300	50	—	Burned deposit
9	Watts Ni, pH = 3	200	5	—	Smooth, semibright, uniform Ni plate

* Each experiment was run for one hour. Some precipitate was present at the end of all runs, except 1.

TABLE II. *Electrolysis of molybdenum solutions under pressure at elevated temperatures**

Expt. No.	Solution	Plating time	Current density	Results
		hr	amp/dm²	
1	80 g/l Na_2MoO_4 + 800 g/l K_2CO_3	4	10	Spongy black deposit containing 7% Mo, 42% Ni†
2	80 g/l Na_2MoO_4 + 800 g/l K_2CO_3	5	5	Spongy black deposit containing 27% Mo, 42% Ni†
3	80 g/l Na_2MoO_4 + 800 g/l K_2CO_3	2	105	Very thin dark deposit containing 2.6% Mo
4	80 g/l Na_2MoO_4 + 300 g/l KOH	4	10	No deposit
5	80 g/l Na_2MoO_4 + 800 g/l K_2CO_3 + 10 g/l Co	4	10	Spongy and powdery Co deposit
6	100 g/l Na_2MoO_4 + 35 cm³/l conc H_2SO_4, pH = 1.0	2.5	50	Blue ppt., blue-black powdery material on cathode, blue soln. Mo = 58%
7	100 g/l Na_2MoO_4 + 35 cm³/l conc H_2SO_4, pH = 3.5	2.5	10	Blue ppt., blue-black powdery material on cathode, blue soln. Mo = 58%

* All runs at 140 to 175 kg/cm² (2000 to 2500 lb/in.²), 300°C, initial N_2 pressure = 49 kg/cm² (700 lb/in.²).
† Solutions 1–5 contained in nickel beaker during run.

Chromium.—A chromium plating solution containing 250 g/l of chromic acid and 2.5 g/l of sulfuric acid was electrolyzed at 75°C, 1 atmosphere pressure, and 52 amp/dm², with a current efficiency of 6 to 7 per cent. Varying the pressure from 1 atmosphere to 200 atmospheres resulted in no significant change in current efficiency. The use of hydrogen or nitrogen to saturate the solution and the

oxide on the cathode which became polarized so that no current could be passed. The use of a solution containing 50 g/l of chromic acid and 0.5 g/l of sulfuric acid at 150°C gave the same results as the more concentrated solution did at 300°C. The same solutions, when heated without electrolysis, underwent considerable decomposition at 300°C, but only negligible decomposition at 150°C. When a solution con-

taining 50 g/l of chromic acid was sealed in a glass tube and heated to 300°C, 15 per cent of the chromium was reduced to the trivalent state and some chromic oxide precipitated. These experiments show that chromic acid solutions are more easily reduced by electrolysis to trivalent chromium at elevated temperatures, but that the reduction to metal is not favored. At 300°C the solutions are thermally unstable and decompose. Solid chromic acid also decomposes at this temperature (6). A chrome alum solution (275 g/l, pH = 1.8) was electrolyzed at 300°C using a porous cup to separate anolyte and catholyte, but no metallic deposit was obtained.

Molybdenum.—The experiments on molybdenum are summarized in Table II. No sound metallic deposits were obtained. The alloy deposits were inferior to those obtainable under ordinary conditions, since they were mostly nonmetallic. In the reduction to blue material (see Table II), the greatly increased tendency for reduction to intermediate stages was again observed. The deposit in run 6, though high in molybdenum, was entirely nonmetallic in appearance. The material on the cathode was evidently a hydrated molybdenum oxide.

Tungsten.—The experiments on tungsten-containing solutions are summarized in Table III. No sound metallic deposits were obtained. In the solutions containing cobalt, tungsten was found in the deposit, but the physical properties of the deposit were much inferior to those obtained at 90°C from the tartrate plating solution (2). The reduction to blue material in solution 3 occurred at a higher pH than is usual at ordinary temperatures. In solutions 7 and 8, at 300°C, the tungsten anodes corroded very well at low voltage (approximately 2 volts). The same solutions at 100°C gave almost instantaneous polarization of the anodes so that even at 12 volts current would not pass. The anodic polarization in this case could be eliminated only after washing the anodes with concentrated ammonium hydroxide. When the voltage was impressed again on the electrodes, a momentary surge of current resulted after which

TABLE III. *Electrolysis of tungsten solutions under pressure at elevated temperatures**

Expt. No.	Solution	Plating time	Current density	Results
		hr	*amp/dm²*	
1	100 g/l Na_2WO_4	2	50	Blue solution. No cathode deposit
2	100 g/l Na_2WO_4 + 2 g/l NaOH	2	95	Blue solution. No cathode deposit
3	100 g/l Na_2WO_4 + 316 cm³/l conc NH_4OH	2	95	Blue solution. No cathode deposit (pH = 10 at end of run)
4	100 g/l Na_2WO_4 + 2.8 g/l Co + 3.4 g/l NH_3	2	95	Irregular, black oxide-containing deposit on cathode, blue ppt. in solution. Deposit contains 44% W
5	100 g/l Na_2WO_4 + 2.8 g/l Co + 3.4 g/l NH_3	5	5	Same appearance as Expt. No. 4 but deposit contains 21.4% W
6	100 g/l Na_2WO_4 + 2.8 g/l Co + 3.4 g/l NH_3	2	650	Same appearance as Expt. No. 4. No W in deposit
7	100 g/l Na_2WO_4 + 80 g/l H_2PO_4 (85%). pH = 1.9	2	5	Blue solution. No cathode deposit
8	100 g/l Na_2WO_4 + 175 g/l H_3BO_3 pH = 5.8	3	5	Blue solution. No cathode deposit
9	100 g/l Na_2WO_4 + 175 g/l H_3BO_3 pH = 5.8	4	100	Thin brown film on cathode, probably WO_2. Blue solution
10	Colloidal dispersion of $WO_3 \cdot H_2O$ in distilled water	4	5	No cathode deposit, colloid migrates to and collects on anode, some blue ppt. Filtration gives original white colloidal dispersion

* All runs at 140–196 kg/cm² (2000 to 2800 lb/in.²), 300°C, initial nitrogen pressure before heating = 49 kg/cm² (700 lb/in.²)

polarization set in again. No thermal decomposition of sodium tungstate solution was observed.

The last group investigated were elements not hitherto deposited in any form from aqueous solutions. These are vanadium, zirconium, and titanium.

Vanadium.—Table IV summarizes the work with vanadium-containing solutions. The deposits from solutions 1 and 2 were highly crystalline, black by reflected light and red by transmitted light. They dissolved in nitric acid, emitting brown fumes and forming a blue solution. From their chemical properties they were evidently an oxide of vanadium in which the valence of vanadium is 4 or less. Since no thermal decomposition of vanadyl or vanadate solutions was detected when heated to 300°C in a sealed glass vessel, the cathode deposits must have been a result of electrolytic reduction, probably to the trivalent or lower state. After drying at 110°C, the deposits from solutions 1 and 2 were found to contain 45 and 58 per cent vanadium, respectively. These values do not approximate any simple lower oxide of vanadium and it must be presumed that the deposit is complex in structure. An x-ray diffraction pattern of this material showed it to be cubic with a lattice parameter of 10.325 Å. This large dimension also indicates that the compound is not a simple oxide, but rather that a large number of atoms form the unit cell. No further work was done on identifying this deposit, since it was certain that it was nonmetallic and did not contain an appreciable amount of free metal. Solutions similar to those in Table IV at 100°C gave only thin films or discolorations at the cathode.

Zirconium and Titanium.—Heating acidified solutions of zirconium sulfate or titanium chloride to 300°C resulted in complete hydrolysis and precipitation of the compounds. A solution containing 500 cm³ of zirconium sulfate (100 g/l), 80 cm³ glycolic acid (70%) and 150 cm³ of concentrated ammonium hydroxide, pH = 9.5, was electrolyzed at 300°C, and no cathode deposit was obtained. The zirconium salt was completely hydrolyzed, no zirconium being detectable in the solution after the run. At the end of the run the solution was found to contain carbonate, resulting either from decarboxylation or anodic oxidation of the glycolate. In addition, it had a very foul odor, indicating the possibility that at the high pressure and temperature the organic compound had been aminated.

Electrolytic runs were not made with titanium since compounds stable in solution at high temperature were not available.

TABLE IV. *Electrolysis of vanadium solutions under pressure at elevated temperatures**

Expt. No.	Solution	Plating time	Current density	Results
		hrs	*amp/dm²*	
1	100 g/l $V_2O_2CL_4$, 50 cm³/l H_2SO_4	3	10	Deposit of reddish black crystals on cathode
2	100 g/l $NaVO_3 \cdot 4H_2O$, pH = 8.0	2.5	10	Crystalline, black anode and cathode deposits
3	100 g/l $NaVO_3 \cdot 4H_2O$, 2.5 g/l Ni, pH = 5	3	5	Black cathode deposit. No nickel
4	Watts Ni solution† + 20 g/l $VOSO_4$	2.5	5	Warty black and brown deposit. Solution of brown material in KOH leaves dark metallic matrix of Ni with approximately 5% V
5	500 cm³ Watts Ni,† 250 cm³ conc NH_4OH, 100 cm³ 61 g/l NH_4VO_3 (= 3.0 g V)	3	5	Nickel deposit on cathode. No vanadium, large ppt. of $Ni(OH)_2$

* Run at 300°C, 140 to 210 kg/cm² (2000 to 3000 lb/in.² pressure), anolyte and catholyte separated by a porous cup in all cases.

† Run at 200°C.

Conclusions

The temperature range around 300°C has been shown to be unsuitable for the electrodeposition of several metals from aqueous solutions. Some of the probable causes of the failures to deposit metals are as follows:

1. The instability of solutions of metal salts at this temperature results in hydrolysis or precipitation, thereby removing the metal ion from solution.
2. At this temperature, reduction of polyvalent ions to an intermediate valence state is favored over reduction to metal.
3. Where gas evolution and metal deposition occur simultaneously the efficiency of metal deposition is decreased, probably because the overvoltage of gas evolution is reduced more than that of metal deposition.

It was found, however, that high temperatures are beneficial for anode corrosion. In at least one case (acid tungstate solutions) anodes corroded well at 300°C, although they were completely passive and prevented flow of current at 100°C.

Any discussion of this paper will appear in a Discussion Section, to be published in the June 1951 issue of the JOURNAL.

REFERENCES

1. H. L. BENNER AND C. J. WERNLUND, "Modern Electroplating," p. 176, The Electrochemical Society, Inc., New York (1942).
A. K. GRAHAM AND H. J. READ, *ibid.*, p. 190.
W. L. PINNER, G. SODERBERG, AND E. M. BAKER, *ibid.*, p. 247.
W. BLUM AND C. KASPER, *Trans. Faraday Soc.*, **31**, 1203 (1935).
2. A. BRENNER, P. BURKHEAD, AND E. SEEGMILLER, *J. Research Nat. Bur. Standards*, **39**, 351 (1947).
3. S. GLASSTONE, "Introduction to Electrochemistry," p. 466, D. Van Nostrand, New York (1942).
4. J. W. MELLOR, "Comprehensive Treatise on Inorganic and Theoretical Chemistry," Vol. III, p. 231, Longmans Green, London (1923).
5. M. ETARD, *Ann. chim. et phys.* [7] 2, 552 (1894).
6. W. H. HARTFORD, *Ind. Eng. Chem.*, **41**, 1993 (1949).

Instrumentation in a Modern Chlorine Handling Plant[1]

J. M. Hildyard

Hooker Electrochemical Company, Niagara Falls, N. Y.

ABSTRACT

The control equipment for a modern chlorine handling plant is described and analyzed. The process consists of equipment for collecting, cooling, drying, compressing, and liquefying chlorine gas. Personal supervision of the equipment by the operators has been reduced by the control means employed. Some information is given for the selection and installation of instruments for chlorine plants.

The primary purpose of this paper is to describe a method of controlling a chlorine handling process; secondly, it is to describe the type of instruments involved and their method of installation. The term 'chlorine handling' refers to that portion of a chlorine plant that collects the chlorine from the cells and performs the necessary treatments for liquefaction.

The control method described herein is used at the Niagara Falls Plant of the Hooker Electrochemical Company, and the selection of the chlorine handling process as the topic of the paper was largely influenced by the interest shown in this recently modernized portion of the plant. This method is not offered as an optimum method for all chlorine plants, but is set forth as a satisfactory solution for the Niagara Falls Plant. The aim of the instruments in a process should be to reduce the production costs, increase quality, or aid and simplify the operations. A given installation will, therefore, reflect the desires and needs of the department charged with the operation of the process.

Fig. 1 is the flow diagram for that portion of the process that is within the scope of this paper. The instrument symbols used are in accordance with the recommendations of the Recommended Practices Committee of the Instrument Society of America (1).

This plant uses diaphragm-type cells to produce a chlorine effluent gas saturated with water and essentially at atmospheric pressure. The chlorine handling process consists of units for collecting, cooling, drying, compressing, and liquefying the chlorine.

The flow sheet starts with the chlorine cells which are located in several cell houses, each of which has a pressure control for the use of the cell attendants. The effluent gas from the cell houses is conducted by pipelines to a common header at the inlet of the chlorine cooling system, which consists of two banks of primary coolers and a bank of secondary coolers. The primary coolers are cooled by plant water the year around. Plant water is also used on the secondary coolers during the winter months, but during the warmer months, it is necessary to use refrigerated water which is obtained by the heat exchange system shown above the coolers on the flow sheet.

From the coolers, the gas flows to the drying towers where it is contacted with sulfuric acid. The dry gas is next compressed in Nash Hytor Compressors (called turbines in accordance with common plant usage) and discharged into tanks for separating the chlorine from the sulfuric acid that is used as a sealing fluid for the compressors. The sealing acid is recirculated by the turbines through a heat exchanger that removes the heat of compression of the chlorine.

After separation from the acid, the gas goes to the refrigeration building where the chlorine is liquefied and separated into the liquid and noncondensible fractions. Liquid chlorine is sent to storage and the "sniff gas" or noncondensible portion is sent to other plant processes that are able to utilize this gas.

When the plant was modernized, the equipment and control means were engineered and installed so that personal attendance of an operator would be minimized. To achieve this, the equipment, after the cells, was installed in two buildings. The first contains the units for cooling, drying, and compressing the chlorine. The second building contains the refrigeration machines and the chlorine liquefaction units. The refrigeration building also contains a panel that has instruments showing the operating conditions both in the liquefaction building and the cooling and compression building. An operator normally stays in the liquefaction building but by means of the remote instruments can keep the equipment in the other building under surveillance.

The instruments used in the process are shown in fairly complete detail on the flow sheet. Most of the temperatures in the two buildings are taken by means of thermocouples. The panel in the liquefaction building has two recording potentiometers and a self-balancing indicating potentiometer with rotary

[1] Manuscript received February 20, 1950. This paper prepared for delivery before the Cleveland Meeting, April 19 to 22, 1950.

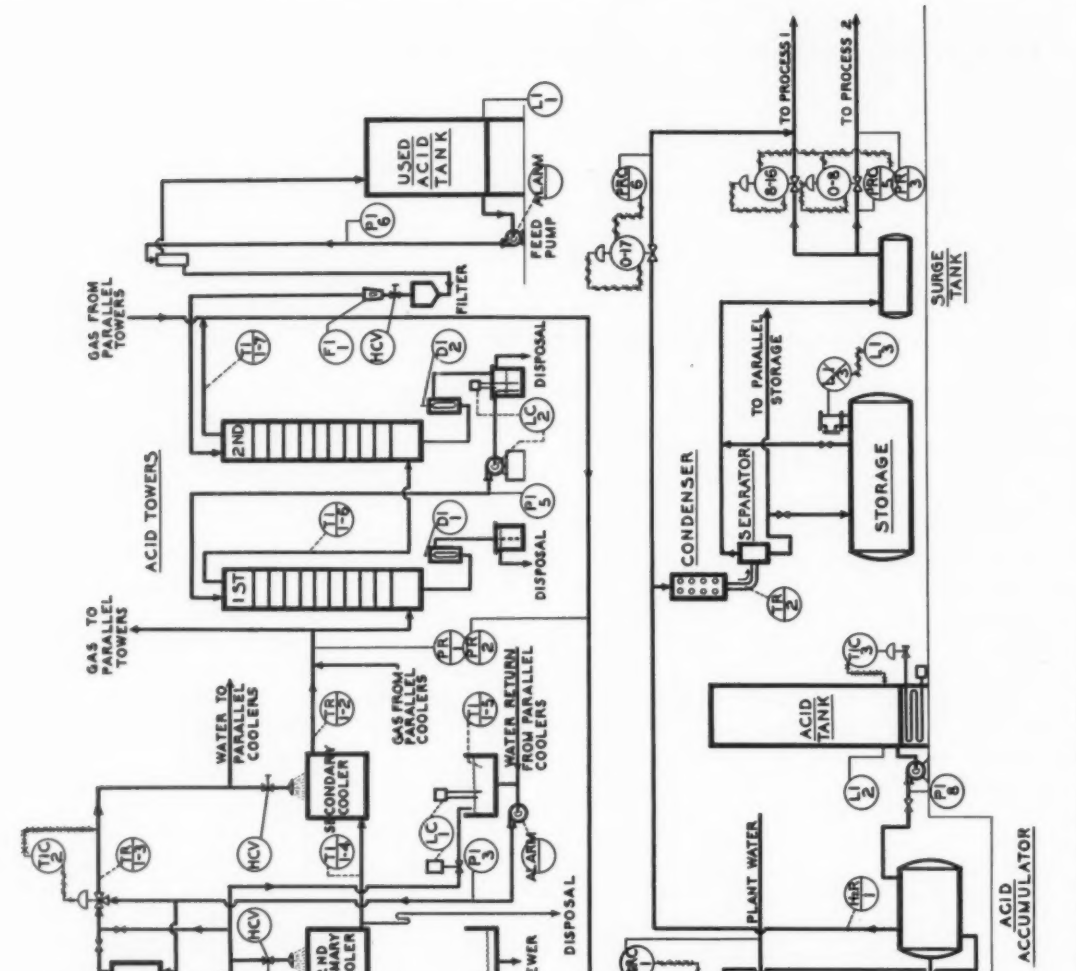

FIG. 1. Flow sheet of chlorine handling process

selector switches. The pressures on the suction side of the turbines and after the cells are obtained by U tube manometers inserted in the pipelines or by bellows type gauges either installed on the panel or transmitting to the panel. The turbine discharge pressures are obtained by bourdon gauges sealed with diaphragm protectors or protected by a purge. A thermal-conductivity-type gas analyzer samples the turbine effluent and analyzes it for percentage of hydrogen. This paper will not consider all of the instruments in detail but will be limited only to the items of greater interest.

Process Pressure Control

Pressure is probably the most important single variable in the process. Temperatures may drift without causing any immediate difficulty, but if the pressures should become unbalanced, the effects are almost instantly reflected to the rest of the process. This process is stabilized by controlling the pressure of three points, namely: (1) the back pressure of each cell house or cell suction, (2) the turbine suction, and (3) the turbine discharge.

The control of each of these points will be considered separately.

Cell Suction Control

Each cell house has a pressure control which regulates the pressure on the cells therein. The controllers are designated PRC-1,2,3 on Fig. 1. Normally, the cell pressure is kept slightly below atmospheric pressure and the controller can maintain this pressure even during severe load changes. If the rate of chlorine generation is increased, the control valve opens to keep the pressure on the cells from increasing and thus backing up the chlorine into the cell house. Regulation of the cell pressure prevents surging of the electrolyte through the diaphragm and thus is of material benefit in maintaining good cell performance.

Automatic control also compensates for the different lengths and sizes of pipelines used on the collection network. The gas from all the cell houses goes into a common cooling and drying system. The collection paths are of different lengths, hence there are different pressure drops between each cell house and the collection point. The difference in pressure drops along each path is absorbed by the motor valve. In the absence of a controller, it would be necessary to insert a slide or baffle in the pipeline to absorb this pressure drop.

The set point of each controller is accessible to the cell-house attendant so that he may increase the suction if he desires. This procedure is desirable for certain types of maintenance on the cells so that chlorine will not diffuse into the cell house.

The controllers have a range of 0 to 2 inches (0–5 cm) of water suction and have proportional plus reset response. Each controller is provided with an automatic-manual transfer switch so that manual operation is possible. The motor valves are lever operated butterfly valves that open with air failure. These valves should have as tight a shut-off as possible to minimize the leakage of air through cell safety seals during those rare occasions when a complete cell house is off stream.

Turbine Suction Control

This term is one that has acquired wide usage in the industry, but it is not descriptive of the results achieved. Actually, the impulse point of the turbine suction controller, PRC-4, is located at the conjunction of all the collection lines and its purpose is to control the suction at this point. The suction is set high enough to insure removal of all the chlorine from the most remote cell house and still permit the cell attendants to operate the cells at any reasonable higher suction.

A secondary purpose of the controller is to keep the suction of the cooling and drying system to a low value. Without the controller, the suction in the collection lines and the cooling and drying system would increase to a value determined by the operating characteristics of the turbines and the volume of chlorine being compressed. Increased suction on this system would increase the air leakage into the chlorine system and thus increase the volume of noncondensibles going to the liquefaction system.

There are two generally accepted methods of controlling the suction on the turbines. These are: (1) throttling the inlet of the turbines, and (2) bypassing some of the compressed gas back to the inlet. The Hooker Electrochemical Company uses the by-pass method of control because it is the more economical of the two systems. Nash turbines operate as a compromise between a centrifugal and displacement pump. Fig. 2 is a reproduction of the operating characteristics of a Type HC-7 turbine used for chlorine compression. These curves reveal that at any given speed a decrease in volume is associated with an increase in pressure and an increase in horsepower requirements. Thus if a turbine has excess capacity and the inlet is throttled, the Δp across the compressor and the horsepower will both increase. If the turbine is discharging into a system operating at constant pressure, this effect is achieved by an increased suction at the turbine inlet. If, however, the inlet is not throttled and the excess compressed gas is by-passed, the Δp across the turbine and compression horsepower remain constant. A further advantage to by-pass control is that a small motor valve can be used to by-pass a portion

of the gas, whereas a valve in the turbine inlet line would be much larger. A typical comparison of this would be a 2 inch by-pass valve as compared to a 15 inch butterfly damper in the turbine inlet line.

The by-passed gas is returned directly to the turbine suction. Somewhat better control could be achieved if the controller operated on the combined characteristics of the turbines and the pressure drop characteristics of the preceding equipment rather than on the turbine alone. This proves to be impractical, however, because the efficiency of the drying towers or coolers would be reduced by introducing the by-pass gas any further back.

When the control of the process was planned, it was decided to have the controller on the panel-board in the liquefaction building. As the plant layout developed, it was found that the distance between the controller at the panel and the impulse point and control valve was so great that the quality of control would be impaired. As a result the method shown on the flow sheet was adopted. A pressure transmitter and a blind controller are located next to the pressure impulse point. The distance between the controller and the motor valve is relatively short so that pneumatic transmission lag is not a factor of concern. A recording receiver and a remote setter for the controller are located at the control panel. With this arrangement, the operator can see the control record and also vary the set point as he wills. There are two gauges PI-1 and PI-2, showing the pressure on the motor valve. One of these is a large 12 inch gauge located on the wall of the compressor room and the other is on the panel. The operators use the first gauge as a guide when they are starting up or shutting down a turbine. The panel gauge is used by the operators to judge how much margin there is between the required capacity and the actual capacity of the turbines in operation.

The suction controller has a range of 0 to 5 inches (0–13 cm) of water suction and has proportional plus reset response. The panel has an automatic-manual transfer switch so that the position of the by-pass valve can be regulated from the operating area. The motor valve closes with air failure.

Turbine Discharge Control

The function of the turbine discharge control is to remove the noncondensibles or "sniff gas" from the system and maintain a constant pressure at the chlorine condensers. "Sniff gas" from the condensers discharges into a surge tank which also receives various slugs of air and chlorine resulting from the transfer of liquid chlorine by air pressure.

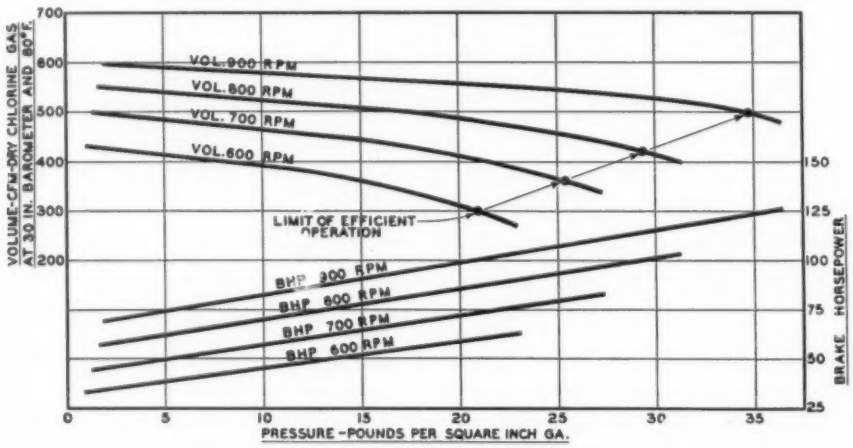

FIG. 2. Estimated performance of HC7 compressor handling chlorine gas

This gas is normally used by one of the plant processes labeled "Process 1." The chlorine requirements of Process 1 may be less than or exceed the supply of "sniff gas." If the requirements were less, the operators of Process 1 formerly proceeded to turn off the chlorine with great abandon and with practically no consideration of what the effect would be on the turbine discharge pressure. Shortly thereafter the suction pressure would rise and immediately thereafter chlorine would back up into the cell house. This difficulty has now been overcome by the scheme shown on the flow sheet. Process 2 is a unit that can take the total supply of "sniff gas" and can operate with virtually no attendance. A pressure controller, PRC-5 operates two air-to-close motor valves having split range positioners. The 8–16 lb positioner first opens its valve to let "sniff gas" go to Process 1. If the pressure of PRC-5 does not return to the control point, corrective action continues until the 0–8 lb positioner opens its valve to relieve the pressure to Process 2. PRC-6 maintains a

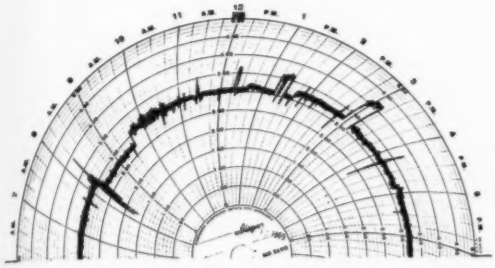

FIG. 3A TURBINE SUCTION
CHART = IN. WATER SUCTION

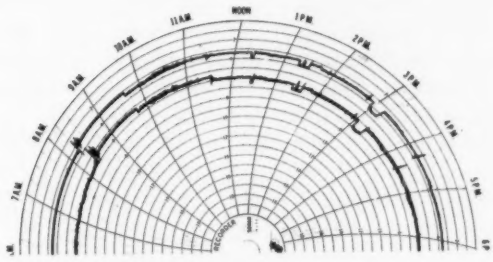

FIG. 3B TOWER INLET AND OUTLET
CHART = IN. WATER SUCTION

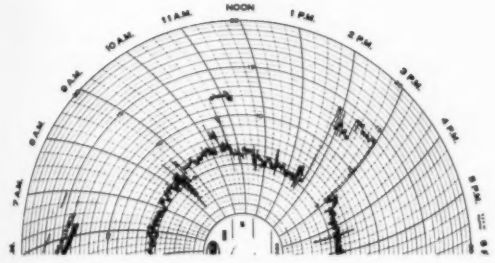

FIG. 3C CELL HOUSE
CHART X 0.1 = IN. WATER SUCTION

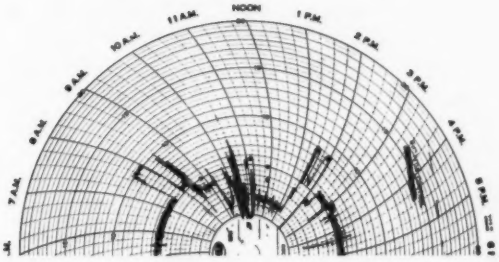

FIG. 3D CELL HOUSE
CHART X 0.1 = IN. WATER SUCTION

FIG. 3. Charts of suction controls

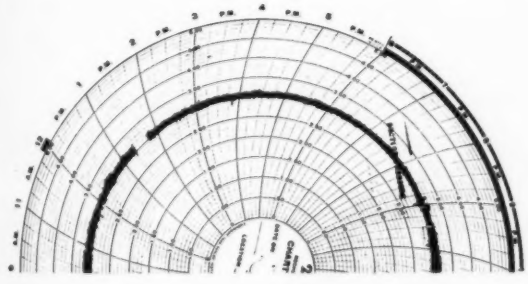

FIG. 4A TURBINE SUCTION
CHART = IN. WATER SUCTION

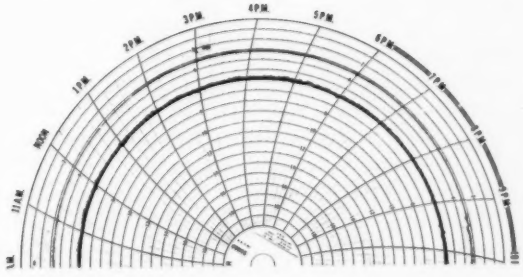

FIG. 4B TOWER INLET AND OUTLET
CHART = IN. WATER SUCTION

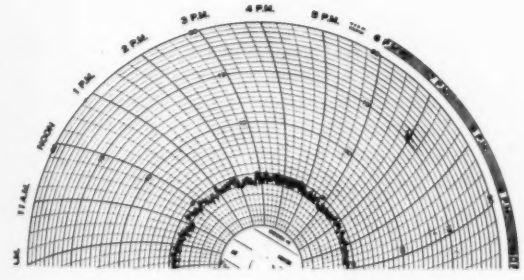

FIG. 4C CELL HOUSE
CHART X 0.1 = IN. WATER SUCTION

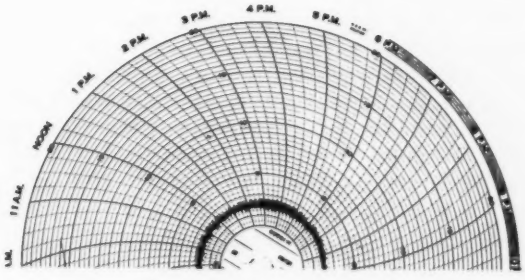

FIG. 4D CELL HOUSE
CHART X 0.1 = IN. WATER SUCTION

FIG. 4. Charts of suction controls

minimum pressure on the line going to Process 1. If the chlorine requirements of Process 1 exceed the "sniff gas" supply, pressure controller PRC-6 opens its motor valve to admit turbine gas to supplement the "sniff gas." By these combined controls, Process 1 always has a minimum supply pressure and the discharge of the turbines is never blocked off. PRC-5 has proportional plus reset response and PRC-6 has proportional response only.

Fig. 3 is a reproduction of some pressure charts of the chlorine handling process. The portions of the charts shown were selected to show how the system behaves under severe operating conditions. The remainder of the charts had smooth continuous lines similar to those of Fig. 4. The charts were put on the instruments at about 10:15 A.M. on the 11th of August 1949 and were removed at about 11:00 A.M. the following day, so there is roughly 45 minutes overlap.

The record shows (Fig. 3B) that there was an increase in load at 11:25 A.M. and that another turbine was turned on to take care of the increase. The increase in load is shown by the change in pressure drop across the acid towers.

Also the record of Fig. 3A shows that at 12:20 P.M., 1:20 P.M., and 2:55 P.M. the operator in the liquefaction building increased the suction on the turbines for short periods. These increases were made in response to a request of the cell attendant of a remote circuit to give him "more pull" to assist in clearing his cells for maintenance. The records of different cell houses (Fig. 3C and 3D) show that at these times there were transient pressure surges of one or two tenths of an inch (0.5 cm) of water for a short time. The change in suction of Fig. 3D at 1:20 P.M. is coincidental and was done by the cell attendant of these cells for his own maintenance purposes. Inspection of Fig. 3C shows that between 1:45 P.M. and 2:58 P.M. the attendant of these cells increased the suction on his cells with only a slightly increased pull at the turbines. This same feature is shown in Fig. 3D at 1:45 P.M. and 7:30 A.M. The pips on the record of Fig. 3A at 1:52 P.M., 2:45 P.M., and 4:13 P.M. are usually associated with changing the number of turbines on the line. The difference in length of the pips can be attributed to the way the various operators manipulate the turbine valves during a change. The "hash" on Fig. 3 at 8:15 A.M. occurred when a string of cells dropped their load. The hash is usually caused by sucking air through the cell seals and subsequent air binding in the condensers. Even so, the cells of Fig. 3C and 3D stayed within good operating limits. The hash on Fig. 3D between 9:15 A.M. and 11:15 A.M. was due to causes that cannot be determined from the plant record. At any rate, the cells were operating at reduced loads and between 10:30 A.M. and 11:15 A.M. were almost down entirely. At no time during the disturbance was the suction outside the limits of the cell seals. It is interesting to contrast the records of Fig. 3C and 3D with that of Fig. 5. This latter record is from a string of cells that were under manual control on a different day. Note that the suction varies from the hub at the center to the outer edge of the chart. It is also interesting to note from Fig. 3C and 4C that the reset rate of this controller is improperly adjusted. This is apparent from the sawteeth which are caused by slow return of the pressure to the set point after a load change.

Fig. 4 shows the same series of records as Fig. 3 except that they were taken on a day of almost uninterrupted operation. Only half the charts are shown, but the other halves are smooth continuations of the same arcs.

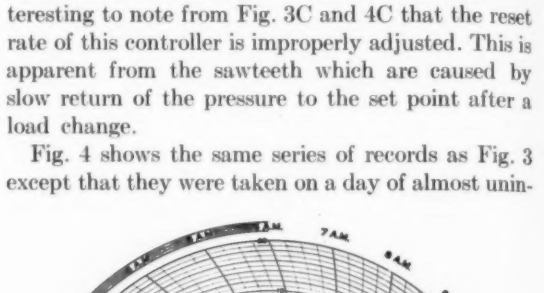

FIG. 5. Cell house suction—manual control

CHLORINE COOLING SYSTEM

The distribution of the water to the coolers is done by manual control. The adjustment of the cooling water valves is not critical because the coolers have sufficient capacity to cool the chlorine to within one or two degrees C of the cooling water temperature. After once adjusting the valves they can usually be left alone for several hours without further adjustment.

The only controls on the chlorine cooling system are those associated with the refrigerated water supply. Brine for cooling the water is obtained from a refrigeration system that is used jointly by this process and one other. The brine is not used on the

chlorine coolers directly because there is a possibility of contamination by chlorine with resultant damage to the refrigeration system by the recirculated brine.

The refrigerated water is sent to the secondary coolers at a temperature just above the freezing point of chlorine hydrate. The water leaving the secondary coolers is recirculated by a pump, the effluent of which is split by a three-way valve so that a portion of the water goes through the brine-water heat exchanger and the remainder by-passes it. A temperature controller, TIC-2, has its impulse point just beyond the point where the split streams are recombined. This controller varies the ratio of the split to maintain a constant temperature at the impulse point.

A recirculation system is also used on the brine side of the brine-water heat exchanger. Enough cold brine is added to the recirculated brine to keep the temperature of the combined stream at 1°C. The temperature controller, TIC-1, has its impulse point just after the recirculating pump discharge and the brine make-up is added directly at the inlet. The purpose of TIC-1 is to prevent too cold a brine from freezing the recirculated water in the heat exchanger.

The loss of water by the evaporation of refrigerated water is compensated for by LC-1, a two-probe, conductor-type level control that operates a solenoid on the plant water line.

During the winter months the refrigerated water is not needed. The plant water itself is too cold for the secondary coolers so the effluent water from the secondary coolers is recirculated and plant water is blended with the recirculated stream to provide the proper temperature.

This blending is currently done manually by adding water directly to the cooling water receiver below the secondary coolers. The blending can be accomplished by TIC-2, however, in the manner shown by the flow sheet. It is planned to make this change to the system in the near future.

With this control system and the cooling capacity of the coolers, it is possible to bring the chlorine gas to within a degree or two of the temperature of chlorine hydrate formation. With this system the maximum quantity of water possible is removed from the gas prior to the acid towers. Before the installation of this cooling system, the coolers would frequently start to freeze out chlorine hydrate with consequent upsets in the cell house pressures. Now, however, this difficulty never arises. Alarms are provided for each recirculating pump to give the operators instant notice if either pump should cease running.

The controllers, TIC-1 and TIC-2, have proportional response only. They operate at extremely high sensitivity and have about 0.4°C throttling range. This is achieved by virtue of direct immersion bulbs having fast response and the fact that the bulb location and control method employed result in very short transportation lags. The motor valves are provided with bellows-sealed stems so that there will be no leakage of water or brine into the pipe insulation.

Acid Towers

The chlorine is dried by used acid from the turbines. The acid is pumped to a head tank to give a constant head for feeding the acid towers. The rate at which acid should be added to the towers is determined by observation of hydrometers, DI-1 and DI-2, located in the tower effluent acid lines. The acid feed rate is adjusted by manual regulation and observation of rotameter, FI-1. There is an alarm to warn the operators if the acid feed pump should cease running.

The acid rate is so low that batchwise addition of the acid would be equally effective if the increments were made small enough. The acid going to the towers is such that a small trickle is the result, and the effect of a rising gas contacting a falling liquid is essentially zero. The principal drying effect is surface absorption as the gas is constrained to travel close to the surface of successive trays of acid. Batchwise addition was the method adopted for feeding the effluent acid of the second tower to the top of the first tower. The acid draining from the second tower is caught in a small receiver at the bottom. The acid level rises in this receiver until the pump casing is flooded and an electrical contact is made by the rising liquid. This contact turns on the pump and the level in the receiver is lowered until a second contact opens, thus stopping the pump. The acid remaining in the pump discharge lines drains back into the receiver. The advantages of this system are:

1. The packing glands of the pump are under suction most of the time since the duty cycle is down to about 0.5 per cent or less.
2. Acid leakage is kept low.
3. The pump does not operate at maximum head when running as would be the case if the discharge were throttled, and the pump were operated continuously.
4. With continuous flow, the acid stream is so small that the pump would overheat with a consequent increase in corrosion rate.

Turbine Acid System

The total turbine effluent, consisting of compressed chlorine gas and sealing acid, is discharged into separating tanks which also serve as acid accumulators. Acid from the accumulators returns to the

turbine suction through the acid coolers and a fixed orifice at the turbine inlet.

The acid rate through the turbines is not critical, although there are several factors involved. The chlorine handling capacity of Nash turbines rises through a maximum and then falls off as the sealing medium is increased above a certain minimum rate. The horsepower requirements increase as the acid seal rate increases; thus there is an optimum acid rate to get maximum capacity per horsepower. This optimum condition is counterbalanced by consideration of the fact that at higher acid rates the turbines will operate cooler. The fixed orifice is sized to circulate enough acid to keep a satisfactory outlet temperature.

Water to the acid cooler is manually regulated. There is a motor valve in the water line that is actuated by a differential pressure controller. This motor valve is normally wide open, but if the condition arises that the water pressure approaches the acid pressure, the valve begins to throttle the water to maintain its pressure a fixed differential below the acid pressure. This is to prevent any leakage of the water into the acid system and consequent damage to the turbines. An "in-line" type conductivity cell is immersed in the water leaving the acid cooler. This conductivity cell is connected to a conductivity meter and alarm, CIA, located at the panel and warns the operators when and if a leak develops in the acid cooler.

Tank Gauges for Liquid Chlorine

Three years ago this plant started using displacement-float-type liquid-level transmitters. The floats are different from standard displacement floats in that they have two cross-sectional areas, the larger area being twice the smaller. The change in section occurs at the level which corresponds to a "full" chlorine tank, with the larger section being in the vapor space. If the level should rise further, the apparent level rises much faster than the actual level. This is a precaution that is used in case the transmitter or receiver should shift calibration. The oversize section gives a bump to the indicated level that will assist the operators in knowing if the instruments are off calibration.

Instrument Specifications and Installation

Pressure Gauges

Each pressure element for measuring chlorine pressure is protected by a diaphragm seal, a gas purge, or both, depending on the conditions of installation. Bourdon pressure elements are protected by commercial diaphragm protectors having cast iron bodies and silver diaphragms. A light oil is used for the sealing fluid.

Diaphragm protectors are satisfactory if three conditions are met:

1. The volumetric change of the pressure element is quite small through the entire range of its operation.
2. The spring rate of the diaphragm is small compared to the spring rate of the pressure element.
3. The diaphragm does not pass through a point of inflection of its spring rate, thus producing an "oil-can" effect.

These conditions can be satisfied with commercial protectors and bourdon gauges if care is exercised in their assembly and calibration. The protected gauges in use at the Niagara Falls Plant are prepared and calibrated by the instrument maintenance group.

Protected bourdon gauges are used to measure chlorine pressure after the turbine discharge. Pressure taps are always made on the top of a chlorine line. If the gauge is to be installed near the pressure tap a direct connection with $\frac{1}{4}$ inch standard

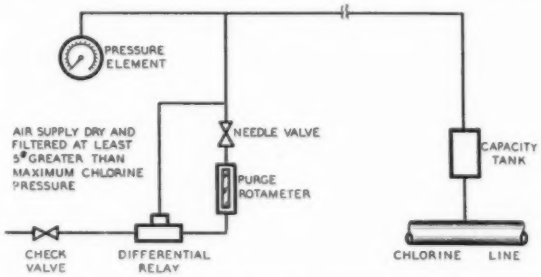

FIG. 6. Purge system for pressure elements

pipe is used. If a remote installation of the gauge is required, the connecting line is purged.

Low pressure elements cannot be sealed by diaphragm protectors without altering their characteristics materially. Low pressure elements are installed on the suction side of the turbines and are protected by a gas purge.

Fig. 6 shows a method of installing the purge assembly. A differential relay provides a constant differential pressure across a needle valve used to regulate the purge rate. A small rotameter or bubbler indicates the rate of purge which is between 0.2 and 2 ft^3/hour (5.7 and 57 l/hour) of air. A needle valve passing this quantity of air from a 20 psi air supply has small clearances between the seat and the plug; consequently very minute particles in the air stream will plug the valve. The differential relay minimizes this difficulty because it keeps about $1\frac{1}{2}$ lb pressure across the needle valve, thus permitting the valve to be much wider open for the same purge rate.

There are two methods of purging an impulse line. In one method, the gas purge enters the impulse line very close to the pressure tap. The other method,

and the one preferred here, is to purge the entire length of the impulse line between the pressure element and the pressure tap. This means that the impulse line must be large enough to pass the purge rate with a negligible pressure drop, or if a smaller line is used, the pressure drop must be constant. This latter condition is realized by a combination of differential relay and needle valve which together constitute a flow controller. From a practical standpoint, all impulse lines used on this installation are either $\frac{1}{4}$ inch tubing or are $\frac{1}{4}$ inch standard pipe.

The capacity tank shown in the diagram is a one foot length of 2 inch pipe with $\frac{1}{4}$ inch taps at both ends. The tank provides a padding of air so that if the pressure surges suddenly, chlorine will not be forced back into the pressure element or impulse line.

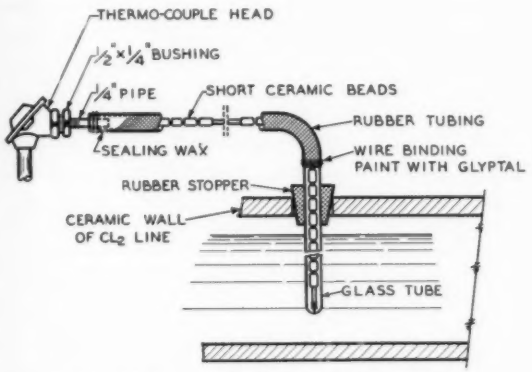

FIG. 7. Thermocouple and well line for wet Cl_2

Thermocouples for Wet Chlorine

The thermocouples were installed in glass thermowells. Details of the construction are shown in Fig. 7. Short ceramic insulators are used on the thermocouple wires so that there will be sufficient flexibility to move the assembled couple. The protecting well is a length of glass tubing closed at one end and inserted in a rubber stopper. A piece of laboratory rubber tubing covers the ceramic insulators and is wired to the glass tubing and the thermocouple head. The assembly is sealed with sealing compound so that if the glass well breaks, chlorine will not pass through the conduit and into the potentiometer.

Motor Valves for Chlorine

Selection of motor valves is a very controversial subject in a chlorine plant. If the chlorine is absolutely dry and the lines are dry, valves with cast iron bodies and stainless trim, except for stems, are acceptable. Stainless steel stems are not permissible on sliding stem valves but are acceptable on rotary stem valves. The stems of sliding stem valves should be made of Hastelloy "C." It seems that chlorine fills the surface pores of a sliding stem valve and as the valve moves up and down the chlorine is pumped to the outside. Moisture working on the pores filled with chlorine gas leads to the inevitable result—a corroded stem.

The catch to the preceding discussion is the term "dry line." The standard remedy for cleaning out a chlorine line is to steam it out and then dry it. Some of the crevices in the valves do not dry out, and when the line is used again, valve trouble nearly always develops. The most satisfactory solution, therefore, is to use Hastelloy "C" trim throughout. Valves in lines that are subjected to frequent steaming should have stainless steel bodies to resist the corrosive action of ferric chloride which forms when the line is returned to use.

A deep stuffing box should be used on all chlorine valves in order to retain the chlorine. With insufficient packing depth, the pumping of chlorine by a sliding stem will soon cause corrosion of the stem. The material with which the packing is impregnated has a great deal to do with the valve operation. Most impregnants will chlorinate and in the chlorinated state become hard or gummy and seize the valve stem. The Hooker Electrochemical Company has experimented with the use of fluorocarbon greases for impregnating the packing. Results of these experiments have been quite promising.

Bellows-sealed packing glands have been tried, but they are not a panacea for chlorine valves. This type of seal has been found suitable for liquid chlorine service but the results on gaseous chlorine have been disappointing. The principal cause of failure has been improper drying of the seals after steaming out the line in which they were installed. Each droplet of condensate has been a nucleus for corrosion. Another cause of failure has been rupture of the bellows caused by a collection of solids in the convolutions and subsequent compression of the bellows by movement of the valve stem.

Molded Teflon and shredded Teflon packing have been tried without success. These packings were not suitable because of Teflon's tendency to cold flow and its lack of resiliency. A Teflon packing having a special shape and operating on a superfinished valve stem has been tried on the turbine by-pass valve with excellent results. There is enough acid mist going through this valve to keep the valve clean, thus preventing injury to the Teflon seal. The Hooker Electrochemical Company does not have data on using this particular seal in other locations.

The packing on a rotary stem valve lasts much longer without maintenance than the sliding stem counterpart. This is because there is no drag-out of

the chlorine through the packing as the valve operates.

One of the difficulties with chlorine valves is caused by seizure of the moving parts, resulting in valve hysteresis. The principal sources of this trouble lie in the bottom guides, the skirt guides, or in too close tolerances in the upper guide. At the Hooker Plant the valves are selected to have a long upper guide. Contour plugs are used and the bottom guides are removed. Sometimes it is necessary to remove a a bit of the upper guide to give more clearance between the guide and the plug. In those applications that permit the use of a quick opening valve, satisfactory operation can be obtained with a wing guided plug. It is strongly recommended that all chlorine valves be equipped with a valve positioner. These instruments will minimize the difficulties that arise from internal friction. A valve with a positioner will operate long after a valve without a positioner has ceased to function.

The choice between a rotary stem valve and a sliding stem valve is purely arbitrary, and both types are used at the Hooker Plant. A rotary stem motor valve has not been available on the market, hence it has been necessary to assemble the valves from a lever motor, a rotary stem valve, and a home-fabricated bracket. Care must be exercised in the assembly of the units to make sure that backlash is kept down to a minimum. These valves operate much longer without maintenance than the sliding stem valves, but they are more difficult to service when the need arises. They are bulky and awkward to install and are generally not appreciated by the instrument repair men. A rotary stem valve must be wing guided since it will not function with a contour plug having a single top guide. Its use, therefore, is limited to those control problems which will permit a quick opening valve.

Summary

At the Niagara Falls Plant of the Hooker Electrochemical Company, the chlorine handling process has been modernized, using an engineering layout and control aids to minimize personal supervision by the operators. Instruments have been provided for process pressure control, chlorine cooling control, acid addition, sealing acid recirculation, determination of hydrogen in chlorine, and liquid chlorine tank gauging. More instrumentation in the cooling and drying building could have reduced further the attention required of the operators, but the added features did not seem to be justified. Furthermore, it was deemed advisable to leave a few details that required an operator's attention so that he would have to make occasional trips to the building. These trips afford an opportunity to check on chlorine leaks and turbine operation. This plant provides a good example of the modern steps that are being taken to ease the burden of the operator and increase the dignity of his job. The paper also gives some guides for the selection and installation of instruments for a chlorine handling plant.

Any discussion of this paper will appear in a Discussion Section, to be published in the June 1951 issue of the JOURNAL.

REFERENCE

1. DAVID HOSTEDLER, "Instrumentation Flow Panel Symbols." A report of the Recommended Practices Committee of the Instrument Society of America. Presented at the Technical Sessions of the I.S.A. National Convention in St. Louis, Missouri, September, 1949.

The Fluorescence of Magnesium Germanate Activated by Manganese[1]

F. A. Kroeger and J. van den Boomgaard

Philips Research Laboratories, N. V. Philips Gloeilampenfabrieken, Eindhoven, Holland

ABSTRACT

Magnesium germanate activated by manganese may contain the activator in different valencies. When this valency is higher than two, fluorescence excited by ultraviolet occurs in seven narrow bands decaying with the same time constant. The variation of this decay constant and the intensity of fluorescence with temperature is explained by the assumption that the relative contribution of radiative and nonradiative transitions is determined by a Boltzmann equilibrium regulating the population of various excited states.

Introduction

The red fluorescence of magnesium germanate activated by manganese, first mentioned by Leverenz (1), has been further investigated by Williams and Patten (2, 3). In these investigations it was found that the spectral distribution of the fluorescence excited by ultraviolet showed six narrow bands in the red part of the spectrum. In a great majority of cases the fluorescence of solids activated by manganese is due to manganese in the divalent state. Williams and Patten have likewise attributed the red fluorescence of magnesium germanate to manganese in divalent form. The structure of the fluorescence spectrum of this system, however, is unusual for divalent manganese. The bands due to Mn^{2+} are normally broad, and show a fine structure only at low temperatures (4, 5). On the other hand, bands of a width comparable with that reported by Patten and Williams have been observed with systems containing tetravalent manganese (6, 7). Therefore, it seemed worthwhile to us to investigate whether manganese of a valency higher than two is active in this case also.[2]

We have, furthermore, studied the quenching of fluorescence with temperature and its influence on the decay, and have explained the results on the basis of a term scheme derived from the spectral data.

Experimental

Magnesium germanate, pure as well as activated with manganese, was prepared by firing mixtures of GeO_2, MgO, and $MnCO_3$ which contained these components in proportions corresponding to $4MgO \cdot GeO_2$:0.01Mn and $2MgO \cdot GeO_2$:0.01 Mn, respectively. The firing was carried out at 1100°C either in an oxidizing atmosphere (air or oxygen), or in a neutral atmosphere (N_2), or in a reducing atmosphere (H_2). The latter products decomposed and will not be discussed further.

Samples of composition $4MgO \cdot GeO_2$:0.01 Mn prepared under oxidizing conditions are slightly pink and show a strong red fluorescence upon excitation by wavelength of either 3650 or 2537 Å. The samples fired in N_2 are white and nonluminescent. Samples of composition $2MgO \cdot GeO_2$:0.01Mn are white and nonluminescent independent of the atmosphere of preparation. The properties of $4MgO \cdot GeO_2$:0.01Mn can be reversibly changed by refiring in a different atmosphere. Thus a sample, first heated in N_2, turns pink and develops the red fluorescence with excitation by ultraviolet upon refiring for three hours at 1100°C in air. On the other hand, samples first prepared in air and then refired in N_2 are bleached and their red fluorescence is diminished.

We have determined the spectral distribution of the red fluorescence photographically with the aid of a prism-spectrograph. The spectrum consists of seven narrow sub-bands at 6180 Å (*a*), 6270 Å (*b*), 6360 Å (*c*), 6450 Å (*d*), 6550 Å (*e*), 6640 Å (*f*), and 6710 Å (*g*). [The last six bands were also observed by Patten and Williams (3); the first band, which is extremely weak, escaped their notice.] The relative intensities in the various sub-bands were determined roughly by measuring the peak heights without trying to separate the bands. The results for temperatures varying from 83° to 568°K are given in Table I. Data taken from Fig. 4 of the paper by Patten and Williams are also included.

It is seen that the intensity of *b* and *c* relative to that of *e* and *f* increases with temperature, but that the ratios *b*:*c* and *e*:*f* are practically constant. Although the intensities in *a* and *d* were not measured, we have the impression that *a* behaves similarly to *b*

[1] Manuscript received February 3, 1950. This paper prepared for delivery before the Cleveland Meeting, April 19 to 22, 1950.

[2] The abstract of a recent paper by Thorington, *J. Optical Soc. Am.*, **40**, 260 (1950) has just come to our attention. We understand that the author has also demonstrated the presence of high valency manganese in a magnesium fluogermanate phosphor.

and c, and d similarly to e and f. This behavior indicates that the fluorescence is due to electronic transitions from two excited states with a separation of $\gamma_b - \gamma_c = 680$ cm^{-1}, to three or four lower states with a separation of $\gamma_b - \gamma_c = \gamma_e - \gamma_f \simeq 230$ cm^{-1}. The term scheme[3] together with the electronic transitions is given in Fig. 1*b*, and a schematic drawing of the fluorescence spectrum corresponding to it is shown in Fig. 1*c*. It appears likely that the four ground levels are vibration levels; the two excited levels may either be different electronic excited states of Mn^{4+} or also vibration levels.

TABLE I. *Relative intensities of the sub-bands of $4MgO \cdot 1GeO_2$:0.01Mn for excitation by $\lambda = 2537$Å at various temperatures*

Temp	6170 Å (*a*)	6270 Å (*b*)	6360 Å (*c*)	6450 Å (*d*)	6550 Å (*e*)	6640 Å (*f*)	6710 Å (*g*)	$= \frac{I_c}{I_f} e^{680/kT}$
°K								
83	0	0	0	~6	50	100	~15	—
83*	0	0	0		27	100		—
195*	0	0	5		44	100		8.7
293*	0	14.5	33		77	100		9
296	~2	24.5	36		66	100		9.5
363*		13.4	27		65	100		3.9
438		40	53		71	100		4.8
568		50	63		71	100		3.5

* Data taken from Fig. 4 of ref. (3).

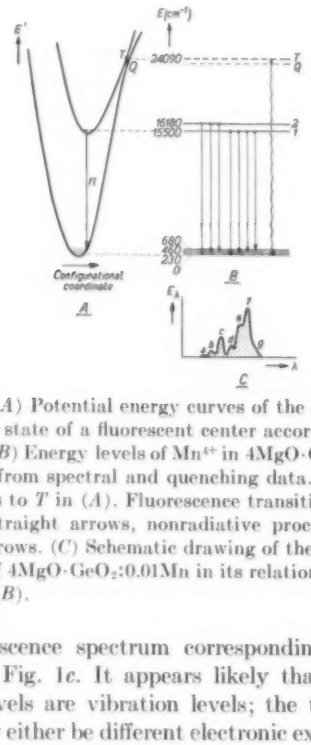

FIG. 1. (*A*) Potential energy curves of the excited state and ground state of a fluorescent center according to Mott and Seitz. (*B*) Energy levels of Mn^{4+} in $4MgO \cdot GeO_2$:0.01Mn as derived from spectral and quenching data. The level T corresponds to T in (*A*). Fluorescence transitions are indicated by straight arrows, nonradiative processes by undulating arrows. (*C*) Schematic drawing of the fluorescence spectrum of $4MgO \cdot GeO_2$:0.01Mn in its relation to the term scheme of (*B*).

Quantitatively, the agreement between the relative intensities of the two multiplets as determined experimentally and as calculated with Boltzmann statistics is not as good as might be expected. The proportion between the two multiplets must be

$$\frac{I_2}{I_1} \sim \frac{I_c}{I_f} = \frac{\gamma_2 g_2 e^{-\epsilon/kT}}{\gamma_1 g_1}$$

in which γ_2 and γ_1 are the transition probabilities, g_2 and g_1 the statistical weights of the two excited levels, while ϵ is the separation between these levels, namely, 680 cm^{-1}. Therefore, the term $\frac{I_c}{I_f} e^{680/kT}$ should be constant which, however, is not found to be the case (Table I, last column). The discrepancy is not eliminated by choosing a different value for ϵ. Although the term scheme of Fig. 1 is, therefore, not quite established, we have nevertheless used it for the considerations described below.

The reflection of the various samples is shown in Fig. 2. Samples without manganese have a very low absorption down to 2500 Å. The samples containing manganese have an absorption band starting in the visible and increasing toward shorter wavelengths. The absorption is relatively strong for the samples prepared under oxidizing conditions, and weak for those made in N_2. It is this absorption in the visible which is responsible for the pink color of the oxidized samples. Refiring in N_2 of a sample originally prepared in air causes the absorption to decrease. However, it does not reach the low level found with samples made directly in this atmosphere.

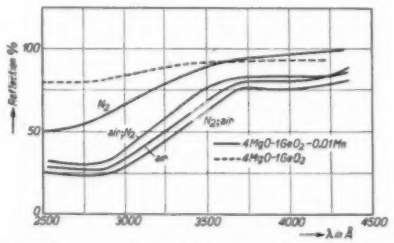

FIG. 2. Reflection of $4MgO \cdot GeO_2$ with and without manganese, prepared in nitrogen or air, or in both of these atmospheres (first air and then nitrogen, or the reverse).

In order to see whether manganese of a valency higher than two is present, a chemical method was used as described previously (7). The sample was dissolved in an aqueous solution of HCl; a current of oxygen-free N_2 was passed through the solution into a second vessel containing an aqueous solution of KI, H_2SO_4, and fresh starch. If manganese in a higher oxidation state is present, HCl is oxidized to Cl_2; the chlorine is carried over to the KI solution by the N_2 current and liberates I_2, which can be titrated with thiosulfate in normal manner. It was found that samples prepared in air have a considerable oxidizing power which is absent with the samples made in N_2.

[3] The significance of the high level T will be discussed later in this paper.

The results are given in Table II, together with values of the reflection for ultraviolet, and the relative intensities of the red fluorescence for excitation by $\lambda = 3650$ Å or 2537 Å. There appears to be a clear correlation between the oxidizing power and the optical properties: strong fluorescence and strong ultraviolet absorption correspond to a strong oxidizing power, and vice versa. Accordingly, the fluorescence as well as the absorption must be attributed to manganese of a valency higher than two.

The values found for the average valency of the manganese can be explained by the presence of manganese of valency three or four, or even higher. As the spectrum observed is similar to that of Mg_2TiO_4:Mn which is activated by tetravalent manganese (6, 7), we are inclined to believe that we are also dealing with Mn^{4+} in this case. The average valencies found then indicate that the products prepared in N_2 contain practically only Mn^{2+} ions, but

TABLE II. *Intensity of fluorescence, reflection, and oxidizing power of $4MgO \cdot 1GeO_2$:0.01Mn, prepared in various atmospheres*

Conditions of firing	Oxidizing power in equivalents per Mn	Average valency of Mn	Intensity of fluorescence		Reflection for	
			exc. 3650	exc. 2537	$\lambda = 3650$	$\lambda = 2537$
1 hr 1100°C, air	0.71	2.71	77	87	0.79	0.28
1 hr 1100°C, N_2	0.05	2.05	7.7	14.7	0.94	0.50
1 hr 1100°C N_2; 3 hr. 1100°C air	0.90	2.90	100	100	0.75	0.25
1 hr 1100°C air; 15 hr. 1100°C N_2	0.27	2.27	48	57	0.83	0.32

that the oxidized samples contain Mn^{4+} as well as Mn^{2+}.

As the base lattice has no absorption in the ultraviolet, irradiation with ultraviolet causes fluorescence only in centers which absorb this radiation, i.e., in the Mn^{4+}. Excitation with ultraviolet of shorter wavelengths, or with x-rays or cathode rays, however, which leads to excited states in the base lattice, must cause fluorescence in Mn^{2+} as well as in Mn^{4+}. This is actually found to be the case. Upon excitation by cathode rays (6 kv), both the reduced and the oxidized samples show a red fluorescence; in fact, the product of true ortho composition in which the manganese cannot be oxidized shows the strongest fluorescence. We have measured the spectral distribution of the fluorescence by means of a double-monochromator in connection with a photomultiplier. The fluorescence is different for the various products. Samples of $4MgO \cdot 1GeO_2$:0.01Mn prepared in nitrogen and containing manganese only in the divalent state show a fluorescence in two rather broad, overlapping bands with maxima at 6550 Å and 7400 Å, i.e., close to those observed with $Mg_2SiO_4:Mn^{2+}$ (8) (Fig. 3*c*). The spectrum of the oxidized samples (Fig. 3*b*) is a superposition of the Mn^{2+} bands and the narrow peaks of Mn^{4+}. Owing to the large width of the slit used, the separate sub-bands of the Mn^{4+} are not resolved, but a comparison of the spectrum with that of the red fluorescence excited by $\lambda = 2537$ Å measured with the same apparatus (Fig. 3*a*) clearly shows that the same emission is present in both cases. An approximate separation of the bands of Fig. 3*b* into Mn^{2+} and Mn^{4+} bands is indicated in the diagram. The contributions of Mn^{2+} and Mn^{4+} are of the same order, indicating that the concentration of manganese in these two valencies is also approximately equal. This, together with the average valency 2.7–2.9 observed, gives further support to the view that it is the tetravalent manganese which is responsible for the red fluorescence in the oxidized

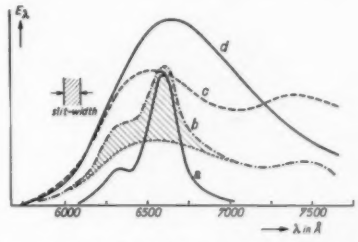

FIG. 3. Spectral distribution of fluorescence. (*a*) The red fluorescence of $4MgO \cdot GeO_2$:0.01Mn (1100°C, air) excited by λ 2537 Å at room temperature. (*b*) Cathodofluorescence of $4MgO \cdot GeO_2$:0.01Mn (1100°C, air). (*c*) Cathodofluorescence of a product of the same composition, but fired in nitrogen instead of air. (*d*) Cathodofluorescence of $2MgO \cdot GeO_2$:0.01 Mn (1100°C, air). For curve *b* a separation into bands of shape *a* and *c* has been indicated.

products. The sample of the stoichiometric ortho-composition ($2MgO \cdot 1GeO_2:Mn^{2+}$) shows fluorescence in one broad band with a maximum at 6600 Å, i.e., at a longer wavelength than the main band of $4MgO \cdot 1GeO_2:Mn^{2+}$. As the x-ray diffraction patterns of these products are very similar,[4] the reason for this difference is still uncertain.

The decay of the cathodofluorescence of the reduced samples is exponential with a time constant of 110 sec^{-1} as is normal for divalent manganese; it is identical for $2MgO \cdot GeO_2:Mn^{2+}$ and $4MgO \cdot 1GeO_2:Mn^{2+}$. The decay of the red fluorescence of Mn^{4+}, excited by λ 2537 Å is also exponential but has a larger time constant $\tau^{-1} = 330$ sec^{-1} (at room temperature). The decay of the cathodofluorescence of the oxidized $4MgO \cdot 1GeO_2:Mn$ samples is not purely exponential: the t vs. log I_{fl} plot is slightly

[4] According to Goldschmidt (13), magnesium germanate should have either the olivine structure (Mg_2SiO_4) or the spinel structure ($MgAl_2O_4$, Mg_2TiO_4). The patterns found by us indicate neither of these two structures.

concave and has an average slope of ~265 sec^{-1} over the first 10^{-2} sec. This corresponds roughly to what should be expected for a superposition of two emissions with time constants 110 and 330 sec^{-1}.

The decay of $4MgO \cdot 1GeO_2:Mn^{4+}$ for excitation by λ 2537 Å was measured as a function of temperature by means of a method described elsewhere (10). With this method the exciting radiation is chopped by means of a rotating disk and the fluorescence is registered by means of a photomultiplier the output of which is fed to the horizontal plates of a cathode ray oscilloscope. The latter is provided with a variable exponential time base, which is triggered by the rotating disk. Although the decay proved to be exponential over the entire temperature range investigated (83°–800°K), the decay "constant" showed a considerable variation with temperature. Between 83° and 180°K it is practically constant; from 180° to 600°K it increases approximately linearly with temperature; above 600°K it increases much more rapidly (Fig. 4). The intensity of the fluorescence is approximately constant from low temperatures up to 600°K, and it decreases strongly between 600° and 800°K, i.e., exactly in the range in which the decay increases rapidly (Fig. 4). This indicates that these phenomena must be related, both being due to nonradiative transitions from the excited state(s) of Mn^{4+} (9). In order to measure the decay of the various sub-bands of the fluorescence separately, two methods were followed. The first one was the method described above but modified by letting the fluorescent light fall on the multiplier via a monochromator. In this way the doublets b,c and e,f could be measured separately. The decay proved to be exactly the same for each (Fig. 4). In the second method we used a photographic method as described by Rinck (11) and also by Studer and Rosenbaum (12) In this method the fluorescence spectrum is photographed at various times after the excitation is interrupted, using a spectrograph placed behind a disk which contains a slit. The disk rotates with the same speed as the disk used for chopping the exciting radiation. In this way the decay of b,c,e, and f was determined separately as in the case of the first method, and was found to be identical for the various bands within the accuracy of the experiment (± 10%). The results are given in Table III.

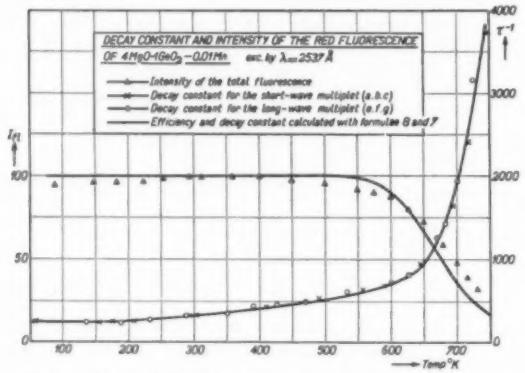

FIG. 4. Variation with temperature, of the efficiency and the decay constant of the red fluorescence of Mn^{4+} in $4MgO \cdot GeO_2$:0.01Mn. Excitation by λ 2537 or λ 3650 Å.

The observed identities of decay and quenching seem to indicate that the various sub-bands correspond to electronic transitions from one excited state to different lower levels, contrary to what was concluded from the variation with temperature of the proportion between the sub-bands. It is possible, however, to account for the effects observed on the basis of the model given above (Fig. 1). If a fluorescent spectrum consists of sub-bands which are due to electronic transitions from various excited levels to one or more ground levels, then it will have a single, purely exponential decay for all the components provided there is Boltzmann equilibrium between the populations of the various excited levels in the stationary state as well as during the decay. This is the case when the processes by which the Boltzmann equilibrium is established are much faster than the fluorescence transitions.

TABLE III. *Intensity of fluorescence in the sub-bands b, c, e, and f at various times after the interception of the exciting radiation, and the decay constants deduced therefrom*

t	b	c	e	f
$0 \cdot 10^{-4}$ sec	100	100	100	100
22	45	58	50	55
44	19	23	23	27
66		9	9	14
t^{-1}(sec^{-1})	368	340	340	310

For a system with i excited states with statistical weights g_i and energies ϵ_i (calculated from the lowest excited state), the population n_i of the level i is related to that of the first level n_1 by the Boltzmann equation:

$$n_i = n_1 \frac{g_i}{g_1} e^{-\epsilon_i/kT}. \qquad \text{(I)}$$

Differentiating logarithmically with respect to time, t:

$$\frac{d \ln n_i}{dt} = \frac{d \ln n_1}{dt}. \qquad \text{(II)}$$

As this is exactly the mathematical expression for the decay constant τ^{-1}, the decay constant is the same for the various transitions starting from the different excited levels. The value of the decay constant is

found by writing down the total number of quanta emitted by the system. This number depends on the transition probabilities of the fluorescence from the various levels, γ_i

$$-\frac{d\sum_i n_i}{dt} = \sum_i \gamma_i n_i. \qquad \text{(III)}$$

With the aid of (I) and (II)

$$-\frac{d \ln n_1}{dt} = \tau^{-1} = \frac{\sum_i g_i \gamma_i e^{-\epsilon_i/kT}}{\sum_i g_i e^{-\epsilon_i/kT}}. \qquad \text{(IV)}$$

Thus it is seen that the decay is always exponential, but that the time constant is a function of temperature. At low temperatures the time constant is determined only by the probability of the transition from the lowest excited state γ_1; at higher temperatures the other transitions also play a part. If the transition probabilities γ_i for the higher levels are greater than γ_1, this leads to an increase of the time constant with temperature as observed in the system we are discussing in this paper and also in several other cases (9, 10). Formula (IV) holds for the case of transitions from several excited states to one ground level as well as to several lower levels. In the latter case the transition probabilities γ_i appearing in the formula are the sum of the transition probabilities for the various transitions starting from the same level.

For the case of $4MgO \cdot 1GeO_2:Mn^{4+}$ we have

$$\left.\begin{aligned}\gamma_2 &= \gamma_a + \gamma_b + \gamma_c \\ \gamma_1 &= \gamma_d + \gamma_e + \gamma_f + \gamma_g.\end{aligned}\right\} \qquad \text{(V)}$$

For this system the variation of τ^{-1} with temperature is described satisfactorily by formula (IV) with $\epsilon_2 = 680$ cm^{-1} (as found from the term scheme), $g_2 = g_1$, $\gamma_1 = 234$ sec^{-1} and $\gamma_2 = 2440$ sec^{-1}. An equally good description is given by the same ϵ_2 and γ_1 with $g_2 = 2g_1$ and $\gamma_2 = 1460$ and probably other combinations of g_2/g_1 and γ_2 will also give satisfactory results. The experimental data do not allow a distinction to be made between these possibilities.

The treatment so far applied to the various fluorescence transitions may also be applied to the nonradiative transitions; the fact that the quenching is the same for the various sub-bands proves that the condition of maintenance of Boltzmann equilibrium during the decay is fulfilled also in this case. Such a treatment has in fact already been given by Williams and Eyring (14). The state playing a part in the quenching process is a transition state of the type discussed by Eyring and co-workers. For a statistical weight of the transition state g_q and an energy ϵ_q, and a probability of the transition regulating the rate of the nonradiative process γ_q, the decay constant τ^{-1} over the entire temperature range is given by the expression

$$\tau^{-1} = \frac{\sum_i g_i \gamma_i e^{-\epsilon_i/kT} + g_q \gamma_q e^{-\epsilon_q/kT}}{\sum_i g_i e^{-\epsilon_i/kT} + g_q e^{-\epsilon_q/kT}}. \qquad \text{(VI)}$$

This expression is different from that derived in a previous paper (9) in which the decay constant was simply the sum of the transition probabilities of the radiative and nonradiative transitions γ and $\delta = \delta_0 e^{-\epsilon/kT}$. However, the difference is negligible; normally $\gamma_q g_q > \gamma_i$ and, therefore, the quenching is already appreciable when the value of $e^{-\epsilon_q/kT}$ is still very small. Consequently, this factor may be neglected in the denominator. Further, the contribution of the other exponential functions in the denominator varies but slowly with temperature and is practically constant over the quenching range. Thus we arrive at the original formula.

This way of treating the temperature quenching shows that the constant appearing before the exponential function in the expression for the probability of the nonradiative transitions contains a factor γ_q which is comparable to the transition probability of fluorescence. In the Mott and Seitz model it probably corresponds to the transition between the potential energy curves of the electronic excited state and the ground state at the point at which they approach one another closely (Fig. 1*a*, $T \rightarrow Q$).

For the case of $4MgO \cdot 1GeO_2:Mn^{4+}$ expression (VI) describes the time constant of the decay for the entire temperature range from 83°K to the point of total quenching with the values of ϵ_2, γ_1, γ_2, g_2/g_1 as given above, and with $\epsilon_q = 8590$ cm^{-1} and $\gamma_q \cdot g_q/g_1 = 6.6 \cdot 10^{10}$. The expression is

$$\tau^{-1} = \frac{234 + 2240\, e^{-680/kT} + 6.6 \cdot 10^{10} e^{-8590/kT}}{1 + e^{-680/kT}}. \qquad \text{(VII)}$$

The efficiency of fluorescence η must then be given by

$$\eta = \frac{\gamma_1 g_1 + \gamma_2 g_2 e^{-\epsilon_2/kT}}{\gamma_1 g_1 + \gamma_2 g_2 e^{-\epsilon_2/kT} + \gamma_q g_q e^{-\epsilon_q/kT}} = \frac{234 + 2240 e^{-680/kT}}{234 + 2240 e^{-680/kT} + 6.6 \cdot 10^{10} e^{-8590/kT}}. \qquad \text{(VIII)}$$

In Fig. 4 curves according to these formulae are compared with the experimental data. For the decay constant the agreement is excellent. As far as the intensity is concerned, it must be emphasized that formula (VII) applies to the efficiency, while the experimental points refer to the intensity; that is to say, a variation of the absorption with temperature has not been accounted for. Furthermore, no correction has been made for the variation of the spectral

distribution with temperature. In view of these facts, the agreement is satisfactory.

Summary

From absorption and fluorescence measurements, and chemical analysis, it was shown that magnesium germanate activated by manganese may contain the activator in different valencies. In samples prepared in N_2 the manganese was divalent. The samples showed no fluorescence upon excitation by λ 3650 Å, but showed red cathodofluorescence in two broad bands. In samples prepared in O_2 or air the manganese was partly oxidized to a valency higher than two, probably four. In this state manganese produced an absorption band in the ultraviolet and a red fluorescence in seven characteristic narrow bands.

The various sub-bands decay with the same time constant which varies with temperature. The intensity of the Mn^{4+} fluorescence upon excitation by λ 2537 Å was constant up to 600°K; above this temperature it decreased rapidly owing to nonradiative transitions from the excited states of Mn^{4+}.

The variations of the decay constant and the intensity of fluorescence with temperature are explained with the assumption that the relative contributions of radiative and nonradiative transitions are determined by a Boltzmann equilibrium governing the population of various excited states.

Acknowledgments

The authors wish to express their appreciation to Mr. Th. P. J. Botden and Dr. A. Bril for their aid in carrying out some of the measurements, to Messrs. W. Hoogenstraaten and P. Zalm for valuable discussions, and to Dr. P. H. Dowling for his aid in editing the manuscript.

Any discussion of this paper will appear in a Discussion Section, to be published in the June 1951 issue of the Journal.

1. H. W. Leverenz, U. S. Pat. 2,066,044, Dec. 29, 1936.
2. F. E. Williams, *J. Optical Soc. Am.*, **37,** 302 (1947).
3. S. H. Patten and F. E. Williams, *J. Optical Soc. Am.*, **39,** 702 (1949).
4. J. T. Randall, *Proc. Roy. Soc. London* **170A,** 272 (1939).
5. R. E. Shrader, *J. Optical Soc. Am.*, **39,** 699 (1949).
6. F. A. Kroeger, *Nature*, **159,** 706 (1947).
7. F. A. Kroeger, "Some Aspects of the Luminescence of Solids," Ch. II, Elsevier, Amsterdam—New York (1948).
8. G. R. Fonda and H. C. Froelich, ' Cornell Symposium on the Preparation and Characteristics of Solid Luminescent Material²," p. 385, John Wiley & Sons, New York (1948).
9. F. A. Kroeger, W. Hoogenstraaten, M. Bottema, and Th. P. J. Botden, *Physica*, **14,** 81 (1949).
10. F. A. Kroeger and W. Hoogenstraaten, *Physica*, **15,** 557 (1949).
11. B. Rinck, *Z. Naturforsch.*, **3a,** 406 (1948).
12. F. Studer and A. Rosenbaum, *J. Optical Soc. Am.*, **39,** 685 (1949).
13. V. M. Goldschmidt, *Nachr. Ges. Wiss. Göttingen, Math.-physik. Klasse*, **1931,** 184.
14. F. E. Williams and H. Eyring, *J. Chem. Phys.*, **15,** 289 (1947).

The Kinetics of the Reactions of Beryllium with Oxygen and Nitrogen and the Effect of Oxide and Nitride Films on its Vapor Pressure

EARL A. GULBRANSEN AND KENNETH F. ANDREW[1]

Westinghouse Research Laboratories, East Pittsburgh, Pennsylvania

ABSTRACT

A systematic study of the reaction of beryllium with oxygen is made over the temperature range of 350° to 950°C. The experimental data may be fitted by the parabolic rate law except for the initial period of the reaction. A plot of log K/T vs. $1/T$ gives an energy of activation of 50,300 calories per mole. A comparison of this rate data with other metals and alloys shows that vacuum-treated beryllium has the smallest parabolic reaction rate constant at 900°C of any metal or alloy that we have studied.

The reaction with nitrogen is studied over the temperature range of 600° to 925°C. The data may be fitted by the parabolic rate law. A comparison with the oxygen reaction shows that the rate of reaction is somewhat smaller. A plot of log K/T vs. $1/T$ gives an energy of activation of 75,000 calories per mole.

No reaction is observed with hydrogen over the temperature range of 300° to 882°C.

A study of the vapor pressure of beryllium and the influence of oxide and nitride films is made using the Langmuir method. Excellent agreement is found for the vacuum-treated specimens with the recent results of Holden, Speiser, and Johnston. Oxide films exert a strong effect in reducing the vapor pressure, the effect varying as the square root of the oxide thickness. A film of 99 micrograms per cm² lowers the vapor pressure 100-fold.

INTRODUCTION

This communication presents the results of studies on the kinetics of the gas phase reactions of beryllium with oxygen and nitrogen. Similar studies have been made on zirconium (3, 4), titanium (3, 5), columbium (3, 6), and tantalum (3, 6). Measurements are also reported on the vapor pressure of beryllium and the effect of oxide and nitride films on the vapor pressure.

From a thermodynamic point of view, beryllium should react readily with many of the common gases since it forms a stable oxide and nitride and perhaps a stable carbide. However, from a kinetic point of view, the reactions with oxygen and nitrogen occur very slowly and there is no evidence that it reacts to any extent with hydrogen (25).

According to the rule of Pilling and Bedworth (23) beryllium should form a protective oxide and nitride, since the ratio of the molecular volume of the oxide to the metal is 1.70 while the corresponding ratio for the nitride is 1.395.

Beryllium has been reported by a number of workers to have the hexagonal close-packed structure. Owen and Pickup (22) report an a_o value of 2.28105 Angstroms and a c_o value of 3.57714 Angstroms at 18°C. The experimental value for the density is given by Vivian (32) to be 1.84 and can be compared to an x-ray value of 1.857. The vapor pressure of beryllium has been studied in the liquid range by Baur and Brunner (1) and in the solid range by Schuman and Garrett (24) and Holden, Speiser, and Johnston (12). The latter work is considered to be the more reliable.

Terem (28) has studied the oxidation of powdered beryllium at 1000°C. The rate of reaction is found to be greater than that for nickel and is 75 per cent complete in 15 minutes. An induction effect in the time course of the oxidation of beryllium is noted which is not explained. In a later paper Terem (29) reports that the oxidation of fine particles does not occur below 500°C and that the rate of reaction is slower in dry air than in ordinary air. He also finds that the Arrhenius law is followed by the oxidation reaction.

Studies by Krylova (15) on the oxidation of a number of metals including beryllium indicate that the velocity of oxidation remains almost unchanged as the temperature is raised until a certain temperature is reached, after which the velocity of oxidation increases rapidly as a function of the temperature.

BeO is reported to have a hexagonal crystal structure of the zincite arrangement. Nitka (21) has found an a_o value of 2.695 Angstroms and a value of c_o of 4.39. The density of BeO is 3.025.

Tzentnershver and Blumenthal (31), in a study of peroxides, have noted a compound BeO_2 which is too unstable to obtain in a pure state.

Gulbransen, Hickman, and Ruka (10) and Yama-

[1] Manuscript received March 27, 1950. This paper prepared for delivery before the Cleveland Meeting, April 19 to 22, 1950.

guchi (34) have observed BeO as the oxide formed on the outer surface during the oxidation of beryllium using the electron diffraction method.

The crystal structure of Be_3N_2 has been observed by Stackelberg and Paulus (26). It has a cubic structure of the Tl_2O_3 arrangement with 16 formula weights in the elementary cell. The a_o value is 8.13 Angstroms. Gulbransen and Ruka (10) have observed Be_3N_2 on the surface of beryllium after nitriding with nitrogen.

Thermodynamic Calculations

Beryllium reacts with many of the common gases to form stable oxides and nitrides and perhaps a stable carbide. No reaction with hydrogen has been observed (25). The chemical equilibrium as a function of the temperature may be calculated when the reaction products are the oxide and nitride. Data from literature sources are not available for the free energy of formation of the carbide.

TABLE I. *Equilibrium calculations on beryllium reactions*

Reaction	Literature reference
(1) $Be(s) + 1/2\ O_2(g) \rightleftarrows BeO(s)$	30
(2) $3Be(s) + N_2(g) \rightleftarrows Be_3N_2(s)$	14
(3) $Be(s) + H_2O(g) \rightleftarrows BeO(s) + H_2(g)$	20, 30
(4) $Be(s) + CO_2(g) \rightleftarrows BeO(s) + CO(g)$	20, 30

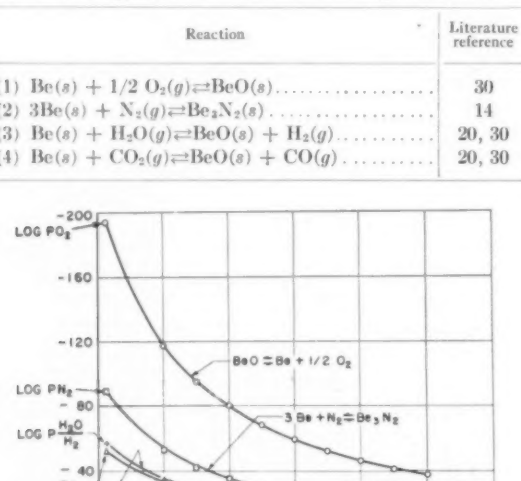

FIG. 1. Equilibrium calculations on Be reactions

Table I shows the reactions for which equilibria calculations are made together with the literature source for the data.

Fig. 1 shows the results of the calculations. The logarithms of the gas pressures or pressure ratios are tabulated as a function of the temperature in °C for the several reactions. The results show the following: (1) BeO and Be_3N_2 are stable over the temperature range of 0° to 1000°C and, from a thermodynamic point of view, beryllium will remove oxygen and nitrogen at the lowest pressures used in modern vacuum technology; and (2) the reaction of water and carbon dioxide to form the oxide and hydrogen and carbon monoxide, respectively, are possible at temperatures up to 1000°C even in vacuums of the order of 10^{-7} mm of Hg.

Samples

The samples of beryllium metal were prepared for us by the Brush Beryllium Company from sintered bars in the form of plates 1.2 cm wide, 8 cm long, and about 0.075 cm thick. Table II shows the chemical and spectrographic analyses of the samples as furnished to us by the supplier.

The as-received samples were cut and filed to approximate weight. Before the final adjustment of the weight, the samples were abraded, starting with 0 grit paper and finishing with 4/0 polishing paper. All abrading operations were carried out under purified kerosene to minimize oxide film formation and the health hazard.

TABLE II. *Analyses of beryllium metal*

%	Chemical analysis	Spectrographic analysis
BeO	1.34	
Slag	0.10	
Assay	98.85	
Ag		0.0005 (approx.)
Al	0.11	0.0500
Cd		0.00002
Co		0.0001
Cu		0.0170
Fe	0.114	0.1070
Li		0.00003
Mg	N.D.	0.0480 (approx.)
Mn		0.0120
Ni		0.0094
Sn		0.0001
Zn		0.0060

The samples weighed 0.4990 g and had surface areas of 6 to 7 cm^2.

One group of samples was pretreated in high vacua at 900°C for several hours to remove volatile impurities. These samples are referred to as vacuum treated.

All samples were stored in a dessicator prior to use.

Apparatus and Method

All of the kinetic measurements were made using the vacuum microbalance and associated equipment (7, 8). The sensitivity of the balance was 0.86 divisions per μg and the weight change could be estimated to 0.3 μg. The vacuum system, double-walled zircon furnace tube, and associated equipment have been described (4, 8, 9). The furnace tube was sealed directly to the all-glass vacuum system. McLeod gage pressures of 10^{-6} mm of Hg or lower

were achieved at temperatures up to 1175°C. With this vacuum system we can heat beryllium without noticeable reaction if the system is properly degassed after exposure to gases at high temperatures.

The oxygen, nitrogen, and hydrogen purification processes have been described (4, 7). Lamp grade nitrogen was used in the preparation of nitrogen. Mass spectrometer analyses of the purified gas showed an oxygen content of about 0.01 per cent.

For the experiments above 750°C, spectroscopically pure argon was added to a pressure of 5 mm of Hg to prevent the evaporation of beryllium during the heat-up period. This gas was removed by evacuating the system immediately before adding the oxygen or nitrogen.

Due to the evaporation of beryllium, the stability of oxide and nitride films cannot be tested directly by weight loss measurements. However, if the furnace tube is shut off from the pumps, the gases given off may be collected and the presssure measured as a function of time. Care must be used to remove the gases which enter the ceramic furnace tube during exposure to oxygen or nitrogen.

The vapor pressure of beryllium and the effect of given thicknesses of oxide and nitride films were studied using the Langmuir method. In this method the vapor pressure P in atm is related to the rate of evaporation m of the beryllium in g/cm²/sec at the absolute temperature T by the formula

$$m = \alpha P \sqrt{\frac{M}{2\pi RT}}$$

where M is the molecular weight of the evaporating molecule or atom and α is the condensation coefficient. The theory and use of these methods have been described by other investigators (12, 13, 16, 17).

The accommodation coefficient, α, is assumed to be unity. This assumption is less correct in our method in which the specimen and surrounding furnace walls were at the same temperature than for methods based upon heating the sample without heating the walls. In the method used here, the measured weight loss depended to some extent upon the geometry of the specimen and furnace tube, since only the difference between the rate of evaporation and condensation was measured. However, for a 1-cm wide sample in a 2.5 cm tube the measured weight loss is probably 80 to 90 per cent of the correct value. This source of error may be small compared to errors due to the presence of films, impurities, or to the measurement of the temperature.

The vacuum conditions under which the specimens are heated and the evaporation rate measured are very critical if vacuum reactions are to be avoided (9). We have found it essential to pump overnight on our system even though pressures of the order of 10^{-6} mm of Hg, as estimated by the McLeod gage, could be obtained within an hour after closing off the system (9). Using this pumping procedure, check results were obtained on successive evaporation experiments. For those experiments involving the addition of an oxide or nitride film, the system was pumped at 750°C for 3 to 4 hours or overnight at room temperature to remove the gases from the ceramic tube.

To measure the rate of weight loss, readings were made of the microbalance and temperature every two minutes in the temperature range of 800° to 970°C. Large-scale plots of the readings were made as a function of time and the slopes evaluated from a smoothed curve by means of Lagrange's formula.

Since the specimens were supported by a 2-mil Nichrome wire from the balance, a direct measurement of the specimen temperature was impractical. Instead, the temperature of the inner ceramic tube between the heater wires and under a surrounding ceramic coating at a point opposite the specimen in the tube was taken as the temperature. Calculations on our system showed that the tube and the specimen had a temperature difference of less than 1°C when the system was heated at a rate of 3° to 4°C per minute at temperatures of 800° to 950°C. The temperature was measured using a platinum and platinum-10 per cent rhodium thermocouple with a White potentiometer.

Although the temperature of the inner ceramic tube at the thermocouple point was maintained to ±1°C the absolute value of the temperature was ±3°C due to variations in the temperature of the cold junction over a period of months.

Results and Discussion

A. High Vacuum Reaction

To obtain reaction rates which have scientific value it is necessary to study the extent of film formation during the process of heating the specimen to the reaction temperature. Many of the reactive metals are excellent getters to the small quantities of gas normally present in the best of high vacua (3, 4, 5, 6). Since the oxides of beryllium cannot be reduced with hydrogen, it is necessary to minimize the oxide films formed during the preparation of the sample and in heating the sample to the reaction temperature. The films formed in the latter operation can only be minimized by heating to the reaction temperature as quickly as is feasible in vacua of at least 10^{-6} mm of Hg and probably lower (9).

Fig. 2 shows the behavior of a sample of beryllium on heating between 300° to 840°C in vacua of 10^{-6} mm of Hg or lower, conditions which were readily obtained after one hour of pumping in our system.

The weight loss in micrograms per cm² was plotted against the time and the temperature noted at the top of the figure. No evidence was found for a vacuum reaction in the sense that zirconium and columbium react with gases in high vacua (4, 6). Above 700°C the specimen lost weight by evaporation. This process increased rapidly with temperature. A

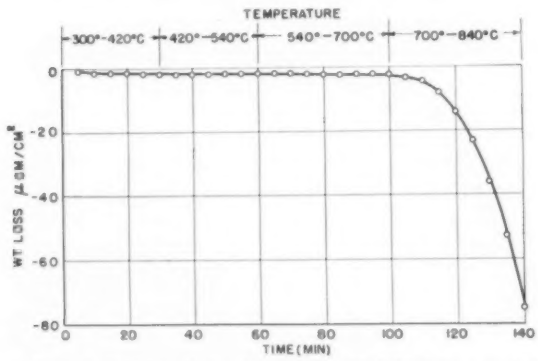

FIG. 2. Vacuum behavior of Be, 300°–840° C, abraded through 4/0.

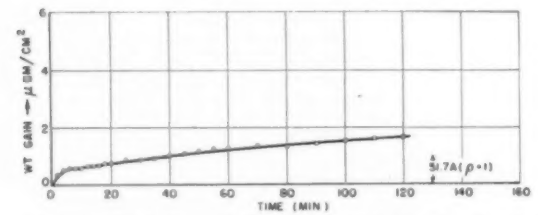

FIG. 3. Oxidation of Be, 350° C, 7.6 cm O_2, abraded through 4/0.

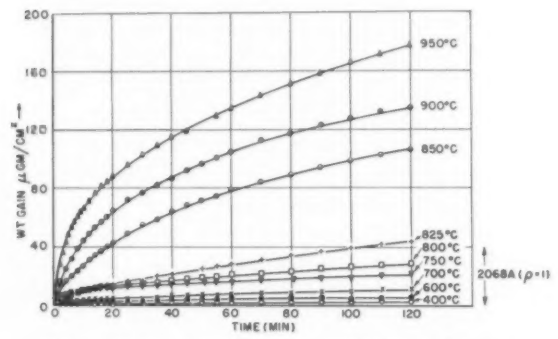

FIG. 4. Effect of temperature, oxidation of Be, 7.6 cm O_2, abraded through 4/0.

reheat of this specimen showed that the onset of evaporation at 700°C was due to impurities present in the metal. The nature of the evaporation process and the influence of oxide and nitride films will be discussed in Section E.

The vacuum heating experiment shows two important facts: (1) beryllium is not an efficient getter in high vacuum systems; and (2) that the volatilization of impurities in beryllium occurs at temperatures of the order of 700°C.

B. Reaction with Oxygen

The reaction was studied as a function of time, temperature, pressure, and vacuum pretreatment.

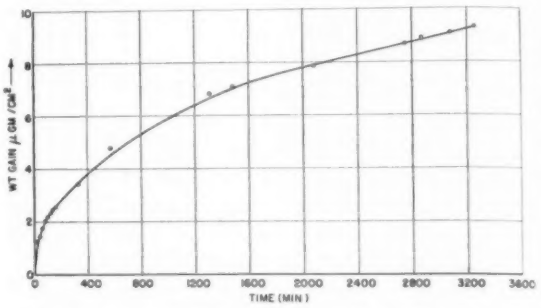

FIG. 5. Reaction of Be with O_2, 500° C, 7.6 cm O_2, long period, abraded through 4/0.

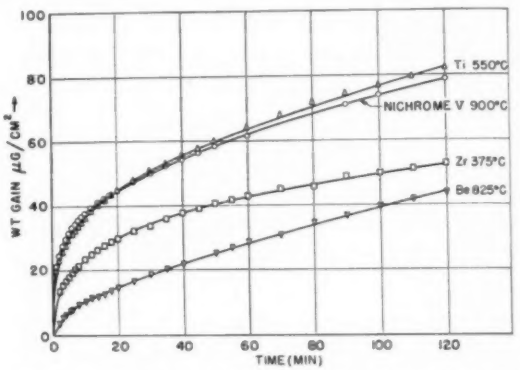

FIG. 6. Comparison oxidation of Be with Zr, Ti, and Nichrome V.

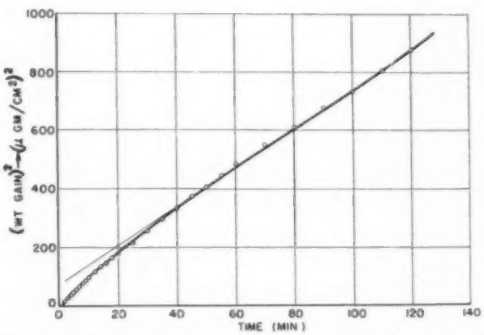

FIG. 7. Oxidation of Be, vacuum treated, 850° C, 7.6 cm O_2, parabolic plot, abraded through 4/0.

The results are shown in Fig. 3 to 12 and Tables III to V. Assuming the ratio of the real to the measured area to be unity ($\rho = 1$) and the oxide to be BeO (10, 34), the thickness of the oxide in Angstroms is related to the weight gain in micrograms per cm² by the factor 51.7.

Time and temperature.—Fig. 3 shows the time course of the oxidation experiment at a temperature

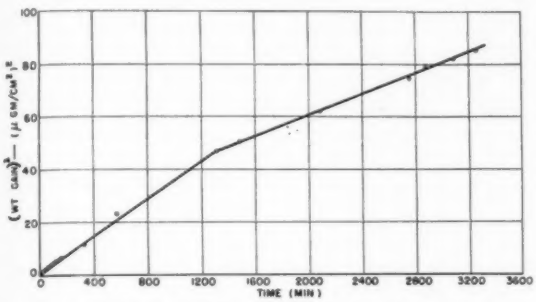

FIG. 8. Oxidation of Be, 500° C, 7.6 cm O_2, long period, parabolic plot, abraded through 4/0.

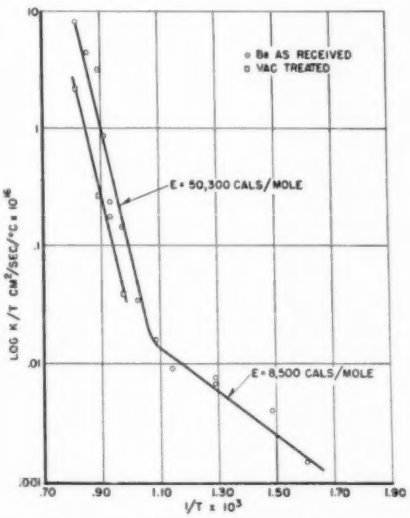

FIG. 9. Reaction of Be with O_2, log K/T vs. $1/T$

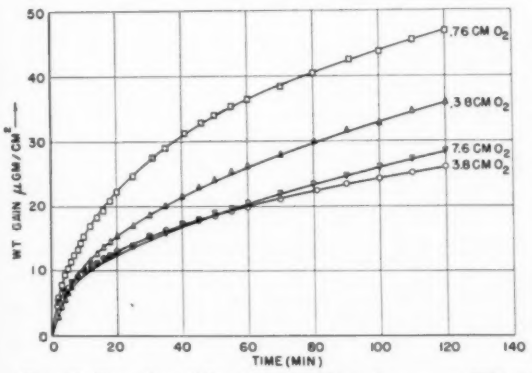

FIG. 10. Reaction of Be with O_2, effect of pressure, 800° C' abraded through 4/0.

of 350°C and an oxygen pressure of 7.6 cm. After 2 hours of reaction a film of 1.65 $\mu g/cm^2$ was formed or a thickness of 85 Angstroms. Compared to other active metals (4, 5, 6) beryllium showed a small reaction under these conditions.

The time course of the oxidation reaction over the temperature range of 400° to 950°C is shown in

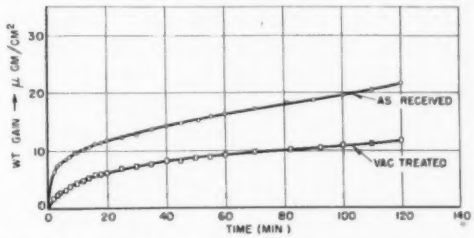

FIG. 11. Oxidation as-received Be vs. vacuum-treated Be, 750° C, 7.6 cm O_2, abraded through 4/0.

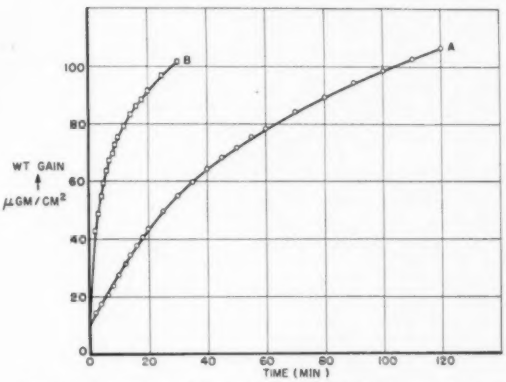

FIG. 12. Reaction of Be with O_2, 850° C, 7.6 cm O_2. A. No film, B. nitrogen film (35.8 $\mu g/cm^2$).

TABLE III. *Color vs. thickness, oxidation of beryllium*

Temp	Thickness (2 hr)		Color
	$\mu g/cm^2$	Å (ρ = 1)	
°C	cm^2		
350	1.65	85	no color
400	3.10	160	no color
500	4.28	221	no color
500	4.56	236	no color
600	4.81	249	no color
700	10.78	557	straw-blue
750	21.8	1128	blue
800	28.2	1510	straw
800	77.6	4010	straw-violet
825	43.7	2260	straw
850	106.7	5520	violet-green
900	135	6980	violet-gray
950	177	9150	gray

Fig. 4. A thickness scale is shown at the right in the figure.

Table III shows a correlation of the oxide thickness with the color of the surface film for two-hour oxidation runs over the temperature range of 350° to 950°C. No colors were observed for oxide films

up to a calculated thickness of 250 Angstroms at 600°C. A straw-blue film was formed at 700°C, having a thickness of 557 Angstroms. Gray films were formed at 900°C and 950°C for thicknesses of 6980 and 9150 Angstroms, respectively.

The effect of temperature on the time course of the oxidation appeared to follow an exponential law.

It is of interest to check the prediction of Terem (28) that an induction effect exists in the course of the oxidation. Fig. 5 shows the time course of the

TABLE IV. *Parabolic rate law constants, entropies, energies, and free energies of activation for the oxidation process*

Temp	K	ΔS^*	E	$-T\Delta S^*$	ΔF^*
°C	cm²/sec	cal/mole/°C	cal/mole	cal/mole	cal/mole
350	0.93×10^{-16}	−51.8	8,500	32,300	40,800
400	1.00×10^{-15}	−54.3	8,500	36,500	45,000
500	1.94×10^{-15}	−51.5	8,500	39,900	48,400
500	2.22×10^{-15}	−51.3	8,500	39,700	48,200
600	2.94×10^{-15}	−52.1	8,500	45,500	54,000
650	5.42×10^{-15}	−51.6	8,500	47,600	56,100
700	1.39×10^{-14}	−50.25	8,500	48,800	57,300
750	1.46×10^{-14}	−7.23	50,300	7500	57,800
800	1.90×10^{-14}	−9.10	50,300	9770	60,070
800	2.88×10^{-14}	−8.28	50,300	8890	59,190
825	8.98×10^{-14}	−7.10	50,300	7800	58,280
850	3.64×10^{-13}	−5.45	50,300	6120	56,420
900	5.55×10^{-13}	−6.58	50,300	7730	58,030
950	1.00×10^{-12}	−7.23	50,300	8840	59,140
*750	4.00×10^{-15}	−9.80	50,300	10,050	60,350
*850	2.99×10^{-14}	−10.45	50,300	11,750	62,050
*950	2.59×10^{-13}	−9.94	50,300	12,170	62,470

* Vacuum treated, 900°C, for two hours.

Time and temperature equations.—The following equations have been used most frequently to explain the time variation of the oxidation rate:

(I) The parabolic law (18, 19, 23, 33) $W^2 = Kt + C$,
(II) The linear law $W = K't + C$, and
(III) The logarithmic law (27) $t = \beta\,(e^{w/\alpha} - 1)$.

In the above equations W refers to the weight gain, t the time, and K', K, C, α, and β are constants.

The following equations are used to interpret the temperature dependence of the parabolic reaction rate constant K:

(I) Arrhenius equation (2) $K = Ae^{-E/RT}$

(II) Transition State Theory (11) $K = \frac{2kT}{h}\lambda^2\, e^{\Delta S^*/R} e^{-E/RT}$

In the first equation A is the frequency factor and E the energy of activation. In the second equation ΔS^* and E are the entropy and energy of activation, λ is the interatomic distance between diffusion sites, k is Boltzman's constant, h is Planck's constant, and R the gas constant. A comparison of the first and second equations shows that the frequency factor A can be identified with universal constants, λ^2, the temperature T, and the temperature independent factor $e^{\Delta S^*/R}$. The term E in the expression $e^{-E/RT}$ results from the assumption that for solid phase reactions $\Delta H^* = E$ since the term $P\Delta V^*$ is small. This assumption has recently been questioned (35).

TABLE V. *Comparison of the parabolic rate law constants and the energies, entropies, and free energies of activation*

	350°C				
	Ta	Ti	Zr	Fe	Be
K cm²/sec	3.37×10^{-14}	1.90×10^{-15}	4.28×10^{-14}	1.2×10^{-15}	0.93×10^{-16}
E cal/mole	27,400	26,000	18,200	22,600	8,500
ΔS^* entropy units	−10.20	−18.00	−25.1	−24.60	−51.8
ΔF^* cal/mole	33,760	37,200	33,800	37,950	40,800

reaction at 500°C over a long reaction time interval of 3200 minutes. The experiment showed no evidence of an induction time for the reaction.

Beryllium is often classed with the active metals. Fig. 6 shows a comparison of the oxidation of beryllium with zirconium, titanium, and the alloy Nichrome V. The figure shows that the oxidation of beryllium at 825°C is similar to that of zirconium at 375°C. In fact at 900°C, the reaction of vacuum-treated beryllium was less than that for Nichrome V. It must not be inferred that beryllium is more protective than Nichrome V until long-term and cycling tests are made.

Time and temperature correlation.—An analysis of Fig. 3, 4, 5, and 6 indicates that the data are not fitted by a linear rate law while plots of the weight gain vs. the logarithm of the time show smooth curves of increasing slope. The logarithmic or linear rate laws do not apply for the conditions studied here.

Fig. 7 shows a parabolic rate law plot for the oxidation of vacuum-treated beryllium at 850°C and 7.6 cm of O_2. The square of the weight gain in μg per cm² is plotted against the time. A reasonable fit is found although some deviation is noted for the

initial stages of the reaction. Deviations of this type are predicted by the recent analysis of Mott (19).

Fig. 8 shows a parabolic plot of the long-time experiment at 500°C and 7.6 cm of O_2. The parabolic plot gives two straight lines and indicates that the metal becomes more protective as the film thickens.

Temperature dependence and the activation energy.—The importance of the evaluation of the temperature coefficient of the reaction rate has been discussed (4). Since the oxidation follows the predictions of the parabolic rate law, it is possible to evaluate the energy and entropy of activation of the rate-limiting process.

The temperature is involved in the transition state theory as part of the exponential term $e^{-E/RT}$ and also directly as T. In previous studies, we neglected the effect of the linear term when compared to the exponential factor. For a more precise evaluation of E for this study we plotted the term log K/T vs. $1/T$ (35). The parabolic rate law constants K were evaluated from parabolic plots of the data in the time range of 60 to 120 minutes. The parabolic rate law constants are given in Table IV.

Fig. 9 shows a plot of log K/T vs. $1/T \times 10^3$. The data may be fitted best by two straight lines. An energy of activation of 50,300 cal per mole was calculated for the temperature range of 750° to 950°C while an energy of activation of 8,500 cal per mole was calculated for the temperature range of 350° to 700°C.

The temperature independent factors $e^{\Delta S^*/R}$ were evaluated from the transition state theory expression for K. Table IV shows the values of the parabolic rate law constants and the energies, entropies, and free energies of activation of the rate-controlling process in the oxidation of beryllium.

Table V shows a comparison of the parabolic rate law constants and the energies, entropies, and free energies of activation for beryllium at 750°C with those for iron, zirconium, tantalum, and titanium at 350°C. The data show that beryllium has a much higher resistance to oxidation than any of the metals indicated.

Pressure effect.—The effect of pressure of the oxygen gas on the reaction is shown in Fig. 10 for a temperature of 800°C. The pressure is varied from 7.6 cm to 0.38 cm of O_2 or by a factor of 20. No simple relationship for the pressure effect can be determined. It is apparent that the reaction rate does not follow a simple linear or square root function of the pressure. These relationships are to be expected if the concentration gradient of the diffusing species is dependent upon the external pressure. We concluded that the small pressure effects are in agreement with the fact that the limiting factor in the reaction is the diffusion of beryllium ions through the oxide film.

Vacuum treatment.—A comparison of the oxidation of the "as-received" beryllium samples with the "vacuum-treated" specimens is shown in Fig. 11. The rate of reaction is smaller for the vacuum-treated specimen. Similar results were obtained for other temperatures. Whether this difference in reaction rates would be maintained over long periods of time has not been determined.

Stability.—A number of tests have been made of the stability of the oxide formed at high temperature by closing the furnace tube from the pumps. No evidence was found for thermal decomposition of the oxide up to 950°C.

Effect of nitride film.—Fig. 12 shows a comparison of the reaction of Be with O_2 with and without

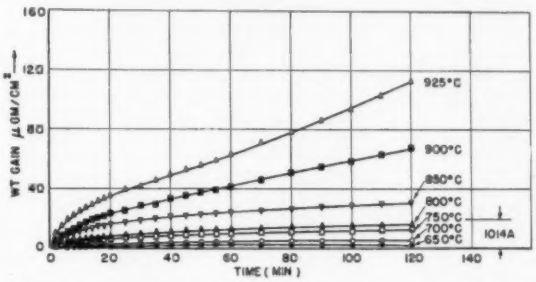

FIG. 13. Reaction of Be with N_2, effect of temperature (650°–925° C), 7.6 cm N_2, abraded through 4/0.

a nitride film. The results show that a nitride film of 35.8 μg per cm² actually increases the reaction rate at 850°C for the time range studied. The nitride film appeared to be very porous to the reaction of beryllium with oxygen.

C. Reaction with Nitrogen

The reactions of beryllium with nitrogen are equally as important as are the reactions with oxygen. The reactions of beryllium with a purified lamp grade of nitrogen were studied as a function of the time, temperature, pressure, and vacuum treatment of the samples. The stability of the nitrogen reaction product was also observed.

Fig. 13 to 20 show the results of our studies. The weight of the nitrogen reacting with the metal in μg per cm² is plotted against the time in minutes for Fig. 13 to 15 and 18 to 20. If we assume that the surface roughness ratio (ρ) is unity and that the formula of the nitride is Be_3N_2 (10), then the thickness of the nitride film is related to the weight gain in μg per cm² by the factor 52.9.

Time and temperature.—Fig. 13 shows the time courses for the reaction of beryllium with nitrogen over the temperature range of 650° to 925°C for purified lamp grade of nitrogen. Except for the 925°C

run, the reaction rate decreases as the reaction proceeds. The effect of temperature appears to follow an exponential law. The scale of 1014 Å is shown at the right in the figure.

Table VI shows a correlation of the nitride thickness with the color of the surface film for two-hour

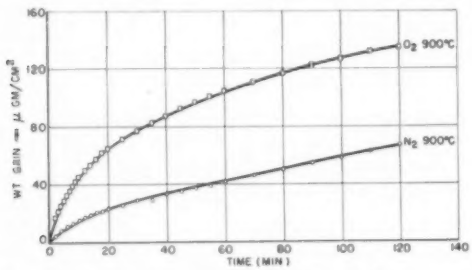

FIG. 14. Comparison reaction of Be with O_2 and N_2, 7.6 cm, 900° C, abraded through 4/0.

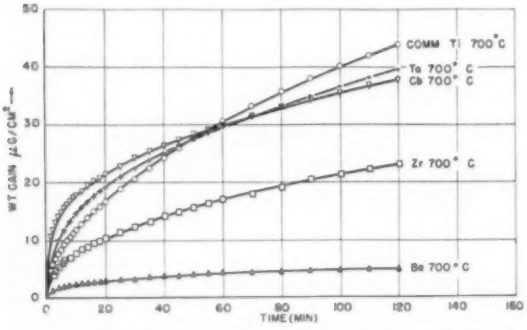

FIG. 15. Comparison of N_2 reaction on Be with Cb, Zr, Ta, and Ti, 700° C, 7.6 cm.

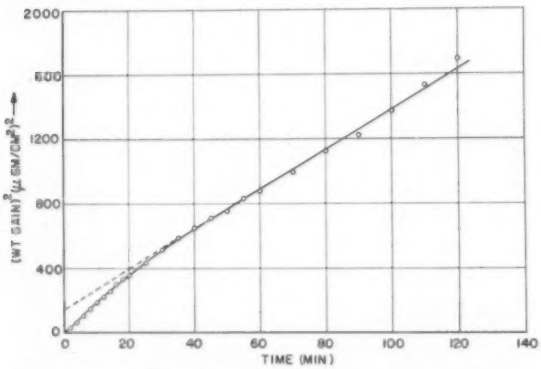

FIG. 16. Nitriding Be, 875°C, 7.6 cm N_2, parabolic plot, abraded through 4/0.

nitride experiments over the temperature range of 650° to 925°C. A straw-colored film was first observed at 700°C for a thickness of 262 Angstroms. The film formed at 925°C and having a thickness of 5810 Angstroms was blue with a whitish tint on the outer surface.

Fig. 14 shows a comparison of the nitrogen reaction with the corresponding oxidation reaction at 900°C. The nitride has the slower rate of reaction.

A comparison of the nitrogen reaction on beryllium with the corresponding reactions on zirconium, titanium, columbium, and tantalum is shown in Fig. 15. Beryllium has the lowest reaction rate of the five metals at 700°C.

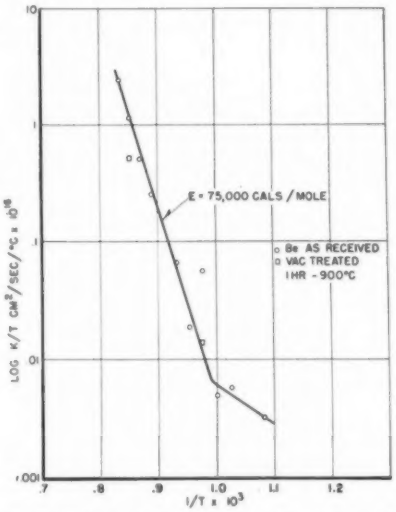

FIG. 17. Reaction of Be with pure N_2, 7.6 cm, log K/T vs. $1/T$ (650°–925° C).

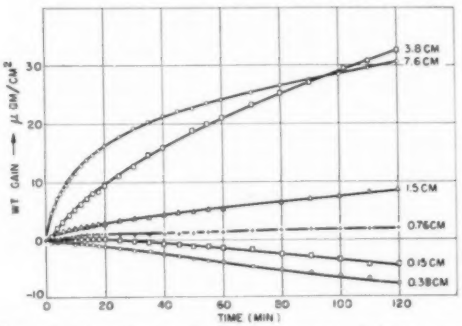

FIG. 18. Reaction of Be with pure N_2, 850° C, effect of pressure, abraded through 4/0.

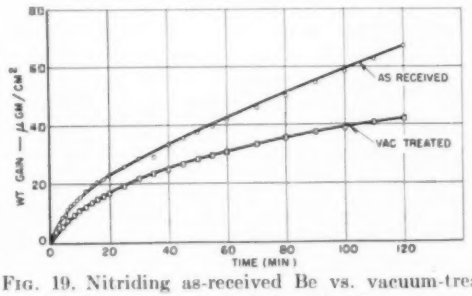

FIG. 19. Nitriding as-received Be vs. vacuum-treated Be, 900° C, 7.6 cm N_2, abraded through 4/0.

The presence of colored films on beryllium in-

dicates that the nitride is not soluble in the metal. Heating in vacua at temperatures between 800° and 970°C over a period of several hours does not dissolve the nitride in the metal.

Since a stable and insoluble nitride film exists on beryllium, it is of interest to see whether the reaction rate follows the parabolic rate law. Fig. 16 shows a plot of the weight gained squared vs. the time in minutes for the nitriding of beryllium at 875°C and 7.6 cm of N_2. A good correlation was found although deviations do occur during the initial stages of the reaction. Similar deviations were found for the oxidation reaction and appeared to be common for many reactions. This plot together with a similar

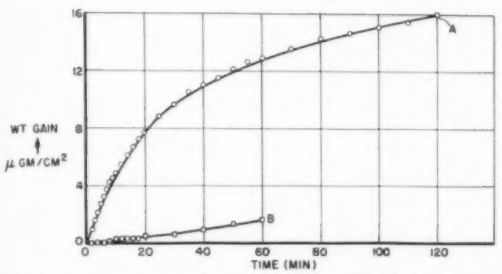

FIG. 20. Reaction of Be with pure N_2, 800° C, 7.6 cm N_2. A. No film, B. oxide film (34.4 μg/cm²).

TABLE VI. *Color vs. thickness, nitriding of beryllium*

Temp	Thickness		Color
	μg/cm²	Å(ρ = 1)	
°C			
650	3.18	168	no color
700	4.95	262	straw
725	4.48	237	straw
750	13.1	693	blue-violet
775	7.75	410	blue-violet
800	16.0	856	light straw-blue background
850	30.6	1620	straw
875	41.1	2170	blue-gray
900	67.0	3540	blue-white
925	111.8	5810	blue-white

analysis for all of the other nitride experiments lead us to conclude that the equation $W^2 = Kt + C$ explains the time variation of the reaction rate.

Parabolic rate law plots of the 900° and 925°C runs show initially a straight line. However, after 60 minutes the slope increases steadily. This may indicate that the nitride film is not as protective at $t > 900$°C as the oxide over long periods of time although the initial reaction rate is smaller. This observation may be correlated with the appearance of a blue-white film at these temperatures.

Temperature dependence and the activation energy.—Since a nitride film is actually formed on the outer surface during reaction, the transition state reaction rate theory may be applied as in the oxidation reaction.

The parabolic rate law constants were evaluated from the parabolic plots of the data in the time range of 60 to 120 minutes except for the 900° and 925°C runs, where they were evaluated for the 0 to 60 minute part of the curve. The parabolic rate law constants are tabulated in Table VII.

Fig. 17 shows a plot of log K/T vs. $1/T \times 10^3$ for both the "as-received" samples and the "vacuum-treated" specimens. The data can be fitted by a straight line although definite evidence was found for deviations from this straight line at the lower temperatures. An energy of activation of 75,000 cal per mole was calculated over the temperature range of 725° to 925°C. This is to be compared to an energy of activation of 50,300 cal per mole for the oxidation reaction. The value of 75,000 cal per mole was the highest energy of activation that we observed and is close to the value of ΔH_0^0 for the evaporation of beryllium (12).

TABLE VII. *Parabolic rate law constants, entropies, energies, and free energies of activation for the nitride reaction*

Temp	K	ΔS^*	E	$T\Delta S^*$	ΔF^*
°C	cm²/sec	cal/mole °C	cal/mole	cal/mole	cal/mole
650	2.95×10^{-16}				
700	5.60×10^{-16}				
725	4.90×10^{-16}	13.1	75,000	13,080	61,900
750	5.78×10^{-15}	16.1	75,000	16,500	58,500
775	1.97×10^{-15}	12.3	75,000	12,900	62,100
800	7.08×10^{-15}	9.9	75,000	10,650	64,350
850	2.86×10^{-14}	12.3	75,000	13,850	61,150
875	5.80×10^{-14}	12.6	75,000	14,470	60,530
900	1.32×10^{-13}	12.7	75,000	14,900	60,100
925	2.88×10^{-13}	13.0	75,000	15,600	59,400
*750	1.41×10^{-15}	13.4	75,000	13,700	61,300
*925	6.01×10^{-14}	14.3	75,000	16,750	58,250

* Vacuum treated.

The temperature independent factors $e^{\Delta S^*/R}$, ΔS^*, and ΔF^* were evaluated from the transition state theory expression for K. Table VII shows the values of the parabolic rate law constants and the energies, entropies, and free energies of activation of the rate-controlling process. The entropies of activation are positive and vary from 9.9 to 16.1 entropy units, the average value being 13.0 entropy units.

The values of ΔS^*, E, and ΔF^* are interesting since they show the importance of considering the entropy (frequency) factor in the rate of oxidation of metals. The difference between the oxidation and nitrogen reaction of beryllium occurs both in the energies of activation and in the entropy terms. The energy of activation is much higher for the nitrogen reaction than for the oxidation reaction but the en-

tropy terms are of opposite signs. This lowers the free energy of activation of the nitrogen reaction so that the two reactions occur at about the same rate. The free energy of activation of the activated state divided by the absolute temperature is one number which can be used in comparing reaction rates which obey the parabolic law. Positive values for ΔS^* indicate a surface reaction product with many possible paths for the metal ion to go to the activated state.

Pressure.—Fig. 18 shows the effect of pressure on the reaction of beryllium with nitrogen for pressures of 0.15 cm to 7.6 cm of Hg of nitrogen at 850°C. The temperature was chosen to be in the range where beryllium evaporates at an appreciable rate in the film-free condition.

The data show that the pressure of the surrounding nitrogen has an important effect not only on the extent of the reaction, but on the shape of the curve. At pressures of the order of 7.6 cm the reaction followed the parabolic law and a considerable reaction was noted, while at a pressure of 0.76 cm the reaction was very small. At lower pressures a weight loss was taking place indicating that evaporation of beryllium occurred at the same time that the nitride reaction was taking place, since blue-gray nitride films were observed for the 0.15 cm and 0.38 cm experiments. These experiments show that beryllium was evaporating faster than nitride was being formed at pressures below 0.76 cm of nitrogen.

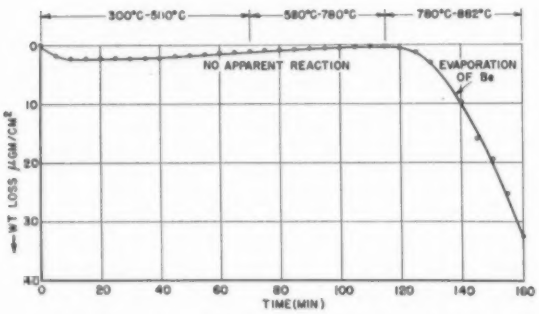

FIG. 21. Reaction of Be with H_2, 300°–882° C, 2.3 cm H_2, abraded through 4/0.

According to studies on the evaporation of beryllium which are discussed in Section E, the rate of evaporation of beryllium at 850°C is approximately 0.6×10^{-6} g/cm²/min for the film-free condition. This rate is sufficient to explain the above results.

Effect of vacuum treatment.—Fig. 19 shows a comparison of the nitrogen reaction at 900°C and 7.6 cm for an as-received and a vacuum-treated sample of beryllium. The vacuum-treated sample reacted at a slower rate than the as-received sample. A parabolic plot of the vacuum-treated experiment at 900°C shows no evidence of an increase in the slope during the time of the experiment. This comparison shows that impurities of the order of 0.01 to 0.10 per cent are important—at least during the early stages of the reaction at 900°C. This is discussed further in section E.

Effect of oxide film on nitride formation.—Fig. 20 shows the effect of an oxide film of 34.4 μg per cm² thickness on the reaction of beryllium with pure N_2 at 800°C and 7.6 cm of N_2. The oxide film was very effective in preventing the reaction, at least in the early stages studied here. These results are in contrast with those observed for the effects of nitride films on the oxidation reaction.

D. Reaction with Hydrogen

Fig. 21 shows an experiment in which a sample of as-received beryllium was heated in a hydrogen atmosphere at a pressure of 2.3 cm of Hg over the temperature range of 300° to 882°C. No appreciable reaction is noted up to a temperature of 780°C at which point the evaporation of beryllium becomes appreciable. We concluded that beryllium did not react with hydrogen over the pressure and temperature range studied. This evidence supports the conclusions of Smith (25) who has carefully reviewed the available information.

E. Vapor Pressure of Beryllium and the Effect of Oxide and Nitride Films

The purpose of these experiments was to study the effects of oxide and nitride films on the vapor pressure of beryllium and to analyze these effects in relation to the reaction rates of beryllium with oxygen. During the course of this study, it became necessary to determine the vapor pressure of beryllium for our particular apparatus although a careful study of the vapor pressure of beryllium has been made recently by Holden, Speiser, and Johnston (12).

Vapor Pressure of Beryllium.—Both as-received and vacuum-treated specimens were used. The experimental method and the treatment of the data were described in a previous section of this report. The vapor pressures, P, are calculated from the measured rates of evaporation, m, by the use of the formula

$$\log P = \log m - 1/2 \log M + 1/2 \log T - 1.647 - \log \alpha.$$

The terminology has been previously discussed.

Table VIII shows the measured rates of evaporation, the absolute temperature, T, and the calculated values of $\log P$ for the two samples. The preliminary heat-up cycle (run 1) is not tabulated in Table VIII since impurities were evaporating during the cycle.

Fig. 22 shows a plot of $\log P$ vs. $1/T$ for five of the experimental runs. The first heating cycle for the as-received sample is shown at the upper right

in the figure and represents the vaporization of volatile impurities in the sample. The second, third, and fourth heating cycles of this sample are shown in the center of the figure (experiments 2, 3, and 4 of Table VIII). The data fit nicely on a straight line. Run 5 in Table VIII for the vacuum-treated specimen is also plotted in Fig. 22. The calculated values for log P for this sample fit nicely with the other data. A curve of the data of Holden, Speiser, and Johnston (12) for log P is also included in the figure. The variation between their work and our studies is about 10 per cent while the earlier work of Schuman and Garrett (24) differs by 300 per cent.

TABLE VIII. *Rates of evaporation and vapor pressure of sintered beryllium*

Run	Temp	Rate	$-\log P$	ΔH_0^0
(*a*) Abraded, as-received specimen and one evaporation heat (Fig. 22)				
	°K	g/cm²/sec × 10⁷	atm	kcal
2	1177	0.468	7.9190	76.92
2	1185	0.577	7.8255	76.93
2	1194	0.681	7.7630	77.19
2	1201	0.850	7.6554	77.04
3	1133	0.117	8.3684	77.72
3	1153	0.168	8.5293	77.20
3	1173	0.398	7.9900	77.02
3	1193	0.625	7.7904	77.27
3	1204	0.971	7.5971	76.92
3	1212	1.29	7.4722	76.73
4	1113	0.0734	8.7357	76.89
4	1153	0.206	8.2799	77.25
4	1173	0.418	7.9688	76.91
4	1193	0.640	7.7802	77.21
4	1204	0.956	7.6039	76.96
4	1215	1.228	7.4931	77.04
4	1221	1.830	7.3188	76.45
4	1229	2.67	7.1533	76.10
Mean				76.98 ± 0.23 (A.D.)
(*b*) Abraded, vacuum treated 1 hr at 900°C				
5	1103	0.05614	8.8540	76.79
5	1141	0.1674	8.3722	76.93
5	1161	0.282	8.1420	77.06
5	1181	0.493	7.8956	77.06
5	1201	0.808	7.6784	77.18
5	1221	1.66	7.3611	76.69
5	1223	1.88	7.3067	76.51
Mean				76.89 ± 0.18 (A.D.)
Overall mean				76.95 ± 0.22 (A.D.)

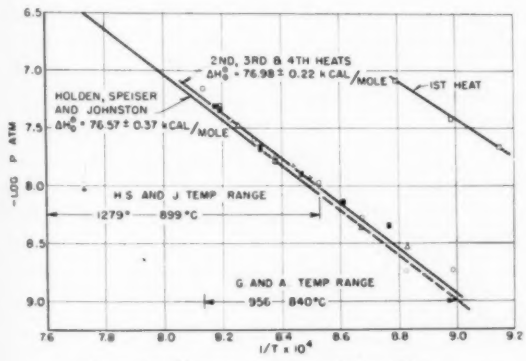
2ND, 3RD & 4TH HEATS
ΔH₀⁰ = 76.98 ± 0.22 KCAL/MOLE
1ST HEAT
HOLDEN, SPEISER AND JOHNSTON
ΔH₀⁰ = 76.57 ± 0.37 KCAL/MOLE
H S AND J TEMP RANGE
1279° — 899°C
G AND A TEMP RANGE
956 — 840°C
-LOG P ATM
1/T x 10⁴

FIG. 22. Vapor pressure of beryllium

Two further points should be noted: (1) the values of log P for the temperature range below 850°C appear to deviate from the straight line; and (2) the actual values of log P may be 10 to 20 per cent higher than the values given here because of the geometry of the experimental setup.

The values of ΔH_0^0 for the evaporation process are calculated from the formula

$$\frac{\Delta H_0^0}{T} = -R \ln P - \frac{(F^0 - H_0^0)}{T}\ \text{gas} + \frac{(F^0 - H_0^0)}{T}\ \text{solid}.$$

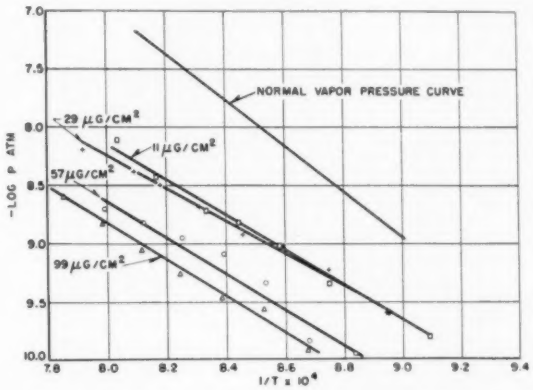

FIG. 23. Effect of oxide films on evaporation, vacuum-treated Be.

The values for the free energy functions are those given by Holden, Speiser, and Johnston (12). Table VIII shows the calculated values of ΔH_0^0 for the several experiments. The mean value is 76.95 ± 0.22 KCal per mole which may be compared to the value of 76.57 ± 0.37 given by Holden, Speiser, and Johnston (12).

The vapor pressure of beryllium may be expressed as a function of the temperature by the equation

$$\log P(\text{atm}) = 6.186 + 1.454 \times 10^{-4} T - \frac{(16{,}800 \pm 48)}{T}.$$

Effect of oxide and nitride films on the vapor pressure.—Fig. 23 and 24 show the results of the effect of oxide and nitride films on the vapor pressure of vacuum-treated samples of beryllium. The normal vapor pressure curve is shown together with the calculated vapor pressure curves for the metal after hav-

ing added oxide and nitride films. The effects of adding four oxide films of 11, 29, 57, and 99 μg per cm^2 and three nitride films of 7.35, 21, and 42 μg per cm^2 are shown.

The calculated vapor pressures are very strongly affected by the presence of oxide films as shown in Fig. 23 and to a lesser extent by nitride films as shown in Fig. 24. An 11 μg per cm^2 oxide film reduces the vapor pressure by a factor of about 10 while a 99 μg per cm^2 oxide film reduces the vapor pressure by a factor of about 60. These effects are dependent upon the temperature since the slopes of the vapor pressure curves for the films are not the same as for the film-free metal.

Fig. 24 shows that a 7.35 μg per cm^2 nitride has no effect while a 42 μg per cm^2 nitride film reduces the calculated vapor pressure by a factor of 4.

It is of interest to note that the change in the vapor pressure is roughly proportional to the square root of the thickness of the oxide and to a linear function of the thickness of the nitride with the exception of the 7.35 μg per cm^2 nitride experiment.

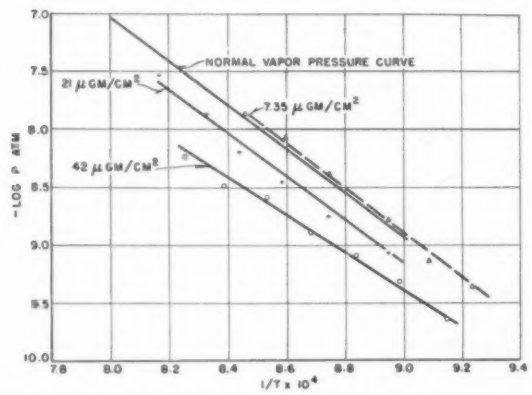

FIG. 24. Effect of nitride films on evaporation, vacuum-treated Be.

SUMMARY

The reactions of beryllium with oxygen, nitrogen, and hydrogen in high vacua were studied using the vacuum microbalance method.

Thermodynamic calculations of the reactions of beryllium to form the oxide and nitride, respectively, showed that the oxide BeO and the nitride Be_3N_2 are stable over the temperature range of 0° to 1000°C in vacua of 10^{-6} mm of Hg. The reactions of water and carbon dioxide to form the oxide BeO and hydrogen and carbon monoxide, respectively, are possible at temperatures up to 1000°C and in vacua of the order of 10^{-7} mm of Hg.

Vacuum heating experiments showed that beryllium is not an efficient getter in high vacuum systems and that volatilization of impurities in sintered beryllium occurs at temperatures of the order of 700°C.

The reaction of beryllium with oxygen was studied over the temperature range of 350° to 950°C. No colored films were observed for a two-hour oxidation at 600°C. However, above this temperature colored oxides formed.

A comparison of the oxidation rate showed that beryllium reacts at 825°C at about the same rate as zirconium at 375°C. The initial reaction rates showed beryllium to react at about the same rate as the Nichrome V series of alloys at 900°C.

A modified form of the parabolic rate law was found to fit the data and an energy of activation of 50,300 cal per mole is calculated from the temperature dependence of the parabolic rate law constants. Using the transition state theory of solid phase reactions, the entropies and free energies of activation of the rate-controlling process were calculated and the values compared to those of other metals.

The reactions of beryllium with nitrogen were studied over the temperature range of 650° to 925°C. Colored films were observed for two-hour reactions at 725°C and higher. The reaction was not sensitive to changes in the pressure and the parabolic rate law could be fitted to the data.

An energy of activation of 75,000 cal per mole was calculated over the temperature range of 725° to 925°C. This value is the highest energy of activation that we have observed and is close to ΔH_0^0 for the evaporation of beryllium. The entropies and free energies of activation were calculated from the temperature dependence of the parabolic rate law constants. Positive entropies were found.

A preliminary study of the reaction with hydrogen was made. No appreciable reaction was found over the temperature range of 300° to 780°C for a pressure of 2.3 cm of Hg.

The vapor pressure of beryllium was studied using the Langmuir method on as-received and vacuum-treated samples. Excellent agreement is found with the results of Holden, Speiser, and Johnston (12). The effect of oxide and nitride films on the vapor pressure was also studied. The vapor pressures are very strongly effected by the presence of oxide films and to a lesser extent by nitride films. An oxide film of 99 μg per cm^2 reduces the vapor pressure by a factor of 60, while a nitride film of 42 μg per cm^2 reduces the vapor pressure by a factor of 4.

Any discussion of this paper will appear in a Discussion Section, to be published in the June 1951 issue of the JOURNAL.

REFERENCES

1. E. BAUR AND R. BRUNNER, *Helv. Chim. Acta*, **17**, 958 (1934).

2. J. S. Dunn, *J. Chem. Soc.*, **1929,** 1149.
3. E. A. Gulbransen and K. Andrew, *J.* (*and Trans.*) *Electrochem. Soc.*, **96,** 364 (1949).
4. E. A. Gulbransen and K. Andrew, *J. Metals* (*Trans. Am. Inst. Mining Met. Engrs.*), **185,** 515 (1949).
5. E. A. Gulbransen and K. Andrew, *J. Metals* (*Trans. Am. Inst. Mining Met. Engrs.*), **185,** 741 (1949).
6. E. A. Gulbransen and K. Andrew, *J. Metals* (*Trans. Am. Inst. Mining Met. Engrs.*), **186,** 586 (1950).
7. E. A. Gulbransen, *Trans. Electrochem. Soc.*, **81,** 187 (1942).
8. E. A. Gulbransen, *Rev. Sci. Instruments*, **15,** 201 (1944).
9. E. A. Gulbransen and K. Andrew, *Ind. Eng. Chem.*, **41,** 2762 (1949).
10. E. A. Gulbransen, J. W. Hickman, and R. Ruka, Unpublished Measurements.
11. E. A. Gulbransen, *Trans. Electrochem. Soc.*, **83,** 301 (1943).
12. R. B. Holden, R. Speiser, and H. L. Johnston, *J. Am. Chem. Soc.*, **70,** 3897 (1948).
13. H. L. Johnston and A. L. Marshall, *J. Am. Chem. Soc.*, **62,** 1382 (1940).
14. K. K. Kelley, *U. S. Bur. Mines Bull.*, **1937,** 407.
15. T. N. Krylova, *Izvest. Akad. Nauk S. S. S. R., Atdel. Tech. Nauk*, **1938** (10), 89; *Khim. Referat. Zhur.*, **6,** 122 (1939); *C. A.*, **34,** 4034[8] (1940).
16. I. Langmuir, *Phys. Rev.*, **2,** 329 (1913).
17. A. L. Marshall, R. W. Dornte, and F. J. Norton, *J. Am. Chem. Soc.*, **59,** 1161 (1937).
18. N. F. Mott, *Trans. Faraday Soc.*, **36,** 472 (1940).
19. N. F. Mott, *J. Inst. Metals*, **72,** 367 (1946).
20. "Natl. Bur. Standards Tables of Selected Values of Thermodynamic Properties," Washington.
21. H. Nitka, *Naturwissenschaften*, **29,** 336 (1941).
22. E. A. Owen and L. Pickup, *Phil. Mag.*, **20,** 1155 (1935).
23. N. B. Pilling and R. E. Bedworth, *J. Inst. Metals*, **29,** 529 (1923).
24. R. Schuman and A. B. Garrett, *J. Am. Chem. Soc.*, **66,** 442 (1944).
25. D. P. Smith, "Hydrogen in Metals," University of of Chicago Press, Chicago, Ill. (1948).
26. M. V. Stackelberg and R. Paulus, *Z. physik. Chem.*, **22B,** 305 (1933).
27. G. Tammann and W. Köster, *Z. anorg. u. allgem. Chem.*, **123,** 196 (1922).
28. H. N. Terem, *Bull. soc. Chim.* [5], **6,** 664 (1939).
29. H. N. Terem, *Rev. faculté sci. univ. Istanbul*, **8A** (1), 9 (1943); *C. A.*, **38,** 4182[6] (1944).
30. M. de Kay Thompson, "The Total and Free Energies of Formation of the Oxides of Thirty-Two Metals," The Electrochemical Society, Inc., New York (1942).
31. M. Tzentnershver and M. Blumenthal, *Bull. intern. acad. polon. sci. Classe sci. math. nat.*, **1935A,** 540; *C. A.*, **30,** 5862[9] (1936).
32. A. C. Vivian, *Trans. Faraday Soc.*, **22,** 211 (1926).
33. C. Wagner and K. Grünewald, *Z. physik. Chem.*, **40B,** 455 (1938).
34. S. Yamaguchi, *Bull. Chem. Soc. Japan*, **18,** 53 (1943).
35. See discussion to papers (2) and (3), *Trans. Am. Inst. Mining Met. Engrs.*, **186,** (1950).

The Kinetics of the Reactions of Vanadium with Oxygen and Nitrogen[1]

EARL A. GULBRANSEN AND KENNETH F. ANDREW

Westinghouse Research Laboratories, East Pittsburgh, Pennsylvania

ABSTRACT

A study is made of the reaction of rolled vanadium sheet with oxygen over the temperature range of 400° to 600°C using specimens weighing 0.1264 g and having a surface area of 1.4 cm². The data may be fitted to the parabolic rate law except for the initial period of the reaction. A plot of log K/T vs. $1/T$ gives an energy of activation of 30,700 calories per mole. The oxidation of vanadium may be compared to the corresponding reactions on columbium and tantalum since the oxide is soluble at high temperatures and the extent of reaction is of the same order of magnitude.

The reaction with nitrogen is studied over the temperature range of 600° to 900°C. The rate of reaction with nitrogen is much less at a given temperature than the corresponding oxidation reaction. The nitrogen reaction is similar to that found for columbium and tantalum in the magnitude of the reaction and in the fact that the nitride film dissolves in the metal as fast as it is formed. The data may be fitted to the parabolic rate law.

INTRODUCTION

Studies have been made on the kinetics of the gas phase reactions of zirconium (9, 10), titanium (9, 11), columbium (9, 12), tantalum (9, 12), and beryllium (13). This paper reports similar work with vanadium.

Thermodynamically vanadium can form the stable oxides V_2O_2, V_2O_3, and V_2O_4, a stable nitride VN, and perhaps a stable carbide. From a kinetic point of view one may predict from an analogy with columbium and tantalum that vanadium reacts with oxygen and hydrogen readily at low temperatures (below 500°C) and nitrogen above this temperature, the nitrogen dissolving in the metal. According to the rule of Pilling and Bedworth (29) vanadium should form a protective oxide since the ratio of the molecular volume of the oxide to the metal is 1.715.

Vanadium forms five oxides: VO(V_2O_2), V_2O_3, V_2O_4, $V_{12}O_{26}$, and V_2O_5. According to Mathewson, Spire, and Samans (25) V_2O_2 has the face-centered cubic lattice with an a_o value of 4.081 Å. These authors were unable to find a lower oxide. V_2O_2 was found to reduce FeO at elevated temperatures. VO has been formed (7) by partial oxidation of VN or by decomposition of ammonium vanadate. It forms solid solutions with VN, the lattice parameters varying with the concentration of VN.

Preparations between V_2O_3 and V_2O_5 have been studied by Hoschek and Klemm (19). Alpha, beta, and gamma phases were found between VO_2 and V_2O_3. The beta phase has the composition $VO_{1.75}$. The gamma phase V_2O_3 was found (35) to have the rhombohedral corundum structure with $a_{Rh} = 5.45 \pm 0.03$ Å and $\alpha = 53° 49' \pm 8'$. The calculated density is 5.04.

The alpha phase is homogeneous between $VO_{1.83}$ and $VO_{2.00}$. Its structure has not been studied although thermodynamic data have been reported on the oxide (2, 5, 20).

Aebi (1) studied the compositions lying between V_2O_4 and V_2O_5 and observed a new oxide corresponding to $VO_{2.17}$. It had a monoclinic structure with $a_o = 11.90$ Å, $b_o = 3.67$ Å, $c_o = 10.12$ Å, and $\beta = 100° 52'$. The density indicates a formula $V_{12}O_{26}$. It was prepared by reduction of V_2O_5 with sulfur dioxide.

Ketelaar (24) found that V_2O_5 has the orthorhombic structure with $a_o = 11.48 \pm 0.01$ Å, $b_o = 4.36 \pm 0.005$ Å, and $c_o = 3.55 \pm 0.005$ Å.

McAdam and Geil (26) made a temper-color study on the oxidation of vanadium at a number of temperatures. A study of the time at 400°C to achieve the first order blue oxide indicated that vanadium oxidizes slower than columbium, zirconium, and iron, but faster than tantalum.

Becker and Ebert (4) found that VN obeys the cubic NaCl arrangement. The most reliable value for a_o is due to Epelbaum and Breger (8) and equals 4.129 ± 0.001 Å, in agreement with the value found by Dawihl and Rix (6). No information is available on the kinetics of the nitrogen reaction.

No hydride has been reported (31).

[1] Manuscript received May 1, 1950. This paper prepared for delivery before the Cleveland Meeting, April 19 to 22, 1950.

Thermodynamic Calculations

The chemical equilibrium may be calculated as a function of temperature from free energy expressions when the reaction products are the oxide and nitride. See Table I.

The logarithms of the equilibrium gas pressures or pressure ratios are tabulated as a function of the temperature in °C for the several reactions. For those reactions involving solid phases alone or for reactions involving complex equilibrium expressions

TABLE I. *Equilibrium reactions on vanadium reactions*

Reaction	References
(1) $2V(s) + 3/2\ O_2(g) \rightleftarrows V_2O_3(s)$	2, 23, 30
(2) $2V(s) + 2O_2(g) \rightleftarrows V_2O_4(s)$	2, 23, 30
(3) $2V(s) + \frac{5}{2}\ O_2(g) \rightleftarrows V_2O_5(s)$	2, 23, 30
(4) $V(s) + \frac{1}{2}\ N_2(g) \rightleftarrows VN\ (s)$	20, 23
(5) $V_2O_3(s) + \frac{1}{2}\ O_2(g) \rightleftarrows V_2O_4(s)$	2, 23, 30
(6) $V_2O_4(s) + \frac{1}{2}\ O_2(g) \rightleftarrows V_2O_5(s)$	2, 23, 30
(7) $V_2O_3(s) + 3H_2(g) \rightleftarrows 2V(s) + 3H_2O(g)$	2, 22, 23, 30
(8) $V_2O_4(s) + 4H_2(g) \rightleftarrows 2V(s) + 4H_2O(g)$	2, 22, 23, 30
(9) $V_2O_5(s) + 5H_2(g) \rightleftarrows 2V(s) + 5H_2O(g)$	2, 22, 23, 30
(10) $V_2O_3(s) + 3CO(g) \rightleftarrows 2V(s) + 3CO_2(g)$	2, 22, 23, 30
(11) $V_2O_4(s) + 4CO(g) \rightleftarrows 2V(s) + 4CO_2(g)$	2, 22, 23, 30
(12) $V_2O_5(s) + 5CO(g) \rightleftarrows 2V(s) + 5CO_2(g)$	2, 22, 23, 30
(13) $4V_2O_5(s) + 2V(s) \rightleftarrows 5V_2O_4(s)$	2, 23, 30
(14) $3V_2O_4(s) + 2V(s) \rightleftarrows 4V_2O_3(s)$	2, 23, 30
(15) $V(s) + NH_3(g) \rightleftarrows VN(s) + \frac{3}{2}\ H_2(g)$	2, 21, 23, 30
(16) $V_2O_3(s) + 2NH_3(g) \rightleftarrows 2V(s) + 3H_2O(g) + N_2(g)$	2, 21, 22, 23, 30
(17) $V_2O_4(s) + \frac{8}{3}\ NH_3(g) \rightleftarrows 2V(s) + 4H_2O(g) + \frac{4}{3}\ N_2(g)$	2, 21, 22, 23, 30
(18) $V_2O_5(s) + \frac{10}{3}\ NH_3(g) \rightleftarrows 2V(s) + 5H_2O(g) + \frac{5}{3}\ N_2(g)$	2, 21, 22, 23, 30
(19) $V_2O_3(s) + 2NH_3(g) \rightleftarrows 2VN(s) + 3H_2O(g)$	2, 21, 22, 23, 30
(20) $V_2O_4(s) + \frac{8}{3}\ NH_3(g) \rightleftarrows 2VN(s) + 4H_2O(g) + \frac{2}{3}\ N_2\ (g)$	2, 21, 22, 23, 30
(21) $V_2O_5(s) + \frac{10}{3}\ NH_3(g) \rightleftarrows 2VN(s) + 5H_2O(g) + \frac{4}{3}\ N_2(g)$	2, 21, 22, 23, 30

Temp	(1) $-\log p_{O_2}$	(2) $-\log p_{O_2}$	(3) $-\log p_{O_2}$	(4) $-\log p_{N_2}$	(5) $-\log p_{O_2}$	(6) $-\log p_{O_2}$	(7) $-\log p_{H_2O}/p_{H_2}$	(8) $-\log p_{H_2O}/p_{H_2}$	(9) $-\log p_{H_2O}/p_{H_2}$	(10) $-\log p_{CO_2}/p_{CO}$	(11) $-\log p_{CO_2}/p_{CO}$
°C											
25	135.5	116	100	51.3	58	36	27.6	17.9	9.9	22.6	12.95
200	81.8	69.5	59.6	28.9	33	20	16.5	10.4	5.4	14.1	8.05
400	54.9	46.3	39.4	17.6	20.4	12	11.2	6.85	3.4	10.1	5.75
600	40.3	34.1	28.4	11.5	15.4	5.6	8.2	5.1	2.25	7.8	4.7
800	31.1	26.25		7.6	11.6		6.4	3.95		6.4	3.9
1000	25.1	21.0		5.1	8.8		5.3	3.2		5.4	3.4
1200	20.5	17.1		3.2	6.8		4.4	2.7		4.8	3.15
1400	17.3	14.4		1.8	5.6		3.9	2.4		4.7	2.9

Temp	(12) $-\log p_{CO_2}/p_{CO}$	(13) $+\log K$	(14) $+\log K$	(15) $+\log K$	(16) $+\log K$	(17) $+\log K$	(18) $+\log K$	(19) $+\log K$	(20) $+\log K$	(21) $+\log K$
°C										
25	4.95	160	116	22.75	−88.5	−79.3	−59.1	−37.2	−28.1	−7.9
200	3.1	99	73	14.6	−49.1	−37.3	−21.9	−20.2	−12.3	+2.2
400	2.3	68.6	51.8	10.6	−29.8	−22.5	−10.8	−12.1	−4.8	+6.7
600	0.5	57	37.4	8.6	−19.1	−12.9	−1.9	−7.5	−1.4	+9.7
800			29.3	7.3	−12.3	−6.6		−4.7	+1.1	
1000			24.4	6.4	−8.1	−2.6		−2.9	+2.5	
1200			20.6	5.8	−5.7	+0.4		−1.6	+3.6	
1400			17.6	5.3	−2.7	+2.2		−0.9	+4.1	

Four types of reactions have been considered: (1) direct formation of the several oxides and nitrides, (2) equilibrium between the several oxides and oxygen, (3) equilibrium between the several oxides and metal, and (4) reduction of the oxides by hydrogen, carbon monoxide, and ammonia.

the logarithms of the equilibrium constant K are tabulated.

The results show the following: (1) V_2O_3, V_2O_4, and V_2O_5 essentially do not decompose to metal and oxygen from 25° to 1400°C in high vacuum; (2) V_2O_5 decomposes to V_2O_4 and O_2 in high vacuum above

500°C; (3) VN may be formed by reaction with nitrogen or ammonia and is stable up to 800°C in high vacuum; (4) V_2O_3 cannot be reduced by hydrogen below 1200°C while V_2O_4 cannot be reduced below 800°C; (5) V_2O_5 may be reduced readily above 400°C; (6) the reduction of the oxides by carbon monoxide without the formation of a carbide are similar to the reduction reactions with hydrogen; (7) the reductions of the oxides with ammonia to form the nitride are more feasible than the corresponding hydrogen and carbon monoxide reductions; and (8) the solid phase reactions of vanadium with the higher oxides to form V_2O_3 are feasible at all temperatures.

The calculations shown in Table I involve certain errors since the data are based on experimental heats of reaction. Since vanadium forms a number of oxides, the extraction of the appropriate values for a particular oxide may lead to errors of the order of ±2000 calories for the heat of reaction alone. These calculations should be used to indicate trends rather than precise values since the degree of error is hard to estimate.

TABLE II. *Chemical and spectrographic analyses of vanadium*

Chemical analyses	%	Spectrographic analyses	%
V	99.7	Mg	≈0.001
N_2	0.1	Ni	<0.0001
O_2	0.06	B	<0.0001
Ca	0.06	U	<0.0001
Fe	0.013		

Apparatus, Method, and Materials

A vacuum microbalance and associated equipment was used for all of the kinetic measurements (15, 16). The sensitivity of the balance is 1.00 divisions per microgram and the weight change can be estimated to 0.25 microgram. The experimental procedures and the purification of O_2, N_2, and H_2 have been described (10, 13, 15, 16).

The vanadium metal used came[2] in two strips 8.5 mils and 15 mils thick. The vanadium was made by calcium reduction of the oxide followed by pressing, vacuum sintering, and warm rolling. Table II shows a chemical and spectrographic analysis of the metal.

The specimens cut from the sheets had surface areas of 2.59 cm² for the 8.5-mil sheet and 1.38 cm² for the 15-mil sheet and weighed 0.1255 gram.

They were abraded, starting with number one grit paper and finishing with 4/0 paper, the last two stages of the abrading being carried out under purified kerosene. The kerosene was removed by washing in soap and water, petroleum ether, and finally with absolute alcohol. They were kept in a dessicator prior to use.

[2] Obtained from the Westinghouse Corporation, Bloomfield, New Jersey, Laboratories.

Results and Discussion

High Vacuum Reaction

Since the oxides of vanadium are not reducible to the metal with hydrogen or carbon monoxide, it is impossible to prepare oxide free surfaces by direct reduction. The procedure adopted minimized formation of oxide films in the abrading process and in heating the specimen to the reaction temperature. The latter operation requires rapid heating in the best of vacua obtainable.

A heating experiment with vanadium showed that a 0.1255 g sample of vanadium lost a total of 6.9 μg between 300° and 700°C over a period of 100 minutes. No further weight change was noted on raising the temperature to 900°C. Above this temperature vanadium acted as a getter under the conditions of the experiment. After longer periods of pumping, no gettering action was noted at temperatures up to 1000°C.

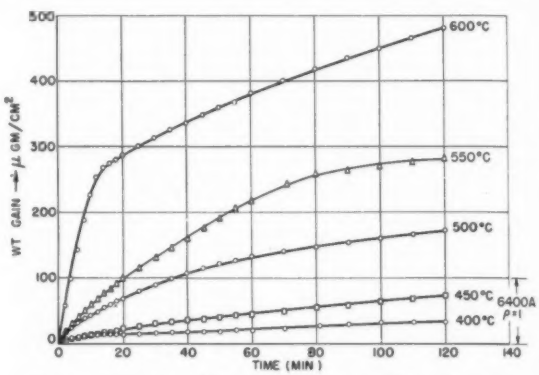

Fig. 1. Reaction of V with O_2, 7.6 cm, effect of temperature, abraded through 4/0.

Reaction with Oxygen

The reaction was studied as a function of time, temperature, and pressure, and the results are shown in Fig. 1 to 7 and Tables III to V. Assuming the ratio of the real to the measured area to be unity ($\rho = 1$) and the oxide to be V_2O_3 (14), the thickness of the oxide in Angstroms is related to the weight gain in micrograms per cm² by the factor 64.

Time and Temperature

Fig. 1 shows the time course of the oxidation experiments for the temperature range of 400° to 600°C for an oxygen pressure of 7.6 cm of Hg. The reaction was rapid initially but the rate decreased as the film

thickened. In this sense the oxide may be said to be protective.

Correlation of the film thickness and the color of the oxide film is shown in Table III. Colored films were observed for all of the runs.

Fig. 2 shows a comparison of the oxidation of vanadium with columbium, zirconium, tantalum, and titanium. Vanadium reacts with oxygen at 400°C and 7.6 cm pressure at a faster rate than titanium but slower than tantalum, zirconium, and columbium. The relative oxidation rates agree with those of McAdam and Geil (26) except for tantalum.

TABLE III. *Color vs. thickness, oxidation of vanadium*

Temp	Thickness		Color
	μg/cm²	Å ($\rho = 1$)	
°C			
400	28	1,790	straw-blue
450	71	4,500	straw
500	171	10,900	blue
550	282	18,050	blue-gray
600	366	23,400	blue
600	395	25,300	gray
600	481	30,800	gray

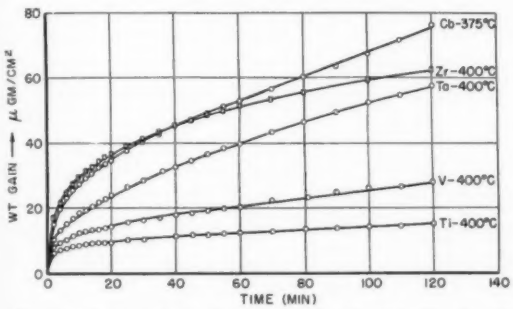

FIG. 2. Comparison of oxidation of V with Cb, Zr, Ta, and Ti.

Time and Temperature Equations

The parabolic rate law and its several modifications (27, 29, 34), the linear rate law, and the logarithmic rate law (32) have been used to interpret the time variation of the oxidation rate. The parabolic law relates the weight gain W to the time of reaction t by the following equation: $W^2 = Kt + C$ where K is the parabolic rate law constant and C is a constant. The constant K has been related to diffusion phenomena and is of fundamental interest in oxidation rate theory. The constant C, usually found by extrapolating the parabolic rate law to time $t = 0$, is as important as K since it may be used to express the initial variations from the parabolic rate law.

The temperature variation of the parabolic rate law constant K may be interpreted by either the Arrhenius equation or the transition state theory (18). The latter theory gives the following expression for K:

$$K = \frac{2kT}{h} \lambda^2 e^{\Delta S^*/R} e^{-E/RT} \qquad \text{(I)}$$

In this equation ΔS^* and E are the entropy change and energy of activation involved in forming the activated state, λ is the interatomic distance between diffusion sites, k is Boltzman's constant, h is Planck's constant, and R the gas constant.

An analysis of Fig. 1 shows that the data are not fitted by the linear rate law. Plots of the weight gain vs. the logarithm of the time show curves of increasing slope.

Fig. 3 shows that the oxidation of vanadium at 400°C and 7.6 cm of O_2 fits the parabolic rate law rather well, with some deviations in the initial stages. This type of deviation has been noted for other metals and has been predicted by Mott (28). At

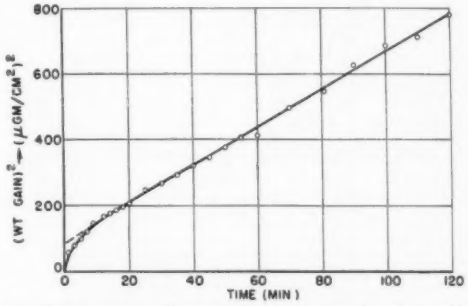

FIG. 3. Reaction of V with O_2, parabolic plot, 400° C, 7.6 cm O_2, abraded through 4/0.

600°C the reaction follows closely the predictions of the parabolic rate law after the initial stage of oxidation (Fig. 7). However, the initial part of the 600°C parabolic plot shows an S-shaped curve joining the straight line after 12 minutes of oxidation. Similar plots at 500° and 550°C show the same initial effect but the linear portion starts after longer periods of time.

The K values used in the analyses of the temperature effect are calculated from the straight line values for the 60 to 120 minute period of reaction except for the 550°C run where an average K value is calculated from the S-shaped curve.

It is to be expected that the initial stages of a surface reaction involving the formation of a film should not follow the long period parabolic rate law for the following reasons: (1) degassing of the metal, (2) change in the surface area as the reaction proceeds, (3) formation of a potential at the oxide to gas interface (27) which aids the diffusion of the metallic ion, (4) solution of gas in the metal, (5) the

500°C; (3) VN may be formed by reaction with nitrogen or ammonia and is stable up to 800°C in high vacuum; (4) V_2O_3 cannot be reduced by hydrogen below 1200°C while V_2O_4 cannot be reduced below 800°C; (5) V_2O_5 may be reduced readily above 400°C; (6) the reduction of the oxides by carbon monoxide without the formation of a carbide are similar to the reduction reactions with hydrogen; (7) the reductions of the oxides with ammonia to form the nitride are more feasible than the corresponding hydrogen and carbon monoxide reductions; and (8) the solid phase reactions of vanadium with the higher oxides to form V_2O_3 are feasible at all temperatures.

The calculations shown in Table I involve certain errors since the data are based on experimental heats of reaction. Since vanadium forms a number of oxides, the extraction of the appropriate values for a particular oxide may lead to errors of the order of ±2000 calories for the heat of reaction alone. These calculations should be used to indicate trends rather than precise values since the degree of error is hard to estimate.

TABLE II. *Chemical and spectrographic analyses of vanadium*

Chemical analyses	%	Spectrographic analyses	%
V	99.7	Mg	≈0.001
N_2	0.1	Ni	<0.0001
O_2	0.06	B	<0.0001
Ca	0.06	U	<0.0001
Fe	0.013		

Apparatus, Method, and Materials

A vacuum microbalance and associated equipment was used for all of the kinetic measurements (15, 16). The sensitivity of the balance is 1.00 divisions per microgram and the weight change can be estimated to 0.25 microgram. The experimental procedures and the purification of O_2, N_2, and H_2 have been described (10, 13, 15, 16).

The vanadium metal used came[2] in two strips 8.5 mils and 15 mils thick. The vanadium was made by calcium reduction of the oxide followed by pressing, vacuum sintering, and warm rolling. Table II shows a chemical and spectrographic analysis of the metal.

The specimens cut from the sheets had surface areas of 2.59 cm² for the 8.5-mil sheet and 1.38 cm² for the 15-mil sheet and weighed 0.1255 gram. .

They were abraded, starting with number one grit paper and finishing with 4/0 paper, the last two stages of the abrading being carried out under purified kerosene. The kerosene was removed by washing in soap and water, petroleum ether, and finally with absolute alcohol. They were kept in a dessicator prior to use.

[2] Obtained from the Westinghouse Corporation, Bloomfield, New Jersey, Laboratories.

Results and Discussion

High Vacuum Reaction

Since the oxides of vanadium are not reducible to the metal with hydrogen or carbon monoxide, it is impossible to prepare oxide free surfaces by direct reduction. The procedure adopted minimized formation of oxide films in the abrading process and in heating the specimen to the reaction temperature. The latter operation requires rapid heating in the best of vacua obtainable.

A heating experiment with vanadium showed that a 0.1255 g sample of vanadium lost a total of 6.9 μg between 300° and 700°C over a period of 100 minutes. No further weight change was noted on raising the temperature to 900°C. Above this temperature vanadium acted as a getter under the conditions of the experiment. After longer periods of pumping, no gettering action was noted at temperatures up to 1000°C.

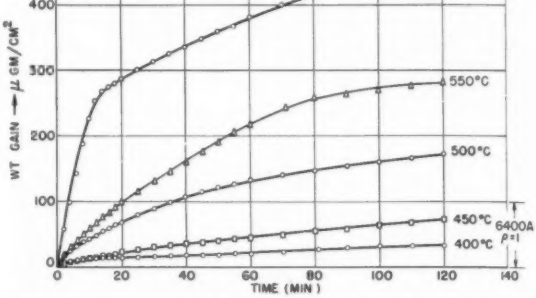

Fig. 1. Reaction of V with O_2, 7.6 cm, effect of temperature, abraded through 4/0.

Reaction with Oxygen

The reaction was studied as a function of time, temperature, and pressure, and the results are shown in Fig. 1 to 7 and Tables III to V. Assuming the ratio of the real to the measured area to be unity ($\rho = 1$) and the oxide to be V_2O_3 (14), the thickness of the oxide in Angstroms is related to the weight gain in micrograms per cm² by the factor 64.

Time and Temperature

Fig. 1 shows the time course of the oxidation experiments for the temperature range of 400° to 600°C for an oxygen pressure of 7.6 cm of Hg. The reaction was rapid initially but the rate decreased as the film

thickened. In this sense the oxide may be said to be protective.

Correlation of the film thickness and the color of the oxide film is shown in Table III. Colored films were observed for all of the runs.

Fig. 2 shows a comparison of the oxidation of vanadium with columbium, zirconium, tantalum, and titanium. Vanadium reacts with oxygen at 400°C and 7.6 cm pressure at a faster rate than titanium but slower than tantalum, zirconium, and columbium. The relative oxidation rates agree with those of McAdam and Geil (26) except for tantalum.

TABLE III. *Color vs. thickness, oxidation of vanadium*

Temp	Thickness		Color
	μg/cm²	Å ($\rho = 1$)	
°C			
400	28	1,790	straw-blue
450	71	4,500	straw
500	171	10,900	blue
550	282	18,050	blue-gray
600	366	23,400	blue
600	395	25,300	gray
600	481	30,800	gray

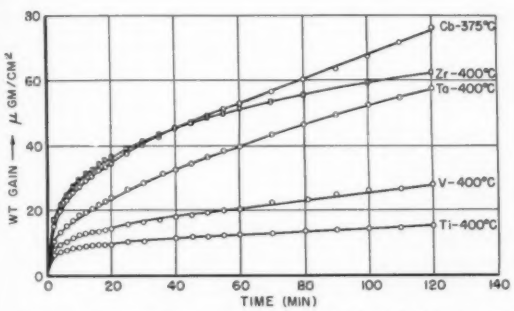

FIG. 2. Comparison of oxidation of V with Cb, Zr, Ta, and Ti.

Time and Temperature Equations

The parabolic rate law and its several modifications (27, 29, 34), the linear rate law, and the logarithmic rate law (32) have been used to interpret the time variation of the oxidation rate. The parabolic law relates the weight gain W to the time of reaction t by the following equation: $W^2 = Kt + C$ where K is the parabolic rate law constant and C is a constant. The constant K has been related to diffusion phenomena and is of fundamental interest in oxidation rate theory. The constant C, usually found by extrapolating the parabolic rate law to time $t = 0$, is as important as K since it may be used to express the initial variations from the parabolic rate law.

The temperature variation of the parabolic rate law constant K may be interpreted by either the Arrhenius equation or the transition state theory (18). The latter theory gives the following expression for K:

$$K = \frac{2kT}{h} \lambda^2 e^{\Delta S^*/R} e^{-E/RT} \qquad (I)$$

In this equation ΔS^* and E are the entropy change and energy of activation involved in forming the activated state, λ is the interatomic distance between diffusion sites, k is Boltzman's constant, h is Planck's constant, and R the gas constant.

An analysis of Fig. 1 shows that the data are not fitted by the linear rate law. Plots of the weight gain vs. the logarithm of the time show curves of increasing slope.

Fig. 3 shows that the oxidation of vanadium at 400°C and 7.6 cm of O_2 fits the parabolic rate law rather well, with some deviations in the initial stages. This type of deviation has been noted for other metals and has been predicted by Mott (28). At

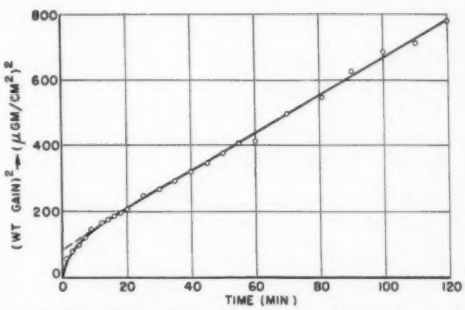

FIG. 3. Reaction of V with O_2, parabolic plot, 400° C, 7.6 cm O_2, abraded through 4/0.

600°C the reaction follows closely the predictions of the parabolic rate law after the initial stage of oxidation (Fig. 7). However, the initial part of the 600°C parabolic plot shows an S-shaped curve joining the straight line after 12 minutes of oxidation. Similar plots at 500° and 550°C show the same initial effect but the linear portion starts after longer periods of time.

The K values used in the analyses of the temperature effect are calculated from the straight line values for the 60 to 120 minute period of reaction except for the 550°C run where an average K value is calculated from the S-shaped curve.

It is to be expected that the initial stages of a surface reaction involving the formation of a film should not follow the long period parabolic rate law for the following reasons: (1) degassing of the metal, (2) change in the surface area as the reaction proceeds, (3) formation of a potential at the oxide to gas interface (27) which aids the diffusion of the metallic ion, (4) solution of gas in the metal, (5) the

effect of these dissolved gases on the transfer of ions and electrons into the oxide, and (6) concentration of impurities from the metal into the oxide during the initial stage of the reaction.

Let us consider each of these mechanisms in turn. The pre-reaction readings show no evidence of degassing which would tend to slow the initial reaction rate. Mechanisms 2, 3, and 4 would make K greater than the long period value.

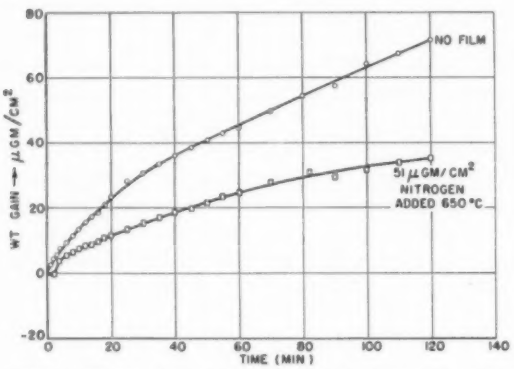

FIG. 4. Effect of nitride film on oxidation of V, 450° C, 7.6 cm O_2, abraded through 4/0.

TABLE IV. *Parabolic rate law constants, entropies, energies, and free energies of activation for the oxidation reaction*

Temp	K	ΔS^*	E	$-T\Delta S^*$	ΔF^*
°C	cm²/sec	cal/mole/°C	cal/mole	cal/mole	cal/mole
400	3.9×10^{-14}	−7.20	30,700	4840	35,540
450	3.5×10^{-13}	−6.14	30,700	4430	35,130
500	1.41×10^{-12}	−6.20	30,700	4790	35,490
550	4.84×10^{-12}	−7.17	30,700	5900	36,600
600	1.025×10^{-11}	−7.07	30,700	6160	36,860

It is difficult to test the effect of dissolved oxygen and nitrogen impurities since one cannot remove these from the metal. However, we have added to one specimen of vanadium at 650°C a total of 70.4 μg of nitrogen (51 μg per cm²) or 0.06 additional weight per cent. The original nitrogen content of the vanadium is 0.10 per cent. Fig. 4 shows a comparison of the oxidation at 450°C of the two samples. The additional nitrogen affects markedly the initial stage of the reaction as well as the ultimate reaction rate. A parabolic plot of this curve shows the characteristic increase of K to the constant value predicted by the parabolic rate law. However, the initial K values are only 30 per cent of the non-nitrided sample. There appears to be a definite correlation between previous nitride treatments and the oxidation rate.

Also, impurities may concentrate in the oxide film and dominate the reaction rate during the initial stage as appears to happen in the oxidation of beryllium and pure iron (13).

Temperature Dependence and Activation Energy

The energy of activation E, evaluated from a plot of $\log K/T$ vs. $1/T$ (Fig. 5), was 30,700 cal per mole between 400° and 600°C.

Table IV shows the values of the parabolic rate law constants and the energies, entropies, and free energies of activation of the rate-controlling process in the oxidation of vanadium. The temperature-independent factor, $e^{\Delta S^*/R}$ was evaluated from the transition state theory equation for K.

Table V shows a comparison of the parabolic rate law constants and the energies, entropies, and free energies of activation for vanadium, tantalum, titanium, and zirconium at 400°C and columbium at 375°C. From an oxidation resistance viewpoint vanadium at 400°C appears to be superior to tantalum, columbium, and zirconium, but not to titanium.

Pressure

The effect of oxygen pressure between 0.15 and 7.6 cm is shown in Fig. 6 for 600°C. The pressure appears to have a strong effect on the initial reaction rate although the long-time rates of reaction are approximately equal. This is best shown by an analyses of the parabolic rate law plots in Fig. 7. The 7.6 cm run shows an initial S-shaped curve which changes to the parabolic rate law after 12 minutes of oxidation. The 0.15 cm run shows a straight line over the complete time range although some evidence for an S-shaped curve is present during the initial stages of the reaction. The long period slope or K value is very similar for these two pressures although the 0.76 cm curve shows a constantly increasing slope.

TABLE V. *Comparison of the parabolic rate law constants and the energies, entropies, and free energies of activation*

	400°C				375°C
	V	Ta	Ti	Zr	Cb
K cm²/sec	3.9×10^{-14}	2.165×10^{-13}	6.67×10^{-15}	1.32×10^{-13}	1.06×10^{-12}
E cal/mole	30,700	27,400	26,000	18,200	22,800
ΔS^*entropy units	−7.20	−9.80	−18.8	−25.2	−12.25
ΔF^*cal/mole	35,540	34,000	38,100	35,200	30,750

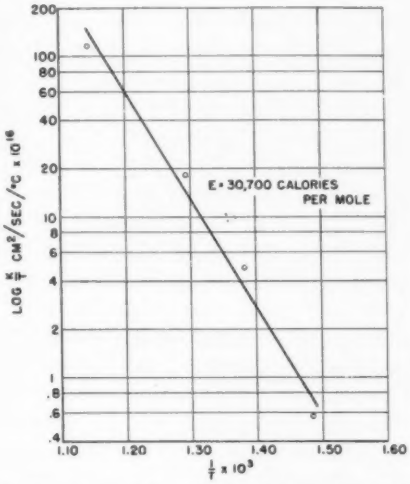

FIG. 5. Reaction of V with O_2, 7.6 cm, log K/T cm²/sec/° C vs. $1/T$ (400°–600° C).

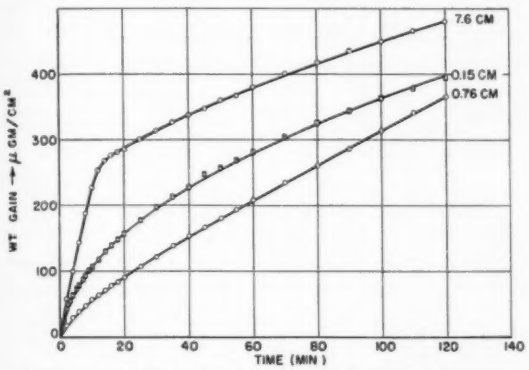

FIG. 6. Reaction of V with O_2, 600° C, effect of pressure abraded through 4/0.

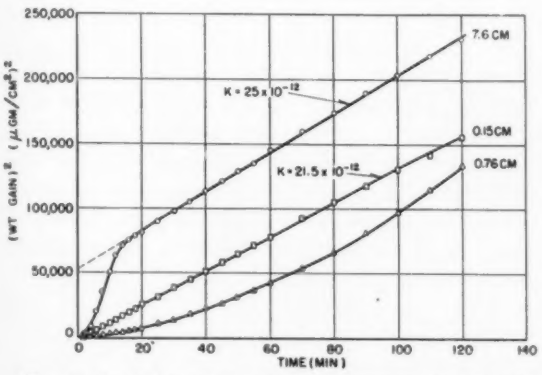

FIG. 7. Oxidation of V, effect of pressure, 600° C, 0.15 cm to 7.6 cm, parabolic plots.

Stability of the Oxide

The oxide formed at 600°C was heated slowly to 940°C in a vacuum of 10^{-6} mm of Hg or better. No evidence was found for decomposition (cf. Table I). However, the surface has a light metallic gray color which indicates that the oxide has dissolved in the metal.

Electron diffraction studies indicated that V_2O_3 was the oxide formed on the surface under the conditions of oxidation, although higher oxides may have disappeared by reaction with the vanadium following the evacuation treatment.

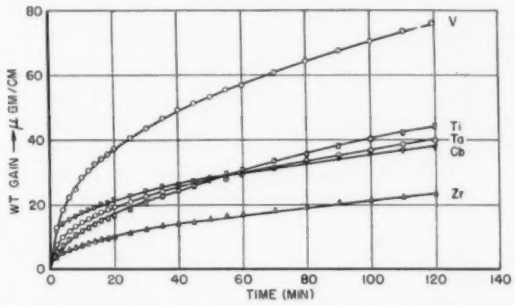

FIG. 8. Comparison nitriding reaction of V with Ti, Ta, Cb, and Zr, 700° C, 7.6 cm N_2.

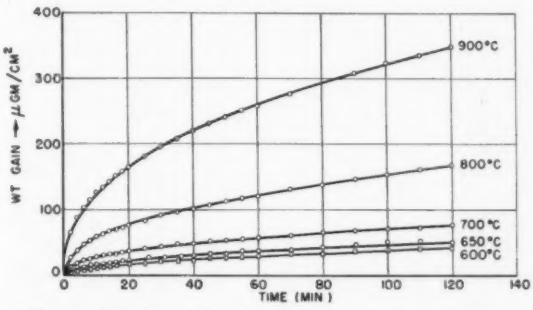

FIG. 9. Reaction of V with N_2, 7.6 cm, effect of temperature, abraded through 4/0.

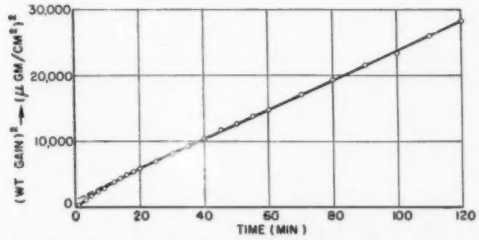

FIG. 10. Reaction of V with N_2, parabolic plot, 800° C, 7.6 cm N_2, abraded through 4/0.

Reaction with Nitrogen

The reactions of vanadium with a purified lamp grade of nitrogen were studied as a function of time, temperature, and pressure. The influence of oxygen pickup on the rate of nitriding and the stability of the nitride to thermal decomposition were also noted. The results are given in Fig. 8 to 13. Thickness calculations were not made because of solution of the nitrogen in the metal.

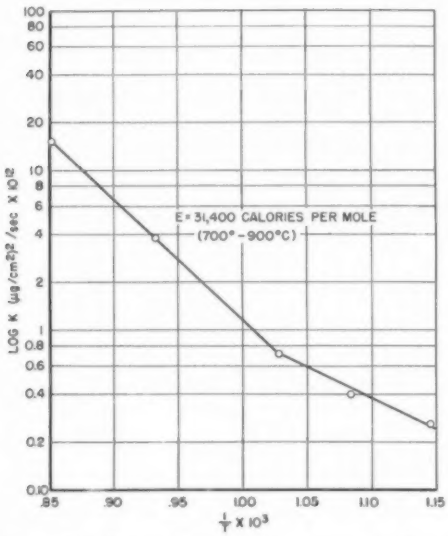

FIG. 11. Reaction of V with N_2, 7.6 cm, log K vs. $1/T$ (700°–900° C).

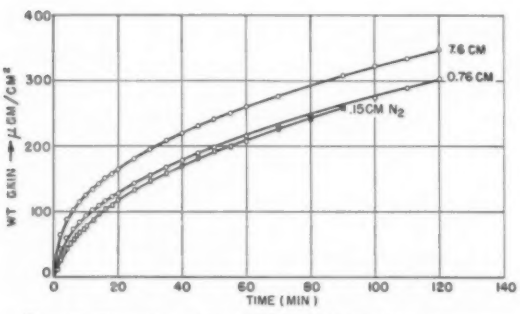

FIG. 12. Reaction of V with N_2, 900° C, effect of pressure, abraded through 4/0.

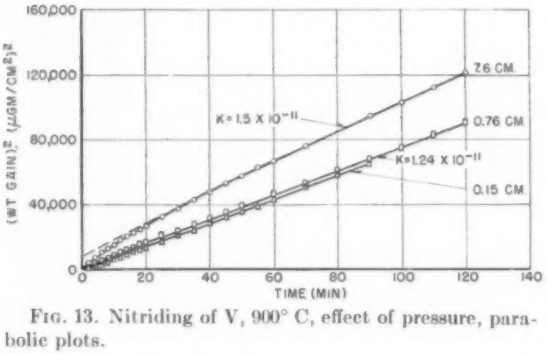

FIG. 13. Nitriding of V, 900° C, effect of pressure, parabolic plots.

Comparison of the Nitrogen Reaction on Vanadium with Titanium, Tantalum, Columbium, and Zirconium

Vanadium reacts with nitrogen faster than the other metals as seen from Fig. 8.

Time and Temperature

Fig. 9 shows that the reaction rate of vanadium with purified lamp grade of nitrogen decreased with time for several temperatures. The temperature effect was uniform and appeared to follow an exponential law. For vanadium at 900°C a total reaction of 348 μg per cm² was observed in two hours while at 600°C 42.9 μg per cm² were obtained for a similar time. The shapes of these curves are similar to what has been observed in other nitrogen reactions (9, 10, 11, 12, 13).

Previous studies on nitriding reactions showed that the parabolic rate law was followed. A similar correlation is found for vanadium as seen from Fig. 10 for the 800°C run. The data fit a straight line except during the early stages of the reaction.

In other papers we have tried to explain the parabolic rate law for a reaction in which the reaction product is partially or completely soluble. We have not observed colored films in any of the nitriding experiments. The method of Van Liempt (33) was suggested to explain the time behavior of the nitriding reaction. Van Liempt used an approximate method for the solution of the diffusion equation for a flat plate:

TABLE VI. *Parabolic rate law constants nitrogen reaction*

Temp	Temp	$1/T \times 10^3$	K sec^{-1}	E
°C	°K		(g/cm²)²	cal/mole
600	873.1	1.14534	2.61×10^{-13}	
650	923.1	1.08342	3.97×10^{-13}	
700	973.1	1.02764	7.08×10^{-13}	31,400
800	1073.1	0.93188	3.75×10^{-12}	
900	1173.1	0.85247	1.50×10^{-11}	

$$Q/Q_o = \frac{8}{d}\sqrt{\frac{Dt}{\pi}}. \qquad \text{(II)}$$

Here Q is the quantity of gas taken up or evolved at any time t, Q_o is the original quantity of gas in the metal, D is the diffusion coefficient, and d is the thickness of the specimen. This expression holds for the reverse process of absorption of gas in the metal except Q_o is the solubility of gas in the metal. It reduces to the parabolic rate law

$$W^2/W_o^2 = Kt + C \qquad \text{(III)}$$

where W is the weight gain and W_o is the solubility at the temperature T. Since K involves the diffusion coefficient D and W_o is temperature dependent, it is impossible to evaluate D unless W_o is known. However, an empirical energy of activation for the reaction can be calculated.

Table VI shows the parabolic rate law constants

for the nitrogen reaction while Fig. 11 shows a logarithmic plot of the parabolic rate law constants K against $1/T$. The data can best be fitted by two straight lines. An empirical energy of activation of 31,400 cal per mole is obtained for the temperature range of 700° to 900°C. This value can be compared to an empirical energy of activation of 39,400 cal per mole for the tantalum reaction and 25,400 cal per mole for the corresponding columbium reaction.

Pressure

Fig. 12 shows the effect of nitrogen pressure, between 0.15 cm and 7.6 cm, on the time course of the reaction at 900°C. The effect is greatest in the initial part of the curve. The long period reaction rate is only slightly affected. In general, the effect of pressure is small compared to the predictions of the linear or square root of pressure laws (3).

Barrer (3) has discussed the influence of pressure on the permeability of gases. Two rate-pressure laws have been used to interpret the data. These are: (1) the linear rate law which is based on the mechanism of activated diffusion of nitrogen without dissociation, and (2) the square root law which is based on the mechanism of activated diffusion with dissociation.

The pressure dependence does not fit either of these rate laws and, therefore, the factor W_o in the rate expression is not influenced by the gas pressure following Henry's law. We have found similar behavior for the nitride on other metals (10, 11, 12). It is felt that a film of nitride is present during the reaction which prevents the operation of Henry's law. This film disappears upon removing the reacting gas since the solution process continues after the gas is removed.

Fig. 13 shows the effect of pressure on the parabolic rate law plots at 900°C. It is of interest to note that the long period rate law constants are in reasonable agreement. However the high pressure run at 7.6 cm of nitrogen gives an appreciable initial effect where K is greater than the long period value. The lower pressure runs fit the parabolic rate law nicely over the complete time range.

Stability of Nitrogen Reaction Product

To test the stability, a sample of vanadium was nitrided at 900°C for 2 hours. The uptake of nitrogen was 414 μg, corresponding to 1.2 atomic per cent of nitrogen. The sample was heated to 1000°C with no observable weight change or pressure change in the system. Thus, nitrogen in the vanadium structure was stable to decomposition in vacua of the order of 10^{-6} mm of Hg or better. Thermodynamic predictions show VN decomposing at 1000°C in high vacua.

Effect of Oxide in Nitrogen Reaction

Oxygen was added at 450°C to the extent of 98.2 μg (72 μg per cm²), corresponding to 0.245 atomic per cent of oxygen. Fig. 14 shows the effect of this addition on the rate of reaction. Oxygen increased the initial reaction rate although the final reaction rate was only slightly affected. The specimen containing the additional oxide gave a K value of 4.67×10^{-12} while the as-received specimen gave a K value of 3.75×10^{-12}. The addition of oxide in solid solution increases the reaction rate. This is in contrast to the effect of nitride on the oxidation reaction.

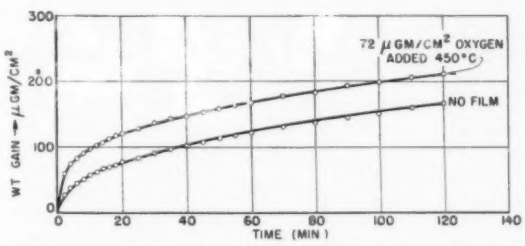

FIG. 14. Reaction of V with N_2, 800° C, 7.6 cm N_2, effect of oxide, abraded through 4/0.

SUMMARY

The reactions of vanadium with oxygen and nitrogen were studied using the vacuum microbalance method.

Thermodynamic calculations were made on the following reactions: (1) decomposition of the several oxides and the nitride, (2) the equilibrium between the several oxides and oxygen, (3) the equilibrium between vanadium and the oxides, and (4) the reduction of the oxides by H_2, CO, and NH_3.

Heating vanadium samples in high vacua showed a loss in weight initially. No reaction was observed with the gases in the vacuum system up to a temperature of 900°C.

The reaction of vanadium with oxygen was studied over the temperature range of 400° to 600°C. Colored films were observed and the parabolic rate law was found to fit the data. However, an initial deviation was observed. A plot of log K/T vs. $1/T$ gave an energy of activation of 30,700 cal per mole. The entropies and free energies of activation were calculated from the transition state theory. Negative entropies of activation were observed. It was shown that vanadium oxidizes faster than titanium but slower than tantalum, columbium, and zirconium.

The reaction of vanadium with nitrogen was

studied over the temperature range of 600° to 900°C. The parabolic rate law fitted the data. The method of Van Liempt was used to derive the parabolic rate law.

The nitrogen reaction was not sensitive to pressure. Since colored films were not observed, it was assumed that a nitride film was present during the reaction but dissolved upon removing the gas. The nitride was stable to 1000°C.

A comparison of the rates of nitriding indicates that vanadium reacts faster than zirconium, titanium, columbium, and tantalum.

Any discussion of this paper will appear in a Discussion Section, to be published in the June 1951 issue of the JOURNAL.

REFERENCES

1. F. AEBI, *Helv. Chim. Acta*, **31**, 8 (1948).
2. C. T. ANDERSON, *J. Am. Chem. Soc.*, **58**, 564 (1936).
3. R. M. BARRER, "Diffusion In and Through Solids," Cambridge University Press, London (1941).
4. K. BECKER AND F. EBERT, *Z. Physik*, **31**, 269 (1925).
5. O. A. COOK, *J. Am. Chem. Soc.*, **69**, 331 (1947).
6. W. DAWIHL AND W. RIX, *Z. anorg. u. allgem. Chem.*, **244**, 191 (1940).
7. V. A. EPELBAUM AND A. KH. BREGER, *J. Phys. Chem. U. S. S. R.*, **20**, 459 (1946). See *C. A.*, **41**, 27g (1947).
8. V. EPELBAUM AND A. KH. BREGER, *Acta Physicochim. U. R. S. S.*, **13**, 600 (1940).
9. E. A. GULBRANSEN AND K. ANDREW, *J. (and Trans.) Electrochem. Soc.*, **96**, 364 (1949).
10. E. A. GULBRANSEN AND K. ANDREW, *J. Metals (Trans. Am. Inst. Mining Met. Engrs.)*, **185**, 515 (1949).
11. E. A. GULBRANSEN AND K. ANDREW, *J. Metals (Trans. Am. Inst. Mining Met. Engrs.)*, **185**, 741 (1949).
12. E. A. GULBRANSEN AND K. ANDREW, *J. Metals (Trans. Am. Inst. Mining Met. Engrs.)*, **186**, 586 (1950).
13. E. A. GULBRANSEN AND K. ANDREW, *J. Electrochem. Soc.*, **97**, 383 (1950).
14. E. A. GULBRANSEN AND R. RUKA, Unpublished Measurements.
15. E. A. GULBRANSEN, *Trans. Electrochem. Soc.*, **81**, 187 (1942).
16. E. A. GULBRANSEN, *Rev. Sci. Instruments*, **15**, 201 (1944).
17. E. A. GULBRANSEN AND K. ANDREW, *Ind. Eng. Chem.*, **41**, 2762 (1949).
18. E. A. GULBRANSEN, *Trans. Electrochem. Soc.*, **83**, 301 (1943).
19. E. HOSCHEK AND W. KLEMM, *Z. anorg. u. allgem. Chem.*, **242**, 63 (1939).
20. K. IWASE AND N. NASU, *Sci. Repts. Tôhoku Imp. Univ.*, Honda Anniversary, **1936**, 476–9.
21. K. K. KELLEY, *U. S. Bur. Mines Bull.*, **407**, 42, 28 (1937).
22. K. K. KELLEY, *U. S. Bur. Mines Bull.*, **384**, 5 (1935).
23. K. K. KELLEY, *U. S. Bur. Mines Bull.*, **476**, 198–201 (1949).
24. J. A. A. KETELAAR, *Z. Krist.*, **95A**, 9 (1936).
25. C. H. MATHEWSON, E. SPIRE, AND C. H. SAMANS, *Trans. Am. Soc. Steel Treating*, **20**, 357 (1932).
26. D. J. MCADAM AND G. G. GEIL, *J. Research Natl. Bur. Standards*, **28**, 593 (1942).
27. N. F. MOTT, *Trans. Faraday Soc.*, **36**, 472 (1940).
28. N. F. MOTT, *J. Inst. Metals London*, **12**, 367 (1946).
29. N. B. PILLING AND R. E. BEDWORTH, *J. Inst. Metals*, **29**, 529 (1923).
30. H. SIEMONSON AND H. ULICK, *Z. Elektrochem.*, **46**, 141 (1940).
31. D. P. SMITH, "Hydrogen in Metals," University of Chicago Press, Chicago (1948).
32. G. TAMMANN AND W. KÖSTER, *Z. anorg. u. allgem. Chem.*, **123**, 196 (1922).
33. J. VAN LIEMPT, Quoted by Barrer (reference 4).
34. C. WAGNER AND K. GRÜNEWALD, *Z. physik. Chem.*, **40B**, 455 (1938).
35. W. H. ZACHARIASEN, *Strukturbericht II*, p. 310.

The Separation of Simple Electrolytes in Solution by an Electro-Gravitational Method[1]

GEORGE W. MURPHY

Department of Chemistry, University of Wisconsin, Madison, Wisconsin

ABSTRACT

The practicality of electrolyte separation by combined effects of electrolysis, electromigration, and convection in cells with suitable reversible electrode systems is demonstrated. The cell consists essentially of vertical silver-silver chloride electrodes between which an aqueous solution of one or more chlorides is contained. Passage of current results in a horizontal concentration and density gradient, which, in turn, leads to a convection current and the concentration of electrolyte species in a bottom chamber. Progress of the separation is followed continuously by conductivity measurements in the case of the single electrolytes NaCl and HCl. Mixtures of these two are analyzed continuously by both conductance and pH measurements. Separations obtained are strikingly large, and the faraday efficiency of the process is reasonably high. Theoretical aspects and applications of the method are discussed.

INTRODUCTION

Some time ago it occurred to the writer that an electrolytic cell might be designed for separation of simple electrolytes in solution, utilizing combined effects of electrolysis, electromigration, and convection. Such a cell would be similar in appearance and analogous in principle to the Clusius thermal diffusion column (1). The electrolyte would be contained between two closely-spaced vertical reversible electrodes; a horizontal concentration, and hence density, gradient would be established by passage of electric current, and a convection current thus begun, resulting in concentration of electrolyte species in a chamber below the electrodes. Partial separation of two electrolyte species could also be accomplished because of differences in ion mobility.

Kirkwood, *et al.* (2) have successfully applied the principle of electrophoresis-convection to the separation of proteins. In their work, the protein is contained between vertical electrodes in a sac permeable to simple ions, but impermeable to the protein. Passage of current through the cell results in concentration of the protein in the lower regions of the sac. Irreversible electrode systems were employed, and their nature is of little consequence, since the material to be separated is in a separate chamber removed from the electrodes. The separation of simple electrolytes requires a considerably different experimental approach.

The separation of ions by electromigration without convection has been in practice for many years, as embodied in the well-known moving boundary technique. The method appears to have been extended almost to the limit in the countercurrent electromigration experiments of Brewer, *et al.* (3).

The combination of electromigration with convection would seem to offer possibilities for improved separations, due to the cascading of a number of elementary separations, in analogy to thermal diffusion-convection, and also to liquid-vapor fractionations.

In the following, practical electro-gravitational cells are described, and the results of some experimental measurements on the separation of simple electrolytes are recorded. The magnitude of the effect is shown to be large, a factor which suggests a number of applications.

EXPERIMENTS WITH CELL I

The choice of electrode and electrolyte material is of fundamental importance in the method. Electrodes of the reversible type must be employed, since convection is to occur at the electrode-electrolyte boundary; gassing would destroy the convection currents. An electrolyte to be separated should have an ion which is involved in the reversible electrode reaction. The Ag, AgCl, Cl^- electrode system was selected for initial study because of its well-known reversibility, and because of its particular utility for cation separation.

The first successful experimental cell is shown in Fig. 1. The electrodes C and D are fine silver concentric tubes[2], 8 in. long. The radial separation is about $\frac{1}{16}$ in., and the mean diameter 1 in. Vessels A and B were made from 500 ml flasks. The neck and the Dewar-sealed glass spacer tubes were made with

[1] Manuscript received April 13, 1950. This paper prepared for delivery before the Washington Meeting, April 8 to 11, 1951.

[2] Obtained from the A. T. Wall Company, Providence, Rhode Island.

precision-bore Pyrex tubing selected to fit the silver tubes closely. Specially machined spacers were used in sealing the glass to insure concentricity. Assembly of glass to silver was accomplished with the aid of Apiezon W wax. Openings in the two vessels are for adding and removing solution, and for introducing detecting elements for pH or conductivity measurements.

A coating of silver chloride on the surface of each electrode was deposited electrolytically in half-normal HCl solution after assembly of the cell. Inasmuch as silver chloride is removed from the cathode and deposited on the anode during operation of the cell, it was anticipated that some means for current reversal must be provided in extended experiments, if the electrodes were to continue to function in a reversible manner. Early experiments were performed on HCl-NaCl mixtures with manual reversal of current at definite time intervals. Some experiments were performed using a repeat cycle interval timer for current reversal. Power for cell operation was taken from a two-volt storage battery.

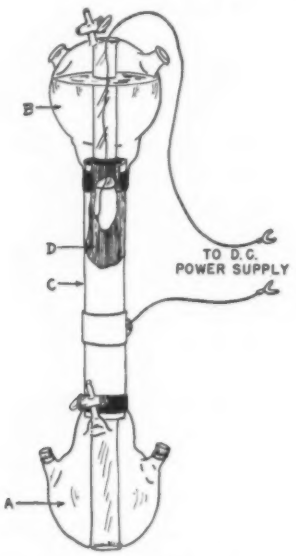

FIG. 1. Cell I

Experiments with Cell I demonstrated the soundness of the principle in a convincing manner. In all cases, convection currents were clearly visible in both upper and lower chambers during the early parts of the experiments. Extended experiments with 0.5N NaCl solution and with 0.35N HCl solution resulted in separation factors c_b/c_t of 20 and 11.5 respectively, where c_b is the concentration in the bottom chamber, and c_t in the top chamber. Experiments with HCl-NaCl mixtures demonstrated that the HCl was removed from the upper chamber much faster than was the NaCl.

Since the above separations were covered later in experiments with Cell II under more closely controlled conditions, they are not described in detail here.

The desirability for a new cell design soon became apparent for three reasons: (1) Under the conditions of operation which had been adopted, the bottom portions of the electrodes had a tendency to short out, due to accumulation of a loose mixture of silver and silver chloride between the electrodes after extended periods. It was felt that the difficulty could be avoided with a wider electrode spacing. (2) The efficiency seemed to be impaired by the necessity for frequent currrent reversal. A greater effective electrode area would allow the deposition of more silver chloride and thus extend the time of a current cycle. Later results with Cell II, however, showed that the amount of electrode material per unit apparent area is by no means the only determining factor in allowable cycle time. (3) The relatively large reservoirs at top and bottom made the time of experiments to a steady state condition inconveniently long.

It was also observed that control of applied voltage was more important than the exact specification of cycle time. This led to a modified method of current reversal based on rising cell potential as cell resistance increased. In particular, if the cell potential rises too high, gassing can be expected.

In closing the subject of Cell I, we note that subsequent experiments have pointed the way toward modified conditions for operating the cell in a satisfactory manner.

Experiments with Cell II

Fig. 2 shows a cell developed along the lines suggested above. C and D are electrodes of fine silver wire mesh, 30 mesh x 0.012 in. diameter wire, 10 in. long each. D consists of two layers of mesh constructed on a form so as to fit snugly in the outer Pyrex tube A, of 1.5 in. OD. The latter was not precision bore, but was selected from stock tubing. C consists of three layers of mesh constructed so as to fit snugly around precision bore tubing B, of $\frac{7}{8}$ in. OD. Radial separation of the electrodes was about $\frac{1}{8}$ in. Fabrication of the silver mesh tubes was accomplished by fine silver brazing. Particular care was exercised in attaching silver lead wires to each electrode. The two Pyrex tubes were Dewar-sealed with the aid of machined spacers to insure concentricity. Before assembly, each electrode was impregnated with freshly precipitated silver chloride. This technique proved to be just as effective as electrolytic deposition.

Fig. 3 shows the means by which progress of the

separation in the upper chamber was followed. The solution flows with the aid of the air lift pump, first through a conductance cell and then through a chamber for pH measurement. The latter was useful only when mixtures of HCl and NaCl were being studied.

The circuit employed for current reversal is shown in Fig. 4. A precision adjustment relay is energized by an applied potential of 0.8 volt or higher, as

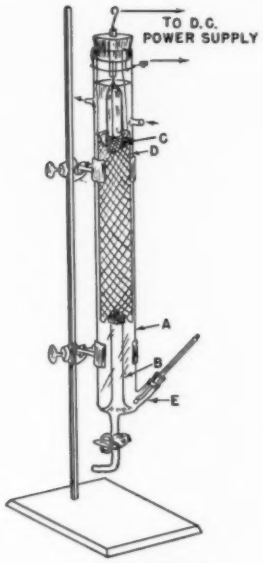

FIG. 2. Cell II

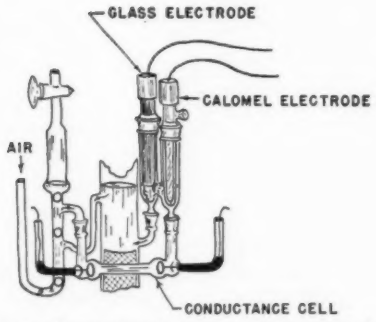

FIG. 3. Continuous analysis system for upper chamber of Cell II.

selected by a series rheostat. Closure of the relay contact starts the timing motor, which introduces a time delay of one minute in the cycle before the reversing switch is closed for a definite polarity. The potential applied to the cell will be below the set point of the relay, because of the low cell resistance at the beginning of a cycle. The resistance of the cell will gradually rise because of polarization effects, the relay will again be energized, and the next half cycle will begin. The time delay at the end of a cycle is introduced in order to allow any convection which has begun substantially to run its course.

Much experimental work had been done before the effect of contact and lead resistances on voltage readings was fully realized. Thus, the reading on the instrument voltmeter (Fig. 4), which corresponds to the voltage at the current reversing relay, is not representative of the voltage at the electrodes, since there are substantial relative drops in voltage in the contacts and leads. Starting voltages at the electrodes as measured subsequently with a separate meter were only 0.14 to 0.26 volt, corresponding to 0.5 volt on the instrument meter. Total contact and lead resistance of the order of only 0.05 ohm would be sufficient to account for the discrepancy. The minimization of contact and lead resistances is a major problem to be considered in the design of future units.

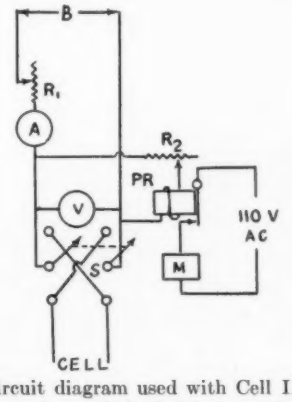

FIG. 4. Circuit diagram used with Cell II. B, 3–2 volt storage batteries in parallel; R_1, 0.5 ohm, 100 watt rheostat, A, ammeter, 10 or 15 amp range; V, voltmeter, 2 volt range; R_2, 10 ohm rheostat; PR, precision adjustment relay, 10 ohm coil; M, timing motor, which operates DPDT switch S, consisting of two interconnected SPDT microswitches.

Separations were carried out on five solutions. The pertinent conditions for each experiment are summarized in Table I. At the beginning of an experiment, the cell was rinsed with the solution to be used and filled to a permanent mark in the upper chamber. No regeneration of electrode material was required between experiments. The volumes of different parts of the cell were as follows: lower chamber, 64 ml; between electrodes, 110.7 ml; upper chamber to mark, analysis cells included, 76.5 ml. An exception to the filling technique was made in Experiment 3, when the upper chamber was filled to only 62.3 ml. Due account has been taken of this difference in subsequent calculations.

In each case, rheostat R_1 was adjusted so that the voltmeter V read about 0.5 volt at the beginning of a cycle. As the resistance of the cell increased, the voltage rose until at about 0.8 volt the relay was

TABLE I. *Conditions of cell operation for five experiments**

Expt. No.	Solution	E_i	E_f	I_i	I_f	R_i	R_f	τ	Temp
								min	°C
7	0.2538*N* NaCl	0.25	0.52	4.0	3.0	0.075	0.18	19	23
8	0.5095*N* NaCl	0.235	0.49	5.2	4.3	0.046	0.12	18	20
5	0.2514*N* HCl	0.26	0.45	8.0	7.0	0.025	0.063	3	24
3	0.6575*N* HCl	0.14	0.40	9.5	8.0	0.014	0.049	4	25
4	0.2495*N* HCl + 0.2621*N* NaCl	0.16	0.40	7.4	5.8	0.020	0.060	9	26

* E is the potential in volts as measured at the electrodes, I is the current in amperes, and R is the cell resistance in ohms computed by Ohm's law. The subscripts i and f refer to the beginning and end of current passage of a half cycle. τ is the time of current passage during a half cycle. All values given are subject to some variation and are representative of the initial phases of the experiment.

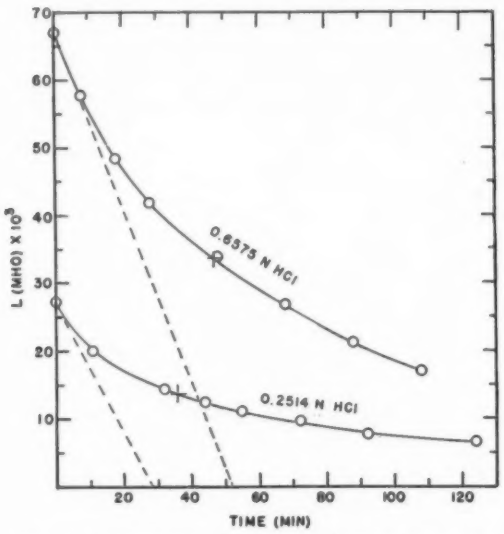

FIG. 5. Conductance, L, of upper chamber during earlier stages of Experiments 3 and 5. Dotted lines are for limiting slopes for convection velocity and efficiency calculations. +, points of half-removal for efficiency calculations.

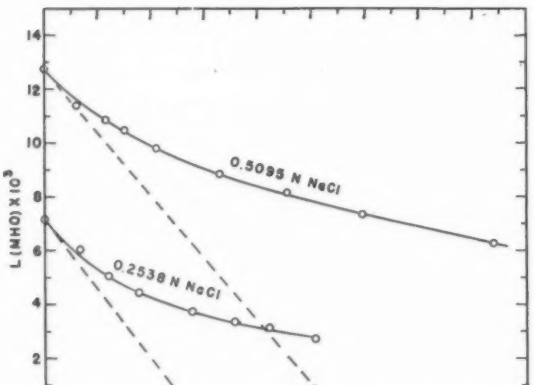

FIG. 6. Conductance, L, of upper chamber during earlier stages of Experiments 7 and 8. For dotted lines see legend to Fig. 5.

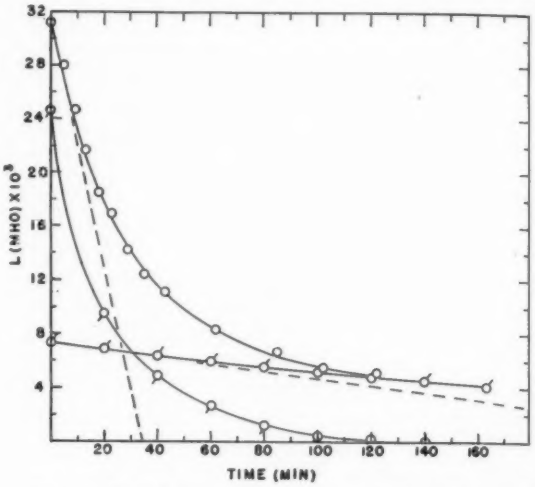

FIG. 7. Experiment 4. ○, measured conductivity of upper chamber; ○, calculated conductivity of HCl; ♂, calculated conductivity of NaCl. Dotted lines, see legend to Fig. 5.

energized. This cycle was repeated for the duration of the experiment, in some cases until a steady-state concentration was reached in the upper chamber. As noted above, the potential on voltmeter V was always higher than obtained directly at the electrodes subsequently with a separate meter.

The progress of the separation was followed continuously by conductance measurements of solution pumped through the analytical chamber. Measurements were made with a cell of 3.476 cm^{-1} cell constant. The measured conductances are plotted on the graphs which follow. In Experiment 4 the pH change was also followed. Conductivities were measured with an Industrial Instruments Model RC-1 conductivity bridge, and pH with a Beckman Model H pH meter. Initial and final concentrations were checked by titration. Acid concentration was determined by the usual procedure, and total chloride by the mercurimetric method.

Results of the experiments are shown in Fig. 5–8. Fig. 5, 6, and 7 show only the initial portions of

conductance vs. time curves, which were used for convection velocity and current efficiency calculations. Fig. 8 illustrates in a striking manner the power of the method for separating single electrolyte species when the apparatus is pushed to the limit. In Experiment 3 the final separation factor for HCl, c_b/c_t was 364 to 1. The corresponding factor for NaCl in Experiment 8 was 100 to 1. It should not be inferred, however, that this type of operation is desirable. As the separation progresses, the current efficiency falls steadily. In addition, the electrodes are subject to two types of deterioration. With HCl solutions the space between the lower portions of the electrodes tends to become clogged with loose Ag-AgCl mixtures after extended periods, thus leading to partial short circuits. This condition is evidenced by ab-

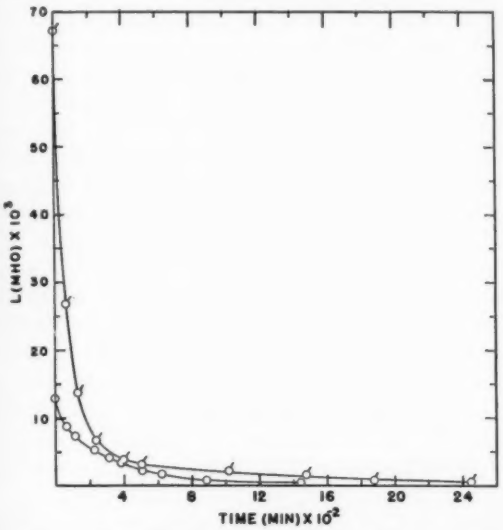

FIG. 8. ♂, Experiment 3, 0.6575*N* HCl, and ○, Experiment 8, 0.5095*N* NaCl, carried to steady state.

normally long periods of current passage in a half cycle. It is probably due both to the relatively large current demand of the lower portion of the electrodes with respect to the upper as the solution in this region becomes more concentrated, and to effects of the increased solubility of AgCl in concentrated HCl solutions. With NaCl solutions, suspended AgCl can be observed in the upper chamber after extended times, particularly with the more dilute solutions. This condition is undoubtedly due to precipitation of AgCl by anodically formed Ag^+ ion in the interior of the solution, rather than on the electrode surface.

One other factor observed in all experiments was the decrease of half-cycle time as the separation progressed. Indeed, when the process was carried to the steady state, current passage was only momentary during a half cycle. The decrease of cycle time is most rapid with dilute solutions. As will be noted from Table I, the shorter initial half-cycle times are to be associated with the more mobile cations.

Results of Experiment 4 on the HCl-NaCl mixture are particularly interesting and are shown in Fig.

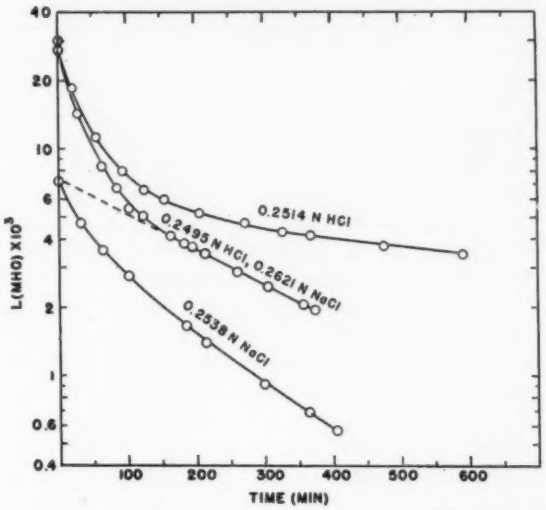

FIG. 9. Experiments 4, 5, and 8 on semilogarithmic plot. The dotted line is an extrapolation of the straight line portion of the middle curve.

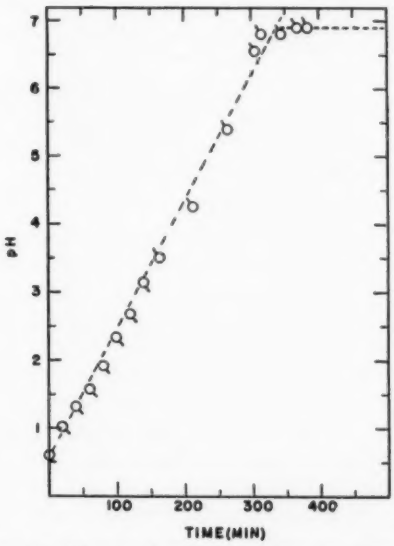

FIG. 10. pH as a function of time for Experiment 4. ○, measured with pH meter; ◎, calculated from conductivities. The dotted line is a straight line approximation used for convection velocity and efficiency calculations.

7, 9, and 10. In this experiment the pH as well as the conductance was determined as a function of time. All pH readings up to about 3.5, however, were unsteady and unreliable, and were therefore discarded. Independent checks were made to verify reliability

of readings above this value. Hydrogen ion concentrations, and hence pH values in the low range, were computed in the following manner: as observed in Fig. 9, a plot of the logarithm of conductance against time is approximately a straight line after about 150 minutes, after which time the upper solution was neutral, according to pH readings. This straight line extrapolates to a value which is very close to the one to be expected from the initial NaCl concentration. The experimental straight portion of the curve and its extrapolation are thus interpreted to represent the logarithm of the conductance of the NaCl alone in the solution as a function of time. By difference, the conductance of HCl alone can be calculated. By assuming that conductance is proportional to concentration and that the latter is numerically equal to activity, the concentration of H^+ and hence the pH could be calculated. The results are shown in Fig. 7 and 10. The removal of HCl is *quantitative* at a point where the NaCl concentration has been reduced by a little more than one third. The outlook for the method as a general means of separating mixtures of cations is thus promising.

Theoretical Considerations

Let us visualize the various processes which occur when the column is operating with a single electrolyte HCl, in the light of current theories of electrochemistry. The following reactions take place at the electrodes:

$$\text{Cathode} \quad AgCl + e = Ag + Cl^-$$
$$\text{Anode} \quad Ag + Cl^- = AgCl + e.$$

Hydrogen ion migrates toward the cathode, and chloride ion toward the anode. There is a net loss of chloride ion in the anolyte because of the electrode reaction, and of hydrogen ion because of migration. There is a net gain of chloride ion in the catholyte because of the electrode reaction, and hydrogen ion because of migration. The catholyte is thus more concentrated in HCl and the anolyte less concentrated; the difference in density gives rise to a convection current, which results in the concentration of HCl in the lower regions of the column.

In a mixture of two electrolytes having chloride as a common anion, the difference in cation mobility results in a preferential distribution of the more mobile cation in the catholyte region, and its resultant greater concentration by convection in the bottom chamber than the less mobile cation.

A mathematical theory of the process, with particular emphasis on the steady state condition, is now being worked out. The interesting theoretical work of Wagner (4) on convection in electrolytic processes will undoubtedly be of assistance in this connection. Kirkwood (2*a*) has developed equations for horizontal electrophoresis superimposed on thermal convection, but these equations cannot be directly applied to our situation. A substantial body of good experimental data is needed as a guide for the development of a detailed theory.

The experimental method employed here makes a general quantitative intercomparison of experiments impractical. The most important requirement for such a comparison would seem to be constant voltage operation with a more involved method for reversing the current flow. The constant time delay interval between half cycles in particular led to results which were not strictly comparable from one experiment to another. The lack of temperature control and the disturbance of convection currents due to the pumping action through the analytical chamber are minor contributing factors. Some conclusions from individual experiments can, however, be drawn.

1. The separation curves for the single electrolyte experiments can in no case be interpreted as a rate process of simple order over the entire range.

2. From the comparison of Experiments 4, 5, and 7 in Fig. 9, it is apparent that the separation curve for the mixture cannot be constructed in a simple manner from the curves for the individual components.

3. The analysis of Experiment 5 (Fig. 8) given at the end of the preceding section indicates that the logarithm of the concentration of the NaCl alone in the solution approximates a straight line, and the continuation of this analysis shows that the logarithm of the concentration of HCl alone in the solution also approximates a straight line (Fig. 10). Thus, in the case of this mixture, the separation of each individual component is a first order overall rate process over the range considered, in contrast to the case for single electrolytes. It is perhaps too early to make a more detailed analysis of this subject.

Horizontal and Vertical Transport Velocity

We may assume that the application of a horizontal electric field results in the movement of a more or less diffuse boundary of electrolyte across the column with a velocity v_x given by the product of the cation mobility and the field strength. These values, given in Table II, range from 0.176 cm/min for the hydrogen ion boundary in Experiment 5 to 0.023 cm/min for the sodium ion boundary in Experiment 8. The width of the gap between the electrodes is not sharply defined and not exactly constant, but a good average value is 0.32 cm. From the current duration per half cycle, τ, the distance λ which the boundary moves has been calculated and listed in Table II. These values are of the same order as the width of the gap but somewhat higher.

It should be recognized first that the electrodes themselves are highly porous, and hence provide additional path length for the ions, and second, that the calculations are only approximate.

In all experiments with single electrolytes the concentration in the upward convection current is undoubtedly less than about 15 per cent of the concentration in the upper chamber. If we assume that the change in concentration is due entirely to convection, that complete mixing occurs in the upper chamber, and ignore the return of electrolyte in the upward current, then the equation $V_u^{-1}(dV/dt) = L_i^{-1}(dL_i/dt)$ should set a lower limit on the rate of convective volume flow dV/dt at any instant. Here V_u is the constant volume of the upper chamber, and L_i is the conductance of the electrolyte. In the case of the mixture, if L_i is the conductance due to HCl alone, then a particularly simple result is obtained, since the concentration of HCl in the upper current must be utterly negligible, and since it has been shown that $L_{HCl}^{-1}(dL_{HCl}/dt)$ is approximately constant. In this case, the calculation should yield the actual convection velocity, and not just a lower limit. If the volume convection velocity is divided by the area of the gap, the linear velocity is obtained.

Convection velocities calculated in this manner are given in Table II. In the case of single electrolytes, the velocity at the beginning of the experiment is recorded, all subsequent values being less. The convection velocity varies from 1.83 cm/min for Experiment 5 to 0.477 cm/min for Experiment 8. It should be noted that the values given are time averages over one or more half cycles. Instantaneous values may be greater or less. In the fourth column, v_y has been multiplied by the ratio of the concentration to the current. These values show a fair degree of constancy for the single electrolytes, and this may prove to be a useful generalization in the development of the theory. Upon introduction of Ohm's law, the convection velocity is seen to be approximately proportional to the product of the applied potential and the equivalent conductance of the electrolyte.

Vertical Distribution of Electrolyte

The only analyses which were made other than by conductance of the upper chamber were titrations of the upper and lower solutions at the end of the experiment. We do not have, therefore, a direct measure of electrolyte distribution throughout the column. On the other hand, our data enable us to calculate by difference an experimental value of n_m, the number of moles of electrolyte between the electrodes, since we also know the total number of moles in the column. Different functional dependences of electrolyte concentration on column height will lead to different theoretical values of n_m. Although the actual functional dependence may be complicated, it is nonetheless of interest to compare the experimental result with assumed simple functional dependences. The two which we select for such comparison are the linear dependence and the exponential dependence, the latter having been predicted by Debye (5) for the analogous case of the thermal diffusion column. In this case, if the concentration dependence is expressed in the form $C = \text{const} \cdot \exp(kV)$, it is readily shown that $n_m = \frac{c_b - c_t}{k}$, where V is the volume corresponding to a given height.

Results of these calculations are given in Table III. The experimental values of n_m are seen to agree much more closely with the exponential than with the linear assumption for those experiments which were carried to the steady state. Two sources of experimental error should be recognized. The removal of electrolyte from the bottom and top chambers cannot be carried out without some mixing.

TABLE II. *Horizontal and vertical transport velocities*

Expt. No.	Solution	v_y	$v_y \cdot C/I$	v_x	λ
		cm/min		*cm/min*	*cm*
3	0.6575*N* HCl	0.81	0.56	0.11	0.44
5	0.2514*N* HCl	1.83	0.58	0.18	0.53
7	0.2538*N* NaCl	0.93	0.58	0.024	0.46
8	0.5095*N* NaCl	0.48	0.47	0.023	0.41
9	0.2495*N* HCl+ 0.2621*N* NaCl	0.97	0.67	0.11* 0.016‡	0.99* 0.14‡

* HCl only.
‡ NaCl only.

Furthermore, the solution in the bottom chamber cannot be perfectly uniform, because of convection during cell operation.

The latter error is the more serious one, tending to make n_m(calc) too large and n_m(expt) too small. For experiments which were carried to the steady state, n_m(calc) may be 15 per cent high and n_m(expt) 15 per cent low. The probable error in experiments which were terminated before reaching the steady state is considerably higher, and for this reason, calculations on Experiments 4 and 5 are included merely for comparison.

To sum up, we may say that experimentally a linear dependence of concentration on column height in the steady state is clearly out of the question, while an exponential dependence is possible.

Efficiency of the Process

The separation process has a distinct limitation imposed by Faraday's law. Ions must move across the column before they can be separated, and the

ultimate efficiency of separation is one equivalent per faraday. The actual efficiency will be less than this because of the opposing process of diffusion, and other factors. Furthermore, the efficiency will fall as the ratio of concentration of solutions in lower to upper chamber increases and diffusion becomes a dominating factor. It is, therefore, of interest to calculate the faraday efficiency of the separations studied here. These efficiency calculations are based on removal of electrolyte from the upper chamber only, and, therefore, are less than the overall efficiency, which should take into account the removal of electrolyte from the region between the electrodes. Overall efficiencies may be up to twice as large. The calculations were made from the knowledge of the volume of solution in the upper chamber, the change in conductance, and the average current. Two calculations were made in each case—the limiting efficiency η_{lim} at zero time, and the efficiency $\eta_{1/2}$ for removal of half the electrolyte. The results of the calculations are given in Table IV. The efficiencies in the case of the single electrolytes are about the same. Perhaps the most impressive figures in the table are for the mixture, Experiment 4. It is interesting to note that the ratio of efficiency of HCl removal to that of NaCl removal is of the same order as the ratio of the respective cation mobilities.

TABLE III. *Vertical distribution of electrolyte—comparison of experimental value of n_m with that calculated from assumed dependence of concentration on column height*

Expt. No.	Solution	C_b	C_t	n_m		
				Calculated from assumed distribution		Experimental
				Linear	Exponential	
		moles liter^{-1}	*moles liter*$^{-1}$			
3	0.6575*N* HCl	1.974	0.0054	0.110	0.037	0.030
5*	0.2514*N* HCl	0.7104	0.2951	0.056	0.0208	0.0153
7	0.2538*N* NaCl	0.7375	0.0101	0.041	0.0190	0.0157
8	0.5095*N* NaCl	1.463	0.01425	0.082	0.0351	0.033
4*	0.2495*N* HCl } HCl only	0.8513	10^{-7}	0.046	0.0059	0.0082
	+ 0.2621*N* NaCl } NaCl only	0.4732	0.0565	0.029	0.0217	0.0314

* These experiments were not carried to the steady state.

TABLE IV. *Per cent faraday efficiency*

Expt. No.	Solution	η_{lim}	$\eta_{1/2}$
3	0.6575*N* HCl	13.1	7.5
5	0.2514*N* HCl	13.6	6.7
7	0.2538*N* NaCl	14.1	7.4
8	0.5095*N* NaCl	11.0	7.5
4	0.2495*N* HCl } HCl only	13.7	12.3
	+0.2621*N* NaCl } NaCl only	1.6	—
	overall	15.3	—

Applications

Numerous applications of the process are suggested. Two or more cations with appreciably different mobilities could be separated in chloride solution with an apparatus of the above type. Other electrode systems would be preferable in some cases. The process is capable of adaptation to large-scale continuous operation. It is attractive from the energy standpoint. Although current efficiencies will always be considerebly less than unity, the voltage requirements are but a fraction of that required for the usual electrolytic process.

On a smaller scale, its use in quantitative analysis of solutions of alkali metal chlorides is suggested. The cations can be separated by the column and determined by some method such as conductance.

A consideration of the possibilities of the process for water purification by removal of electrolyte points to some serious obstacles. Convection currents will not be as pronounced in dilute solutions as in the more concentrated solutions, and the solubility of silver chloride or other active electrode material must be considered. More serious is the probability of formation of suspensions of the electrode material when the solution becomes dilute. This condition was observed in runs 7 and 8 after extended periods of operation.

From the standpoint of theory, this method offers excellent possibilities for the study of separation in general. Voltage and current inputs responsible for the separation are readily measured, and continuous analyses are easily performed. The elementary processes are more readily visualized here than in, say, the corresponding process of thermal diffusion, and the theory of electrolytic transport is more advanced.

The large effects of convection in electrolytic cells demonstrated in these experiments are pertinent to

the recent papers of Reed and Schriever (6*a*), Gordon (6*b*), and MacInnes, Shedlovsky, and Longsworth (6*d*). Reed and Schriever's experiments are claimed to demonstrate the presence of a macroscopic space charge in electrolytes during electrolysis, while Gordon and MacInnes, *et al.*, have disputed this claim. Among several objections raised by the latter to the experimental procedure was the possibility of convection in the cell, which would have led to a vertical concentration gradient. It is apparent from Schriever's reply (6*c*) to Gordon that the magnitude of convection effects has not been fully appreciated. MacInnes, Shedlovsky, and Longsworth have performed a simple experiment similar to Reed and Schriever's except that strictly reversible electrode systems were employed in a vertical cell designed to eliminate convection currents. They report no evidence of a space charge. The magnitude of convection effects which *can* be obtained in electrolytic cells as reported in this paper is substantial evidence that Reed and Schriever's cell was nonuniform in composition in the neighborhood of the electrodes, and that their conclusions may accordingly require modification.

ACKNOWLEDGMENT

The author is indebted to Mr. Harry A. Schopler for the drawings of Figures 1, 2, and 3.

Any discussion of this paper will appear in a Discussion Section, to be published in the June 1951 issue of the JOURNAL.

REFERENCES

1. K. CLUSIUS AND G. DICKEL, *Naturwissenschaften*, **26,** 546 (1938).
2. (*a*) J. G. KIRKWOOD, *J. Chem. Phys.*, **9,** 878 (1941).
   (*b*) L. E. NIELSEN AND J. G. KIRKWOOD, *J. Am. Chem. Soc.*, **68,** 181 (1946).
   (*c*) J. R. CANN, R. R. BROWN, AND J. G. KIRKWOOD, *J. Am. Chem. Soc.*, **71,** 2687 (1949), and earlier papers.
3. A. K. BREWER, S. L. MADORSKY, J. K. TAYLOR, V. H. DIBELER, P. BRADT, O. L. PARHAM, R. J. BRITTEN, AND J. G. REID, JR., *J. Research Natl. Bur. Standards*, **38,** 137 (1947), and earlier papers.
4. C. WAGNER, *J.* (*and Trans.*) *Electrochem. Soc.*, **95,** 161 (1949).
5. P. DEBYE, *Ann. Physik*, **36,** 284 (1939).
6. (*a*) C. A. REED AND W. SCHRIEVER, *J. Chem. Phys.*, **17,** 935 (1949).
   (*b*) A. R. GORDON, *J. Chem. Phys.*, **18,** 146 (1950).
   (*c*) W. SCHRIEVER, *J. Chem. Phys.*, **18,** 146 (1950).
   (*d*) D. A. MACINNES, T. SHEDLOVSKY, AND L. G. LONGSWORTH, *J. Chem. Phys.*, **18,** 233 (1950).

THE ELECTROCHEMICAL SOCIETY, INC.

The Electrochemical Society is an international organization of individuals and companies concerned with or interested in Electrochemistry and allied subjects.

The Society is dedicated to the advancement of the theory and practice of Electrochemistry and related subjects, as shown in the following divisions:

Battery	Electro-Organic
Corrosion	Electrothermic
Electric Insulation	Industrial Electrolytic
Electrodeposition	Theoretical Electrochemistry
Electronics	

Among the means to this end are the holding of meetings for the reading and discussion of professional and scientific papers on these subjects, the publication of such papers, discussions, and communications as may seem appropriate, and cooperation with chemical, electrical, and other scientific and technical societies.

It is an incorporated society without capital stock. The affairs of the Society are managed by a Board of Directors under a Constitution and By-Laws. Officers are nominated by a nominating committee appointed by the Board of Directors and elected by the members.

Direct all general correspondence and inquiries regarding membership to Society headquarters at 235 West 102nd Street, New York 25, N. Y., c/o Mr. W. J. Holian, Assistant Secretary.

Officers of the Society

President ..... CHARLES L. FAUST
Past President ..... ALFRED L. FERGUSON
Vice-President ..... RALPH M. HUNTER
Vice-President ..... J. C. WARNER
Vice-President ..... ROBERT J. MCKAY
Treasurer ..... E. GIDEON WIDELL
Secretary ..... HENRY B. LINFORD